THE INTERACTIONS OF ZINC THIOLATE COMPLEXES AND EXOGENOUS METAL SPECIES: INVESTIGATIONS OF THIOLATE BRIDGING AND METAL EXCHANGE

A Dissertation

by

ELKY ALMARAZ

Submitted to the Office of Graduate Studies of
Texas A&M University
in partial fulfillment of the requirements for the degree of

DOCTOR OF PHILOSOPHY

May 2009

Major Subject: Chemistry

THE INTERACTIONS OF ZINC THIOLATE COMPLEXES AND EXOGENOUS METAL SPECIES: INVESTIGATIONS OF THIOLATE BRIDGING AND METAL EXCHANGE

A Dissertation

by

ELKY ALMARAZ

Submitted to the Office of Graduate Studies of
Texas A&M University
in partial fulfillment of the requirements for the degree of

DOCTOR OF PHILOSOPHY

Approved by:

Chair of Committee,	M. Y. Darensbourg
Committee Members,	David P. Barondeau
	Kim R. Dunbar
	Edward D. Harris
Head of Department,	David H. Russell

May 2009

Major Subject: Chemistry

ABSTRACT

The Interactions of Zinc Thiolate Complexes and Exogenous Metal Species: Investigations of Thiolate Bridging and Metal Exchange. (May 2009)

Elky Almaraz, B.S., The University of Texas – Pan American

Chair of Advisory Committee: Dr. Marcetta Y. Darensbourg

Small molecule Zn(II) complexes containing N- and S- donor environments may serve as appropriate models for mimicking Zn protein sites, and thus, their reactions with heavy metal ions such as Pt(II) and W(0) may provide insight into possible adduct formation and zinc displacement. To study such possible interactions between zinc finger proteins and platinum-bound DNA, the ZnN_2S_2 dimeric complex, *N*,*N*′-bis(2-mercaptoethyl)-1,4-diazacycloheptane zinc (II), $[Zn\text{-}1']_2$, has been examined for Zn-bound thiolate reactivity in the presence of Pt(II) nitrogen – rich compounds. The reactions yielded Zn/Pt di- and tri- nuclear thiolate-bridged adducts and metal-exchanged products, which were initially observed via ESI-mass spectrometry (ESI-MS) analysis of reaction solutions, and ultimately verified by comparison to the ESI-MS analysis, ^{195}Pt NMR spectroscopy, and X-ray crystallography of directly synthesized complexes. The isolation of Zn-(μ-SR)-Pt-bridged [(Zn(bme-dach)Cl)(Pt(dien))]Cl adduct from these studies is, to our knowledge, the first Zn-Pt bimetallic thiolate-bridged model demonstrating the interaction between Zn-bound thiolates and Pt(II).

Additional derivatives involving Pd(II) and Au(III) have been explored to parallel the experiments executed with Pt(II).

The $[Zn\text{-}1']_2$ was then modified by cleavage with $Na^+[ICH_2CO_2]^-$ to produce (N-(3-Thiabutyl)-N'-(3-thiapentaneoate)-1,4-diazacycloheptane) zinc(II), Zn-1'-Ac or $ZnN_2SS'O$, and 1,4-diazacycloheptane-1,4-diylbis(3-thiapentanoato) zinc(II), Zn-1'-Ac_2 or $ZnN_2S'_2O_2$, monomeric complexes (where S = thiolate, S' = thioether). The $[Zn\text{-}1']_2$ di- and Zn-1'-Ac mono-thiolato complexes demonstrated reactivity towards labile-ligand tungsten carbonyl species, $(THF)W(CO)_5$ and $(pip)_2W(CO)_4$, to yield, respectively, the $[(Zn\text{-}1'\text{-}Cl)W(CO)_4]^-$ complex and the $[(Zn\text{-}1'\text{-}Ac)W(CO)_5]_x$ coordination polymer. With the aid of CO ligands for IR spectral monitoring, the products were isolated and characterized spectroscopically, as well as by X-ray diffraction and elemental analysis.

To examine the potential for zinc complexes (or zinc-templated ligands) to possibly serve as a toxic metal remediation agents, Zn-1'-Ac and Zn-1'-Ac_2 were reacted with $Ni(BF_4)_2$. The formation of Zn/Ni exchanged products confirmed the capability of "free" Ni(II) to displace Zn(II) within the N-, S-, and O- chelate environment. The Zn/Ni exchanged complexes were analyzed by ESI-MS, UV-visible spectroscopy, IR spectroscopy of the acetate regions, and X-ray crystallography. They serve as foundation molecules for more noxious metal exchange / zinc displacement products.

DEDICATION

I dedicate this dissertation to my mother and father, Eugenia and Alejandro Almaraz. Their unwavering love, support, guidance, and prayers have given me the strength to conquer the challenges presented along this journey to reaching my goals and dreams.

ACKNOWLEDGEMENTS

I would like to acknowledge the following people who have helped me throughout this journey. I gratefully recognize my advisor, Professor Marcetta Y. Darensbourg, who has provided me with continuous guidance and the encouragement to rise to every challenge in order to reach new heights. I thank my research committee members Professors Kim Dunbar, Edward Harris, David Barondeau, and former committee member, Raymond E. Schaak for their support throughout my graduate studies. I greatly appreciate the collaborators at Virginia Commonwealth University, Professor Nicholas P. Farrell, Quiete de Paula, Qin Liu, and Atilio Anzellotti, and their research ideas and collaborative efforts. I owe many thanks to Dr. Joseph Reibenspies and Dr. Nattamai Bhuvanesh in the X-ray Diffraction Laboratory, and Vanessa Santiago and the Laboratory for Biological Mass Spectrometry for imparting their expertise and assistance. The Women in Science and Engineering (WISE) organization and Dr. Marian Hyman have significantly influenced my development and maturity as a scientist, philanthropist, and as a woman.

I thank my my parents, Alejandro and Eugenia Almaraz, and my sisters, Edna Almaraz, Elda Mora, Elia Ochoa, and Elma Gonzalez, for without their spiritual, emotional, physical, and financial support, I would not have made it this far. I am grateful to German Gonzalez, for his positive words, and for always reminding me that everything is possible when we have faith and trust in God. I also thank Desiree Gonzalez, for being my best friend, for believing in me, and for encouraging me to shoot

for the stars. I also thank German Gonzalez, Jr. for his constant support, respect, and praise. My beautiful ray of sunshine and happiness, Alejandra Ochoa, has always brightened my life with her big smile and tender heart. I greatly appreciate Bryan Dulock, Jr. for taking care of me during my most stressful times, and for reminding me to breathe.

Many thanks to Dr. Jalal Mondal, for his constant mentoring and guidance, and for forever changing my life. I am also grateful to be a part of a great research family, the M. Y. Darensbourg and D. J. Darensbourg research groups. Thank you for the encouraging words, big smiles, and high spirits. I will never forget "Team Zinc", Jason A. Denny, for his fantastic work ethic, multi-tasking wonders, and most importantly for his friendship, and William S. Foley, for always being "on the ball", enthusiastic, and having an open heart and open arms. I have been very blessed to have "My Peeps" in my life, Yatsandra Oyola and Chris Bauer. I thank you for years of devoted support, and look forward to our many years of continued friendship. I also thank one of my very first friends at TAMU, Brad Williams. He has experienced with me and helped me through the adventures of graduate school.

TABLE OF CONTENTS

CHAPTER Page

LIST OF FIGURES

FIGURE Page

FIGURE Page

FIGURE Page

LIST OF TABLES

CHAPTER I

INTRODUCTION

The Properties of Zinc

The zinc(II) d^{10} metal ion, owes its vast assortment of functions to its distinctive chemical and physical properties. As it plays significant roles in nature, industry, and medicine, the non-redox active zinc contains a filled d shell, and thus has no unpaired electrons, no magnetic properties, and rare cases of observable color from its compounds arise from attached ligands.[1-3] This "silent" metal ion is a borderline hard Lewis acid which can accommodate a variety of hard and soft donors such as nitrogen, oxygen, and sulfur.[1,4] Due to its d^{10} configuration and subsequent lack of ligand field stabilization effects, zinc (II) does not possess a typical coordination number or geometry, thus rendering the ion accessible to two- (linear), three- (planar), four- (tetrahedral), five- (trigonal bipyramidal/square pyramidal), six- (octahedral), seven- (pentagonal bipyramidal) and eight- (distorted dodecahedral) membered ligand binding motifs.[1] Within this wide scope of coordination possibilities, the distribution has been estimated to be about 0.2 % three-, 42 % four-, 19 % five-, 35 % six-, and 4 % seven-coordinate.[1,5-7]

The ability to hold various ligand types, numbers, and geometries makes the zinc ion ideal for ligand (and metal) exchange reactivity. These unique properties, or rather "non-properties" as stated by Vahrenkamp, of the zinc ion are the crucial features

---

This dissertation follows the style of *Journal of the American Chemical Society*.

responsible for its pervasiveness and significance in an extensive assortment of chemical reactions.[8] Another unique feature of the zinc ion is that its lower-energy, filled d orbitals cause it to engage ligands strictly in σ donation, with negligible π interactions, such as OH^-, OR^-, and SR^-, hence preserving the nucleophilic character of these anionic ligands. It is through these Zn-ligand interactions that we observe reactivity of Zn-OR and Zn-SR species in the presence of electophilic reagents. The present work exploits these reactive entities by exploring the reactivity of zinc-bound thiolates towards a variety of exogenous metal species to observe both Zn-S-Metal bridging and Zn/Metal exchange within zinc chelate systems.

The Role of Zinc in Biological Systems

Zinc in Humans. Zinc is the second most abundant transition metal found in biology, and plays a critical role in the growth and development of microorganisms, plants, and animals alike.[1-3] The ubiquity of this essential trace element is due to its high prevalence in the environment, in food, and in the make-up of living organisms. The average human adult contains a total of two to three grams of zinc, with an average of 7 ppm in the blood, 75-150 ppm in bone, and 50 ppm in tissues and muscles.[2,3] It is estimated that within the tissue cells of the body, zinc is distributed as 30 – 40% in the nucleus, 50 % in the cytosol, and the remaining percentage is in organelles, vesicles and the cellular membrane.[1] The dietary intake recommended for an average man is about 7.5 to 15 mg per day, and for an average woman is about 5.5 to 12 mg per day.[1,2] While foods such as oysters, liver, beef, wheat, eggs, and cheese may contain between about 1

– 7 mg per 100 g serving, the average adult may consume approximately 5 – 40 mg per day, varying with diet.[1-3] Healthy levels of zinc have been associated with immune system and skin health, normal digestion and fertility.[1-4] In cases where there is a deficiency of zinc in the body, humans may experience symptoms such as growth retardation, skin damage, and a slowing of sexual maturation.[3,4]

Zinc in Enzymes and Proteins. Zinc(II) is crucial in the composition of enzymes which regulate growth and development and in transcription factors, i.e., proteins that aid in the transcription of DNA to RNA.[1,4,9-11] The zinc ion is most frequently observed in such biological sites to be tetrahedrally ligated to N-, S-, and O-donor atoms of amino acid side chains, small molecules, and H_2O. The typical amino acid residues and their respective donor atoms that bind Zn(II) are cysteine thiolate sulfurs, histidine imidazole nitrogens, and the carboxylate oxygens of aspartate and glutamate.[1,4,9-11] There are both mono- and dinuclear zinc enzyme and protein sites, as well as polynuclear sites, in which the latter two are usually bridged via carboxylate, water, and thiolate ligands.[1,4,9]

Zinc (II) participates in key functions within a multitude of enzymes and proteins as both a *catalytic* and a *structural* entity.[1,4,9-11] The zinc ions which play *catalytic* roles, such as carbonic anhydrase and liver alcohol dehydrogenase, more often have a higher incidence of aspartate, glutamate, and water (or hydroxide) O-donor ligands. Many of these zinc sites rely on water ligands to participate in their mechanism of action. For example, carbonic anhydrase requires zinc to generate a deprotonated hydroxide, and liver alcohol dehydrogenase utilizes displacement of water by an alcohol substrate.[1,4,5,9]

In both cases, water plays a key role in "activating" the catalytic cycles. However, there are cases such as the Ada protein and farnesyl transferase in which Zn-$Cys_{thiolate}$ sites act as the vital factor in the functional processes of Zn-thiolate alkylation. Figure I-1 below illustrates the Zn-binding sites within carbonic anhydrase, liver alcohol dehydrogenase, and the Ada protein.

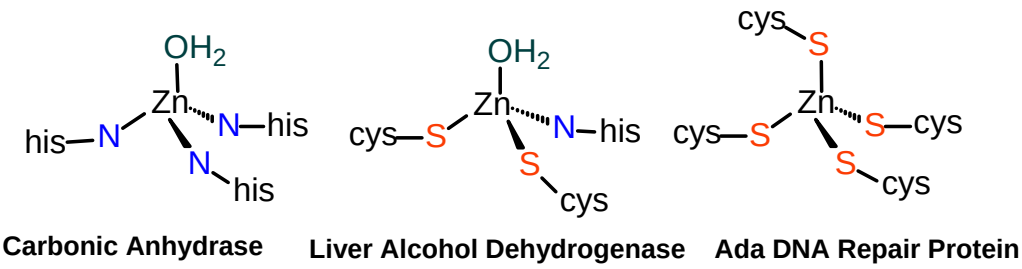

Figure I-1. Zinc (II) coordination sites within carbonic anyhydrase, liver alcohol dehydrogenase, and Ada DNA repair protein.

It is worth mentioning that a dimeric zinc complex employed within the present studies has been cleaved by thiolate alkylation, as in Ada and farnesyl transferase, as well as through metallation with Pt(II), Pd(II), and W(0), suggesting a possible parallel between Zn-S modification via alkylation and metallation.

The usual geometry in *structural* zinc centers, such as zinc finger proteins, is that of tetrahedral (or distorted tetrahedral) binding from cysteine and histidine ligands. Using zinc as a structural scaffold, zinc finger proteins rely on the small metal ion to organize the tertiary structure of the protein for subsequent DNA binding and transcription. [4,9,12] Within such proteins are recognized structural peptide sequences which are referred to as zinc finger domains; these are responsible for Zn^{2+} binding and subsequent DNA interaction. The small (30-40 amino acid residues in length) and stable

domains coordinate Zn^{2+} in a tetrahedral geometry through Cys_2His_2, Cys_3His, or Cys_4 binding sites (Figure I-2), with the Cys_2His_2 motif being the most commonly known.[12-14] The Zn^{2+} ion is chelated in a mononuclear, tetrahedral fashion through the N_xS_{4-x} (x = 0 – 4) non-consecutive amino acid side chain donors, pinning together a beta-hairpin and an alpha helix as in the ZnN_2S_2 site of Transcription Factor IIIA illustrated in Figure I-3.

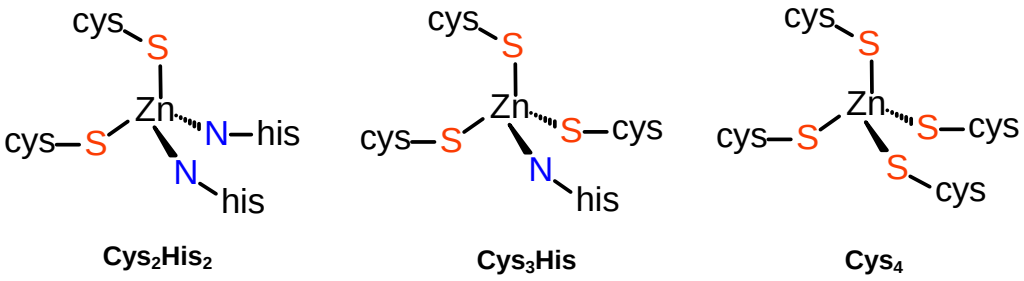

Figure I-2. Common zinc (II) coordination in zinc finger proteins.

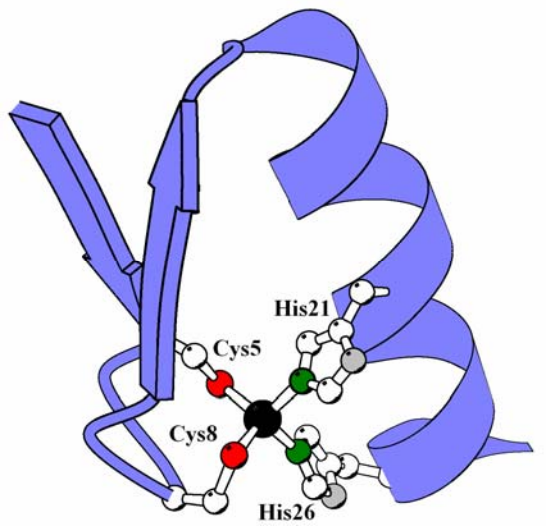

Figure I-3. Zinc finger protein domain in Transcription Factor IIIA (TFIIIA). Adapted from [12].

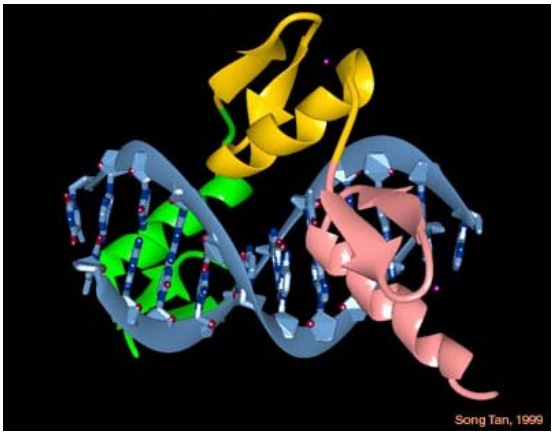

Figure I-4. X-ray structure of Zn finger-DNA complex in Zif268. Figure from [17].

Although Zn^{2+} does not directly mediate zinc finger protein binding to the DNA, zinc is required in order to fold the protein domain into a conformation that is structurally suited for DNA interaction. The typically observed sites of protein – DNA interaction are the arginine and histidine side chain residues of the α helix which hydrogen bond with the guanine bases of DNA, intercalating the zinc finger domains into the major groove, as pictured in Figure I-4 of the X-ray structure of a zinc finger-DNA complex.[13,15-17] Zinc finger domains have been examined for coordination of redox active metal ions, such as Mn^{2+}, Cu^{2+}, Cd^{2+}, Hg^{2+}, Ni^{2+}, Co^{2+} and Fe^{2+} but, always demonstrate a preference for Zn^{2+}.[12,14,18-20]

The first chapters of this work will mainly focus on the reactivity of Zn complexes in N- and S- rich environments, as found frequently within *structural* Zn sites, while the last chapters incorporate additional O- ligands within the Zn chelate environment, somewhat mimicking the *catalytic* sites as well.

Synthetic Small Molecule Models of Biological Zinc Sites

Before the increased emergence of zinc protein and enzyme X-ray crystallography in the late 90's and early 2000's, the colorless and "silent" zinc sites were commonly studied by replacement with cobalt (II), and the other transition metal ions mentioned above.[1,4,9] Additionally, as with common practice in exploring metalloproteins and enzyme active sites, the synthesis of small molecule synthetic analogues for both structural and catalytic investigations have been developed. Following suit, many synthetic models have also been compared to their Co^{2+}, Cd^{2+}, Fe^{2+}, and Ni^{2+} counterparts to determine the first coordination sphere effects, as well as spectroscopic analyses. [21-26]

The library of known synthetic models for zinc- containing sites is vast in number, but is mainly composed of tri- and tetradentate zinc tripodal and scorpionate complexes, with a smaller portion of mono- and bidentate systems.[5] A classic example of the latter is the $[Zn(SC_6H_5)_4]^{2-}$ utilized by Lippard as a mimic of the *E. coli* Ada protein, which is responsible for repair of DNA alkyl phosphotriester lesions through alkylation of zinc-bound thiolates.[27] Many researchers such as Parkin, Carrano, Vahrenkamp, and Riordan have developed small molecule analogs which incorporate the former type of ligands to substantiate a tetrahedral geometry.[5,28] Both types of systems, the $[Zn(SC_6H_5)_4]^{2-}$ and the zinc tripodal complexes, have been examined for their SR^- reactivity via alkylation studies.[5,8,27] Additional Zn-containing models, such as those developed by Grapperhaus and Darensbourg, employ tetradentate N_2S_2 ligands that position Zn in a secure square pyramidal or distorted tetrahedral environment for

investigations on reactivity of their Zn-S sites.[29-31] The pre-organization of multi-dentate N_2S_2 ligands, as implemented in the present work, maintains the structural integrity of the coordination complex, allowing for modification of the terminal thiolate S-atoms by metallation or oxygenation while remaining Zn-bound.

Motive for Studying Zn-Bound Thiolate Reactivity. What is the rationale for specifically modeling the reactivity of Zn in such N- and S- rich sites? The idea of Zn-containing proteins as potential drug-related targets relates to their abundance and locale within the cell, which places them at high risk for interaction with Pt^{2+} in chemotherapy, or other transition metal ions used in drug treatments. As postulated in the mechanism of action of cisplatin (Figure I-5A), upon entering the cell the Pt(II) becomes hydrolyzed and "available" as a cationic species for capture by DNA or, as in resistance modes in Figure I-5B, by S- containing molecules and proteins.[32] Studies on the mechanism have revealed that a minute portion (under five percent) of administered cisplatin actually binds to the intended DNA target.[33,34] This suggests that a large portion of the Pt^{2+} is accessible to interact with a host of small molecules, enzymes, and transcription factors within the cell. It is within this suggested mechanism (and the reactivity studies of cisplatin and its *trans*-derivative) that a foundation for the plausibility of Zn-protein/Pt/DNA ternary adducts has been laid and studies of their potential role in cytotoxicity have ensued.[33-36]

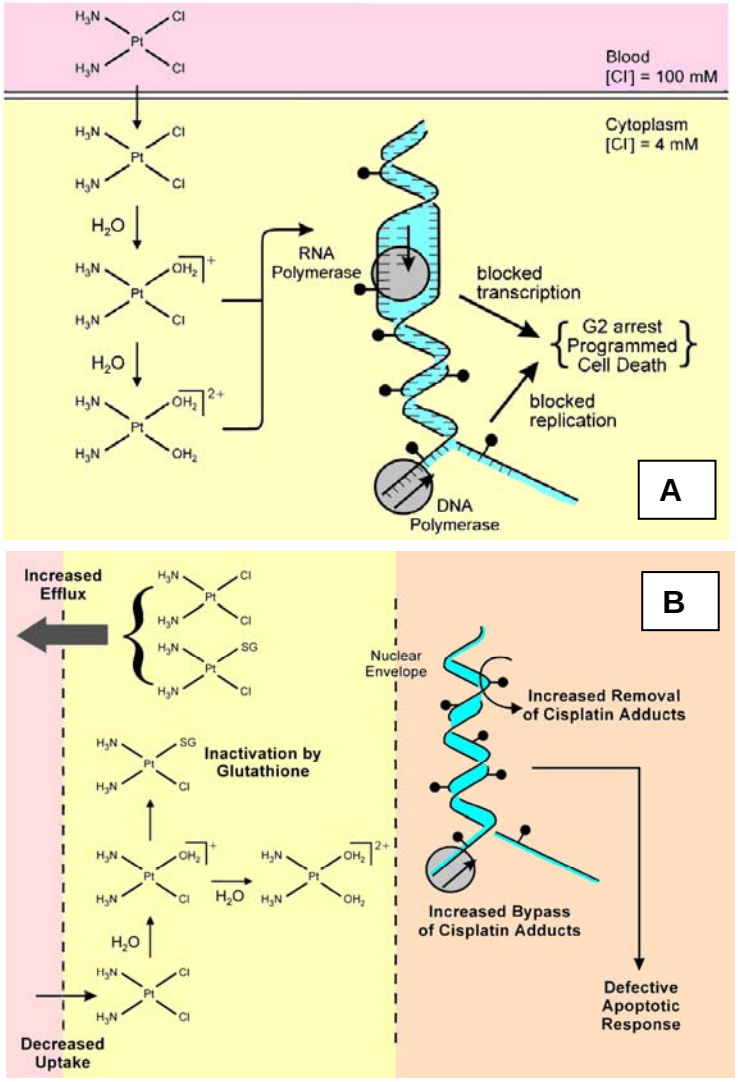

Figure I-5. The proposed cisplatin chemotherapy modes of: A. action / cytotoxicity and B. resistance. Adapted from [32].

There are two proposed implications resulting from such ternary adducts and Zn/Pt metal exchange, depicted in Figure I-6. The first predicts that zinc finger disruption by Pt(II), whether by metal-bridging or exchange, may cause protein conformational changes that would end in the inhibition of DNA-binding and transcription. Considering that the Pt(II) is bound to DNA prior to zinc finger

interaction, the alternate proposed consequence views the Pt-binding to zinc proteins as a mechanism of Pt(II)-removal from DNA, thus allowing the cancerous cell to continue to flourish. This second notion, however, is linked to the first since Pt(II) removal would be coupled with the sacrifice of the protein to which it binds, ultimately altering protein function as well.

Figure I-6. Working hypothesis for the implications of Zn/Pt interactions upon cancerous cells.

The use of small molecule models to investigate such interactions would provide a starting point towards substantiating or negating such hypotheses. Furthermore, synthetic models, as in the typical manner for chemical reactivity analysis, would allow added ease of manipulation and varying conditions, and more rapid isolation and characterization of the models demonstrating the first coordination sphere of interaction.

The occurrence of Zn/Pt metal-exchange in such model systems is introduced within this report, along with the first structurally characterized Zn-Pt thiolate bridged hetero-bimetallic model. As will be discussed in Chapter II, the model may give insight into the Pt displacement of Zn in N- and S- rich sites. Investigations of Pt^{2+} displacement of Zn^{2+} within Zn-S peptidic sites have been reported by Bose, *et al.*, and Farrell, *et. al*, and the structural implications of such transmetallation on cellular

function and apoptosis has been discussed. [35,37] Aside from the initial findings of such Pt- containing adducts and metal exchange, the present investigations of Zn-bound thiolates, reported herein, will expound upon their reactivity with the following: additional drug-related metals (Pd and Au), a heavy, low-valent metal (W^0) with CO ligands attached for IR spectral monitoring, and a first row d^8 toxic metal (Ni) salt for exploration of possible noxious metal chelate therapy. These studies aim to elucidate the capability of Zn-bound thiolates to form stable bridges to exogenous metals, and identify the conditions under which the added metal ions may replace Zn within its coordination environment.

CHAPTER II

THIOLATE BRIDGING AND METAL EXCHANGE IN ADDUCTS OF A ZINC FINGER MODEL AND Pt(II) COMPLEXES: BIOMIMETIC STUDIES OF PROTEIN/Pt/DNA INTERACTIONS*

To provide precedents for the possible interactions of platinum DNA adducts with *zinc finger* proteins, the [Pt(dien)Cl]Cl (dien = diethylenetriamine) and [Pt(terpy)Cl]Cl (terpy = 2,2′:6′,2″- terpyridine) complexes were exposed to the *N*,*N*′-bis(2-mercaptoethyl)-1,4-diazacycloheptanezinc(II) dimer, $[Zn(bme\text{-}dach)]_2$. Through collaborative efforts by the M. Y. Darensbourg (TAMU) and N. Farrell (Virginia Commonwealth University, VCU) research laboratories, the products were defined by electrospray ionization mass spectrometry (ESI-MS), X-ray crystallography and ^{195}Pt NMR spectroscopy. The presence of a leaving chloride in both platinum(II) complexes facilitates electrophilic substitution involving sulfur-containing zinc finger synthetic models or, as in previous studies, zinc finger peptidic sequences. Monitored via ESI-MS, both reactants yielded evidence for Zn-(μ-SR)-Pt bridges followed by zinc ejection from the N_2S_2 coordination sphere and subsequent formation of a trimetallic Zn-(μ-SR)$_2$-Pt-(μ-SR)$_2$-Zn-bridged species. The isolation of Zn-(μ-SR)-Pt-bridged species [(Zn(bme-dach)Cl)(Pt(dien))]Cl is, to our knowledge, the first Zn-Pt bimetallic thiolate-

*Reproduced with permission from: "Thiolate Bridging and Metal Exchange in Adducts of a Zinc Finger Model and Pt^{II} Complexes: Biomimetic Studies of Protein/Pt/DNA Interactions" Almaraz, E.; de Paula, Q. A.; Liu, Q.; Reibenspies, J. H.; Darensbourg, M. Y.; Farrell, N. P. *J. Am. Chem. Soc.,* **2008**, *130*, 6272–6280. Copyright 2008 American Chemical Society.

bridged model demonstrating the interaction between Zn-bound thiolates and Pt^{2+}. In the case of the [Pt(terpy)Cl]Cl reaction with the $[Zn(bme\text{-}dach)]_2$, ESI-MS analysis further suggests metal exchange by formation of $[Zn(terpy)Cl]^+$, whereas the [Pt(dien)Cl]Cl reaction does not yield the corresponding $[Zn(dien)Cl]^+$ ion. Direct synthesis of the Zn-Pt thiolate-bridged species and the $Pt(N_2S_2)$ chelate, where Pt has displaced the Zn from the chelate core, permitted the isolation of X-ray-quality crystals to confirm the bridging and metal-exchanged structures. The ESI-MS, ^{195}Pt NMR spectroscopy, and molecular structures of the di- and trinuclear complexes will be discussed, as they provide insight into the metal-exchange mechanism.

Introduction

Critical biological functions regulated by the docking of cysteine-rich zinc finger proteins onto DNA or RNA include DNA repair, regulation of genetic transcription, and viral-host cell incorporation.[38-40] These important biomolecule interactions may be inhibited upon chemical modification, usually alkylation or oxidation, of the zinc binding ligands. Such chemical modification may result eventually in zinc ejection and loss of protein tertiary structure, resulting in the inhibition of biological function. Especially in the case of the HIV nucleocapsid zinc finger NCp7 protein, this strategy has been used to develop small-molecule inhibitors as a potentially new class of HIV-inhibiting drugs.[41-43] A formal analogy exists between alkylation and platination (metallation); chemical modification of the biomolecular substrate involves in both cases electrophilic attack on the cysteinyl sulfurs of the zinc-binding site. In agreement, *in*

vitro studies using mass spectrometry and other spectroscopic techniques have demonstrated the ability of platinum-nucleobase compounds, such as *trans*-[PtCl(9-EtGua)(pyr)$_2$]+ and *[SP-4-2]*-[PtCl(9-EtGua)(NH$_3$)(quin)]$^+$, to bind to the C-terminal domain of the NCp7 peptide with subsequent ejection of the zinc.[37, 44] It is reasonable to suggest that the mechanism of zinc ejection also involves platination of zinc-binding ligands within the active site, analogous to alkylation, with the formation at some point of a ligand-bridged Zn-Pt species. In support of this notion, the reaction between *cis*-[PtCl$_2$(NH$_3$)$_2$] (*cis*-DDP, cisplatin) and a 31 amino acid zinc finger sequence containing a ZnCys$_4$-binding site proceeds in a stepwise manner in the presence of 2 equiv of *cis*-DDP with complete deligation of Zn^{2+}.[35]

The concept of ternary Zn (protein)/Pt/(DNA/RNA) species may have widespread relevance in biology. Recognition of cisplatin-adducted DNA is seen for many proteins, a number of which contain the Zn-finger motif.[37, 45, 46] Two relevant human examples are the XPA repair protein and the transcription factor Sp1. DNA–protein cross-linking reactions involving zinc finger proteins and site-specific platinated oligonucleotides have also been described. Tetra- and trifunctional dinuclear platinum complexes cross-link the Sp1 protein and components of the bacterial UvrABC repair system to DNA-DNA *interstrand* adducts induced by the complexes.[47-49] Heterodinuclear [Pt,Ru] compounds are also capable of inducing these ternary DNA protein cross-links.[48,50] Incorporation of steric hindrance into an ethylenediamine chelate allows for ternary DNA–protein cross-linking of an initially formed monofunctional DNA adduct with components of the UvrABC repair system, because of

retardation of the second (bifunctional) DNA-binding step and favorable competitive reaction with protein.[51] The use of *trans*-[$PtCl_2(NH_3)_2$] (*trans*-DDP) to cross-link the zinc finger nucleocapsid protein to HIV-1 RNA may proceed through a similar mechanistic pathway.[52]

As stated, the molecular description of ternary DNA–protein complexes involving zinc fingers and platinated DNA may reasonably be considered to involve a zinc-binding site (cysteine) bridging to a platinated nucleobase (polynucleotide). The well-known affinity of platinum(II) compounds for sulfur certainly suggests the feasibility of Zn-(μ-SR)-Pt intermediates in these biological processes. The mechanism of zinc ejection may also involve such intermediates. The alkylation/platination analogy has also been successful in studying model reactions where potential Zn-Pt intermediates were observed by mass spectrometry. Initial results from a study of the zinc protein model $[Zn(bme\text{-}dach)]_2$ (a structural drawing shown in Scheme II-3) and *trans*-$[PtCl(9\text{-}EtGua)(pyr)_2]^+$ showed the formation of putative Zn-Pt species and eventual incorporation of Pt into the chelate to form Pt(bme-dach).[53] Such a small-molecule study may be predictive of chemical models for the proposed biological structures. The earlier biomolecule and mass spectral studies (VCU) may be considered to be on the micro- to nanomolar scale, wherein the reaction between zinc finger synthetic analogues and simple platinum and platinum-nucleotide complexes might mimic the more complicated biological system. In pursuing these analogies, we have made a tandem study at the millimolar (bulk chemical synthesis, TAMU) level for the purpose of adduct and proposed intermediate isolation, which may be structurally characterized, including

X-ray diffraction studies. The latter technique will give detailed information on the feasibility of the possible bonding arrangements in the biological system. A schematic of the possibilities is presented in Scheme II-1. This report describes the study of two representative platinum compounds, $[Pt(dien)Cl]^+$ and $[Pt(terpy)Cl]^+$, with $[Zn(bme\text{-}dach)]_2$, the zinc-bound thiolate.

Scheme II-1. Possible Products Resulting from the Interactions of Zinc-Bound Thiolates with Pt^{2+} Species

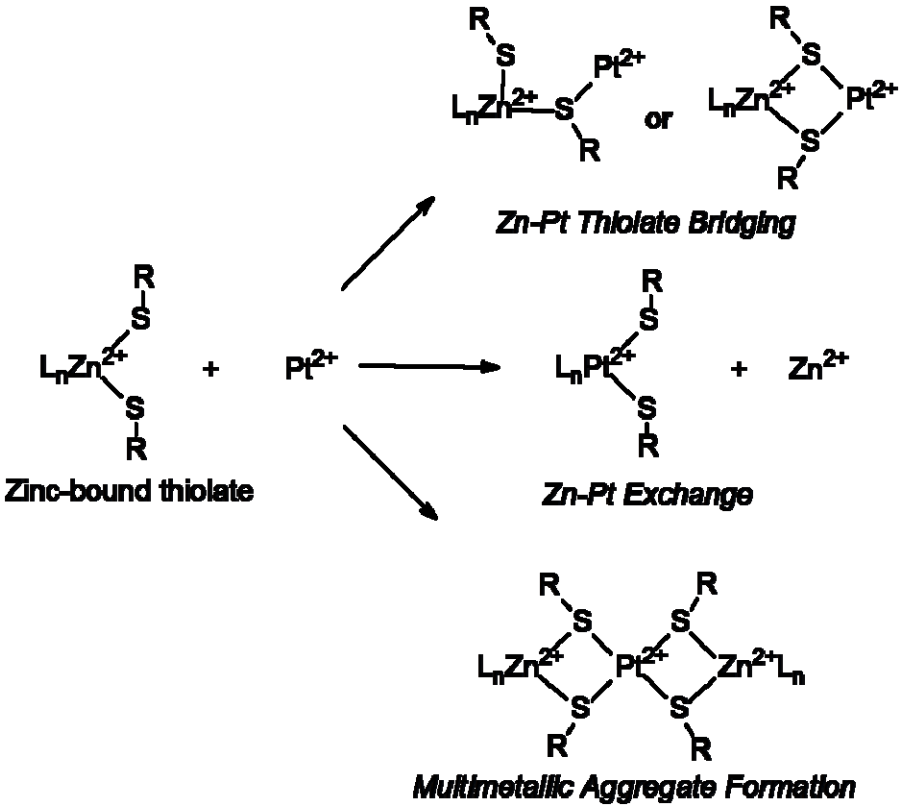

Experimental Details

Materials, Methods, and Reagents. All micro-nanomolar scale, ESI-MS-monitored reactions were carried out at VCU, while all the bulk chemical syntheses (direct syntheses) were performed at TAMU. All reagents and reactants were used without further purification. The [Pt(terpy)Cl]Cl and [Pt(dien)Cl]Cl complexes were prepared from K_2PtCl_4 as described in the literature.[54] The purity of the complexes was confirmed by ^{1}H and ^{195}Pt NMR spectroscopy (VCU) and elemental analyses, which were performed by QTI Laboratory, Whitehouse, NJ, Canadian Microanalytical Services, Ltd., Delta, British Columbia, Canada, or Atlantic Microlab, Inc., Norcross, GA.

Electrospray Ionization Mass Spectrometry (ESI-MS, VCU). Electrospray ionization mass spectra were recorded with a Finnigan LCQ ion-trap electrospray meter (LCQ-MS) in positive-ion mode. The voltage at the electrospray needles was 4.5 kV, and a N_2 sheath gas and Aux/sweep gas were used. The capillary was heated to 150 °C. The solutions were injected into the ESI source directly at a flow rate of 3.0 μL/min. Tandem mass and zoom scan were used to analyze the structure of the product in each of the experiments. Helium was admitted directly into the ion-trapping efficiency and as the collision gas in the collision-induced dissociation (CID) experiment. A maximum ion injection time of 500 ms along with 10 scans was set. To induce collision activation, the relative collision energy was controlled to 10–30% of the maximum, depending upon the precursor ions and MS*n*. In MS/MS and MS*n* experiments, an isolation width of 6 –

12 *m*/*z* units for the precursor ions was used to allow the signature Pt isotopic distribution to be observed.

Sample Preparations for ESI-MS Analysis. A 100 μL sample of 0.01 mM methanolic solution of $[Zn(bme\text{-}dach)]_2$ was mixed with 100 or 200 μL of 0.01 mM water solutions of [Pt(dien)Cl]Cl or [Pt(terpy)Cl]Cl, respectively, and incubated at 37 °C. ESI-MS spectra were recorded by taking a 10 μL solution mixture and diluting with 100 μL of MeOH prior to injection into the mass spectrometer. Mass spectrometry (ESI-MS) on the directly synthesized $[Zn(bme\text{-}dach)]_2$ and complexes **III**, **IV**, and **V** (Scheme II-2) were performed by the Laboratory for Biological Mass Spectrometry at Texas A&M University.

NMR Spectroscopy (VCU). ^{1}H and ^{195}Pt NMR spectra were obtained on a Varian 300 MHz NMR spectrometer at 23 °C, using 5 mm NMR tubes. The chemical shifts (δ) in the ^{1}H NMR spectra were referenced to 98% D_2O (4.79 ppm). The ^{195}Pt chemical shifts were referenced to K_2PtCl_4 in D_2O (– 1614 ppm).

Synthesis of *N*,*N*′-Bis(2-mercaptoethyl)-1,4-diazacycloheptanezinc(II) Dimer, $[Zn(bme\text{-}dach)]_2$, Complex I. The bis(2-mercaptoethyl)-1,4-diazacycloheptane (H_2bme-dach) ligand was prepared according to published procedures.[55] Under N_2, H_2bme-dach (2.530 g, 11.5 mmol) was dissolved in 20 mL of MeOH and NaOMe (1.220 g, 22.6 mmol) in 20 mL of MeOH was slowly added. The solution was vigorously stirred for 2 h at 22 °C. Under N_2, $ZnCl_2$ (1.568 g, 11.5 mmol) dissolved in 35 mL of MeOH was rapidly added to the stirring solution and immediately formed a white precipitate. After 28 h of stirring under an N_2 blanket, the white solid was isolated by

filtration in air and washed 3 times with MeOH to yield, after drying *in vacuo*, 2.64 g (4.7 mmol) of $[Zn(bme\text{-}dach)]_2$ product (81.7% yield). The dimer was dissolved in pyridine and layered with diethyl ether to yield colorless, X-ray quality crystals. ESI-mass spectrum: $[M + H]^+$ m/z = 569. Elemental analysis: calculated (found) C, 38.1 (37.8); H, 6.39 (6.13); N, 9.87 (9.83).

Synthesis of *N,N′*-Bis(2-mercaptoethyl)-1,4-diazacycloheptanezincchloride Platinum Diethylentriamine [(Zn(bme-dach)Cl)(Pt(dien))]Cl, Complex III. Under N_2, the $[Zn(bme\text{-}dach)]_2$ (0.0258 g, 0.0455 mmol) was dissolved in 30 mL of MeOH and heated to 37 °C with stirring. The [Pt(dien)Cl]Cl (0.0330 g, 0.0894 mmol) was dissolved in 3 mL of deionized H_2O and added drop-wise to the clear, colorless $[Zn(bme\text{-}dach)]_2$ solution. The cloudy reaction mixture was stirred at 37-39 °C for 39 h, after which time the stirring was stopped to allow the grayish precipitate to settle. The precipitate was removed by filtration, and the clear colorless solution was concentrated *in vacuo*. X-ray quality crystals were obtained through both layering and vapor diffusion with MeOH/diethyl ether. Approximate yield from recrystallization tubes: 0.016 g (0.024 mmol), 27%. ESI-mass spectrum: $[M]^+$ m/z = 616, $[M - Cl]^{2+}$ m/z = 290.5. ^{195}Pt NMR spectroscopy: – 3267.95 ppm. Elemental analysis: calculated (found) C, 23.91 (22.83); H, 4.79 (5.18); N, 10.73 (10.58). Note: Shorter reaction times were used in attempts to isolate the monothiolate-bridged species, **II** (Scheme II-2). However, crystals of the dithiolate-bridged species were the sole product.

Synthesis of *N, N′* - Bis(2-mercaptoethyl)-1,4-diazacycloheptaneplatinum(II), [Pt(bme-dach)], Complex IV. Under a N_2 atmosphere, H_2bme-dach (0.306 g, 1.39

mmol) was dissolved in 15 mL of MeOH and KOH (0.158 g, 2.82 mmol) in 10 mL of MeOH was added to it slowly. The solution was stirred vigorously for 1.5 h. A portion of K_2PtCl_4 (0.579 g, 1.39 mmol) was dissolved in a 30 mL of solvent mixture comprised of 10 mL of MeOH and 20 mL of H_2O and slowly added to the stirring solution. The reaction mixture was stirred vigorously at room temperature overnight, after which time the bright yellow solution and solid were separated. The solid was washed with 20 mL of MeOH, and all washings were added to the solution. The solution was then reduced in volume *in vacuo* and placed on a silica gel chromatography column, with MeOH as the eluant. The first pale yellow band was collected and dried to yield 0.040 g of pure product, a 7.0% yield. X-ray quality crystals were obtained from slow evaporation from a concentrated MeOH solution. ESI-mass spectrum: $[M + H]^+$ m/z = 414, $[M + Na]^+$ m/z = 436, $[M + K]^+$ m/z = 452. ^{195}Pt NMR spectroscopy: – 3044.4 ppm. Elemental analysis: calculated (found) C, 26.14 (25.17); H, 4.39 (4.27); N, 6.78 (6.56).

Synthesis of *N*, *N*′- Bis(2-mercaptoethyl)-1,4-diazacycloheptane-zincchloroplatinate, [Zn(bme-dach)Cl]$_2$Pt, Complex V. Two methods were implemented to produce (a) pure product in the form of insoluble powder and (b) X-ray quality crystals for molecular structure determination.

(a) A solution of K_2PtCl_4 (0.0215 g, 0.052 mmol) in 5 mL of H_2O was added to $[Zn(bme\text{-}dach)]_2$ (0.0297 g, 0.052 mmol) dissolved in 35 mL of MeOH. After stirring for approx. 2 h, the yellow precipitate was isolated by filtration and washed with H_2O, MeOH, and Et_2O to remove any starting materials or salts. The yellow solid was dried *in vacuo*; yield, 0.0210 g (48.7%). The product was found to be partially soluble in

tetrahydrofuran (THF) and $CHCl_3$. ESI-mass spectrum: $[M - Cl]^+ = 797$ *m*/*z*. ^{195}Pt NMR spectroscopy: – 3472.50 ppm. Elemental analysis: calculated (found) C, 25.94 (25.57); H, 4.35 (4.36); N, 6.72 (6.25).

(b) Stock solutions of K_2PtCl_4 (0.0630 g, 0.152 mmol) in 6 mL of H_2O/MeOH (80/20 V) and $[Zn(bme\text{-}dach)]_2$ (0.0155 g, 0.027 mmol) in 30 mL of MeOH/MeCN (67/33 V) were prepared. A total of 1 mL (0.025 mmol) of the K_2PtCl_4 solution was transferred to a Schlenk tube and layered carefully with 2 mL of MeOH. The $[Zn(bme\text{-}dach)]_2$ solution (25 mL or 0.023 mmol) was then delicately layered above the MeOH layer. The tube was then held at 2 °C for 3 days, after which time the pale yellow needles that developed at the interface were harvested for X-ray diffraction study.

Isolation from NMR Experiments (VCU). When the reaction between [Pt(dien)Cl]Cl and $[Zn(bme\text{-}dach)]_2$ in either a 1:1 or a *2 Pt:1 Zn* molar ratio was monitored by ^{195}Pt NMR spectroscopy, yellowish crystals precipitated within the NMR tube after approx. 2 h. Upon filtration and drying, elemental analysis further supported the formation of the species corresponding to $[Zn(bme\text{-}dach)Cl]_2Pt$; calculated (found) C, 25.94 (25.89); H, 4.35 (4.36); N, 6.72 (6.52).

X-ray Structure Analysis (TAMU). The final structural solutions for the four structures presented in this chapter were finalized and prepared for publication by Dr. J. H. Reibenspies, X-ray Diffraction Laboratory at Texas A&M University. Low-temperature (110 K) X-ray diffraction data were collected on a Bruker SMART 1000 CCD based diffractometer (Mo Kα radiation, λ = 0.71073 Å) for the Pt(bme-dach) single crystal.[56] The [(Zn(bme-dach)Cl)(Pt(dien))]Cl data were collected on the Bruker

– AXS APEX–II CCD three-circle X-ray diffractometer under the same conditions. For the $[Zn(bme\text{-}dach)]_2$ and $[Zn(bme\text{-}dach)Cl]_2Pt$ complexes, data were obtained on a Bruker D8 GADDS general purpose three-circle X-ray diffractometer (Cu Kα radiation, λ = 1.54184 Å), also operating at 110 K. The structures were solved by direct methods. H atoms were added at idealized positions and refined with fixed isotropic displacement parameters equal to 1.2 times the isotropic displacement parameters of the atoms to which they were attached. Anisotropic displacement parameters were determined for all non-hydrogen atoms. Programs used were as follows: data collection and cell refinement, *SHELXTL*[57]; absorption correction, *SADABS*; structure solution, *SHELXS-97* (Sheldrick)[58]; structure refinement, *SHELXL-97* (Sheldrick)[59]; and molecular graphics and preparation of material for publication, *SHELXTLPLUS*, version 5.1 or later (Bruker). X-seed was employed for the final data presentation and structure plots.[60]

Cambridge Crystallographic Data Centre (CCDC) 623889, 661017, 661018, and 661019 contain the supplementary crystallographic data for this paper. These data can be obtained free of charge via www.ccdc.cam.ac.uk/data_request/cif, by e-mailing, or by contacting The Cambridge Crystallographic Data Centre, 12, Union Road, Cambridge CB2 1EZ, U.K.; fax, +44-1223-336033. Furthermore, the crystallographic data reports for the four compounds included in this report are listed in the Appendix.

Results

The reaction between $[Pt(dien)Cl]^+$ and the Zn dithiolate complex $[Zn(bme\text{-}dach)]_2$ was studied using ESI-mass spectrometry, ^{195}Pt NMR spectroscopy, and X-ray crystallography on isolated products. Scheme II-2 lists the compounds that were characterized in this study. The molecular structures of complexes **I**, **III**, **IV**, and **V** were determined by X-ray diffraction analysis, and that of complex **II** was inferred by ^{195}Pt NMR spectroscopy.

Scheme II-2. Compounds **II**, **III** (with dangling amine stabilized by a network of hydrogen bonding), **IV**, and **V** Formed in the Reaction between $[Pt(dien)Cl]^+$ and the Zn Dithiolate Model $[Zn(bme\text{-}dach)]_2$, Complex **I**

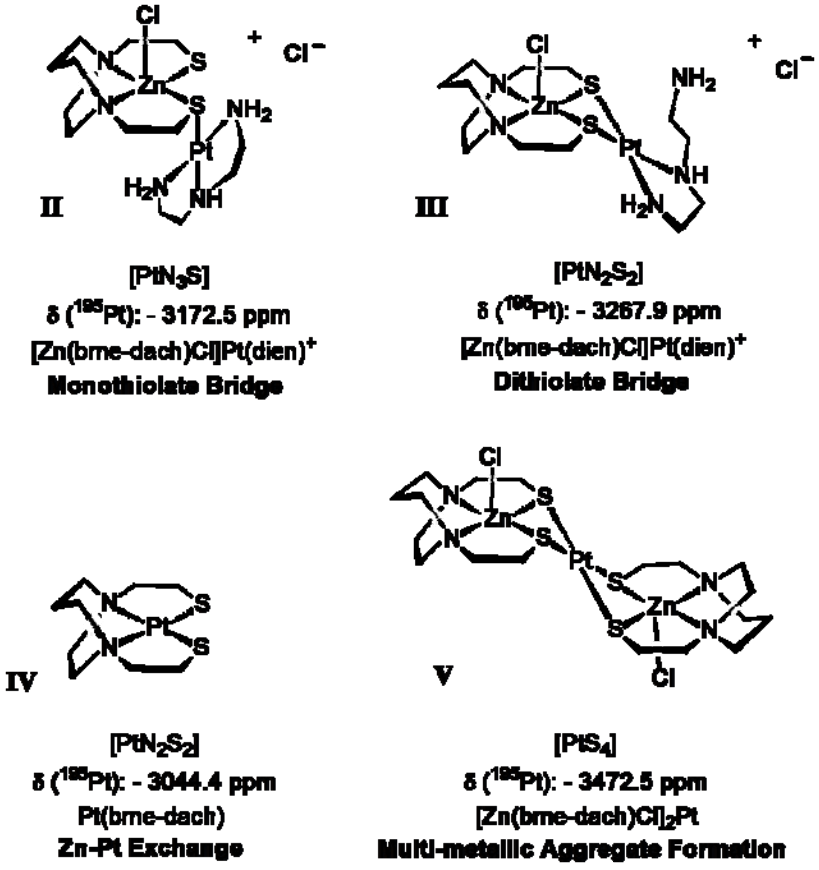

ESI-MS Analysis of the Reaction between [Pt(dien)Cl]Cl and [Zn(bme-dach)]$_2$, Reaction 1. When probed by ESI-mass spectrometry, the reaction between [Pt(dien)Cl]Cl and [Zn(bmedach)]$_2$ gave rise to two new major peaks, which remained invariant with time (Figure II-1, 1a). The *m*/*z* values of 290.9 and 616.3 were assigned to the species corresponding to [Zn(bme-dach)(Pt(dien))]$^{2+}$ and [(Zn(bme-dach)Cl)(Pt(dien))]$^{+}$, respectively. The isotopic distributions of these two peaks agree with the calculated predictions.

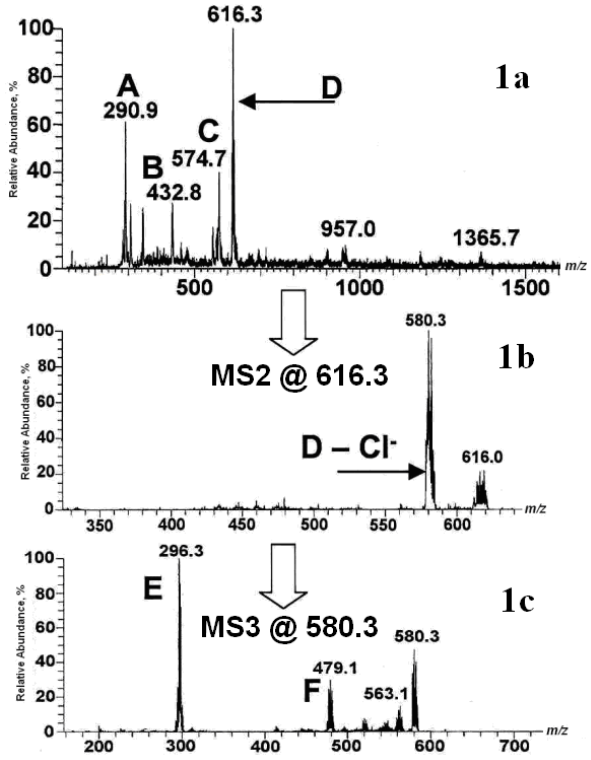

Figure II-1. ESI-MS spectrum of a 1:1 mixture of [Pt(dien)Cl]Cl and [Zn(bme-dach)]$_2$. (1a) after 48 hours of incubation, showing the predominant species [Zn(bme-dach)Pt(dien)]$^{2+}$ (A), {[Zn(bme-dach)]$_2$Pt(dien)}$^{2+}$ (B), {[Zn(bme-dach)]$_3$Pt(dien)}$^{2+}$ (C) and {[Zn(bme-dach)Cl]Pt(dien)}$^{+}$ (D). The MS2 spectrum of D exhibits the D – Cl$^-$ species (1b) and the MS3 of 580.3 yields [Pt(dien) – H$^+$]$^+$ (E) and [Zn(bme-dach)Pt – H$^+$]$^+$ (F) (1c).

The minor peaks shown in 1a of Figure II-1 at m/z = 432.80 and 574.70 may be ascribed to multi-metallic formulations such as $[(Zn(bme\text{-}dach))_2Pt(dien)]^{2+}$ and $[(Zn(bme\text{-}dach))_3Pt(dien)]^{2+}$, respectively. The formation of higher molecular-weight Zn-Pt clusters of the type $[(Zn(bme\text{-}dach))_nPt]^{2+}$, where n = 2–8, has been observed via ESI-MS when the complexes *cis*-$[Pt(NH_3)_2(guanosine)_2]^{2+}$ or *trans*-$[Pt(py)_2(9\text{-}EtGH)_2]$ were incubated with $[Zn(bme\text{-}dach)]_2$.[37]

The composition of the major species was further explored with CID experiments (VCU) to assess the sites of bridging and cleavage. The MS2 of the peak at 616.2 (Figure II-1, 1b) resulted in the daughter ion at 580.3, consistent with the loss of chloride from $[(Zn(bme\text{-}dach)Cl)(Pt(dien))]^+$. As shown in 1c of Figure II-1, the MS3 fragmentation of the signal at 580.3 then produces two parent ions with m/z 296.3 and 479.1, which may be assigned to the ions $[Pt(dien)]^+$ and $[Zn(bme\text{-}dach)Pt]^+$, respectively. The dominant peak at 616.3 thus corresponds to the very stable heterodinuclear species $[(Zn(bme\text{-}dach)Cl)(Pt(dien))]^+$, indicative of the high affinity of platinum(II) compounds to sulfur.[37]

^{195}Pt NMR Spectroscopic Analysis of Reaction 1: Evidence of a Monothiolate-Bridged Intermediate and Dithiolate-Bridged Product. ESI-mass spectrometry cannot distinguish between the putative structures **II** and **III**. The reactions and nature of the products were further explored by NMR spectroscopy. The ^{195}Pt NMR spectrum of the [Pt(dien)Cl]Cl gave a single peak with a chemical shift at – 2280.8 ppm, as is typical of Pt^{2+} in a N_3Cl donor environment.[61] Upon reaction of 2 equiv of [Pt(dien)Cl]Cl with 1 equiv of $[Zn(bme\text{-}dach)]_2$ (i.e., 1 Pt:1 Zn) over the course

of 30 min at 37 °C, a new ^{195}Pt NMR resonance appeared at – 3172.53 ppm (Figure II-2). This chemical shift is typical of a PtN_3S coordination sphere. Furthermore, after 1 h, an additional resonance was observed at – 3267.95 ppm, which grew in intensity with time. The downfield shift of this singlet in the ^{195}Pt NMR spectrum is consistent with a $[PtN_2S_2]$ species. After 3 h (Figure II-2), this latter signal at – 3267.95 ppm was clearly visible as the major component. After 2 days, the same species as observed in the 3 h spectrum were observed in the solution in a similar ratio, indicating that the reaction had attained equilibrium. The most reasonable assignments for these species are shown in Scheme II-2, and in the case of complex **III**, this assignment was confirmed by X-ray crystallography.

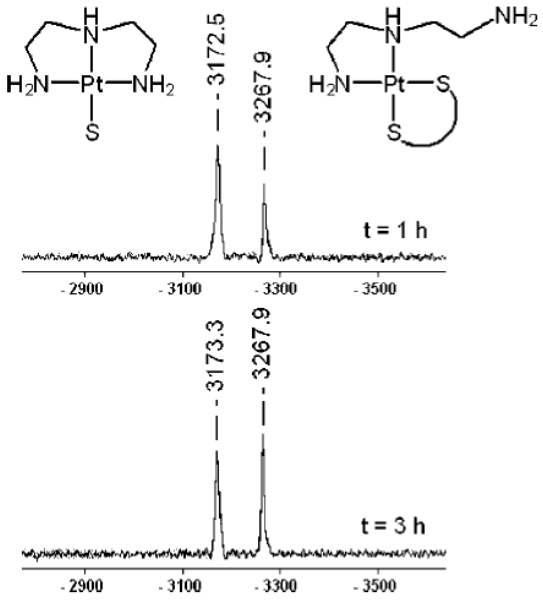

Figure II-2. ^{195}Pt NMR spectra obtained from the reaction between [Pt(dien)Cl]Cl and $[Zn(bme\text{-}dach]_2$ (2 Pt:1 Zn ratio) in MeOH after 1 h (top) and after 3 h (bottom).

After approximately 2 h, a yellowish precipitate appeared, which yielded (after isolation and drying) an elemental analysis corresponding to $[Zn(bme\text{-}dach)Cl]_2Pt$, complex **V** (Scheme II-2). The ^{195}Pt NMR spectrum of this species has a δ(Pt) chemical shift of – 3472.5 ppm, and is likely to be a Pt^{2+} in an S_4 coordination sphere[62] ; again, this structure was confirmed by X-ray crystallography.

Structural Analyses. $[Zn(bme\text{-}dach)]_2$, Complex I, and Pt(bme-dach), Complex IV. The four compounds essential to this study were subjected to X-ray diffraction studies, and the ball and stick drawings of their molecular structures are shown in Figures II-3 to II-9. Figure II-3 shows the $[Zn(bme\text{-}dach)]_2$ dimeric complex used as a zinc finger model in this and previous work to have a penta-coordinate zinc in N_2S_3 coordination. The dimeric partners are related such that one-half of the dimer is the symmetry-generated product of the other. In terms of pseudo-trigonal bipyramidal geometry, the N_2S_2 donor set about Zn(1) produces axial N(2) and S(1) donors with ∠N(2) – Zn – S(1) of 157°, while the equatorial trigonal plane is defined by ∠N(1) – Zn – S(2) = 128.5°, ∠N(1) – Zn – S(1)′ = 113.2°, and ∠S(2) – Zn – S(1)′ = 115.3°. The S(1)′ sulfur donor is bridging between the two partners of the dimer and would thus be in an equatorial site of a pseudo-trigonal bipyramid with respect to Zn(1). The alternate description of a distorted square pyramidal structure is also applicable according to the *tau* value of 0.47, where a value of 0 indicates a perfect square pyramid and a value of 1.00 denotes a trigonal bipyramidal geometry.[63] In this case, the S(1) and S(1)′ are in the apical positions, while the N(1), N(2), S(1), and S(2) are in a very distorted basal plane. Pertinent distance parameters are given in the caption of Figure II-3.

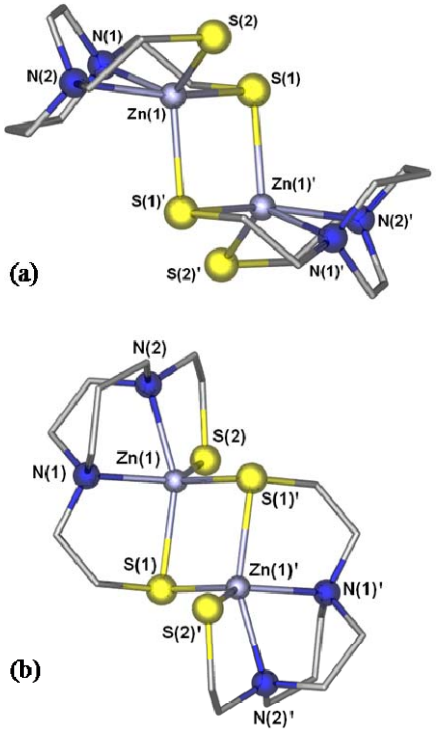

Figure II-3. (a) Ball and stick representation of the molecular structure of Zn(bme-dach)$_2$ emphasizing square pyramidal geometry and (b) an alternate drawing of the coordination sphere emphasizing the trigonal bipyramidal geometry about Zn. Selected bond lengths (Å): Zn(1)-N(1), 2.181(6); Zn(1)-N(2), 2.274(5); Zn(1)-S(1), 2.4960(17); Zn(1)-S(2), 2.3077(17); Zn(1)-S(1)', 2.4170(16); S(1)-Zn(1)', 2.4170(16). Selected bond angles (deg): N(1)-Zn(1)-N(2), 71.94(19); N(1)-Zn(1)-S(2), 128.51(17); N(2)-Zn(1)-S(2), 85.11(13), N(1)-Zn(1)-S(1)', 113.18(18), N(2)-Zn(1)-S(1)', 98.13(13), S(2)-Zn(1)-S(1)', 115.34(7); N(1)-Zn(1)-S(1), 84.83(15); N(2)-Zn(1)-S(1), 156.62(13); S(2)-Zn(1)-S(1), 108.28(6); S(1)'-Zn(1)-S(1), 93.30(6); Zn(1)'-S(1)-Zn(1), 86.70(6).

The Pt(bme-dach) molecular structure shown in Figure II-4 is a highly regular square plane (deviation of Pt^{2+} from the perfect N_2S_2 plane = 0.0003 Å). The difficulty in isolating the yellow crystals of this monomeric PtN_2S_2 compound from the insoluble yellow powder is ascribed to the presence of extended π-stacking interactions as has been seen in linear chain platinum(II) diimine complexes among others.[64-66]

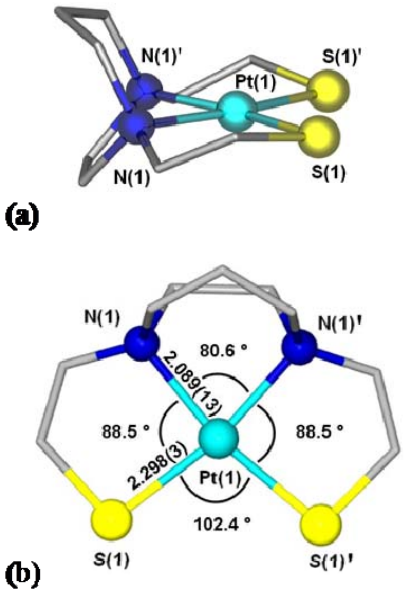

Figure II-4. (a) Ball and stick representation of the Pt(bme-dach) structure and (b) alternate view displaying angles and distances.

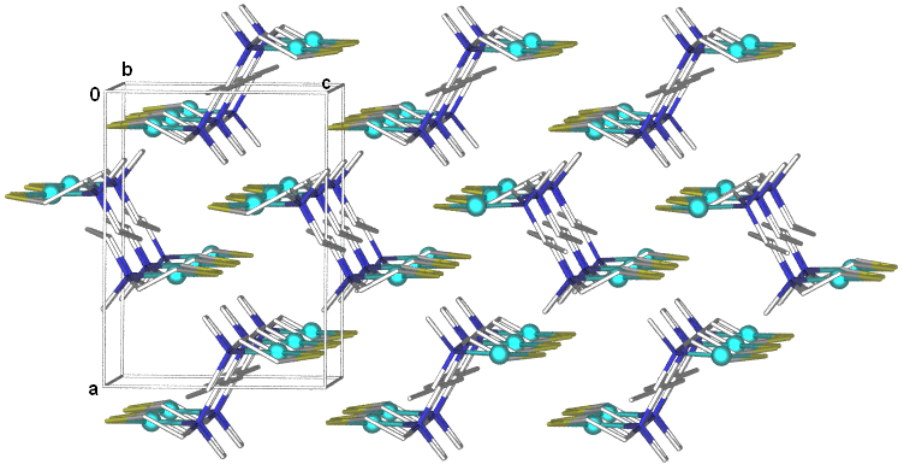

Figure II-5. The packing diagram of Pt(bme-dach), with the unit cell displayed.

Nevertheless, the packing diagram (Figure II-5) for monomeric Pt(bme-dach) shows no such interactions; the closest intermolecular Pt · · · Pt distance is 5.049 Å, while the closest Pt · · · $S_{intermolecular}$ distance is 5.714 Å.

The effect of the large Pt^{2+} ion in the N_2S_2 donor set as contrasted to the analogous Ni(bme-dach) structure is to open the S-M-S angle by approx. 7°; i.e., for M = Ni^{2+} and Pt^{2+}, the values are 95.4° and 102.4°, respectively. A concomitant restriction of the N – Pt – N angle to 80.6° relative to the N – Ni – N angle of 82.5° is then observed.

Structural Analyses. [(Zn(bme-dach)Cl)(Pt(dien))]Cl, Complex III. Figure II-6 displays the molecular structure of the dithiolate bridged [(Zn(bmedach)Cl)(Pt(dien))]Cl, complex **III**. The extended structure of this salt (Figure II-7) finds the chloride counterion, along with H_2O and MeOH solvent molecules, within the unit cell. As seen in Figure II-6, the Zn^{2+} is penta-coordinate, with the bme-dach N_2S_2 ligand forming the base of a square pyramid from which zinc is displaced by 0.863 Å toward a chloride that occupies the apical position of the square pyramid. This unit serves as a metallodithiolate bidentate ligand to platinum(II), which is further coordinated by two of the three nitrogen atoms of the diethylenetriamine ligand in the $Pt(dien)Cl^+$ precursor. The alternate view of Figure II-6 (b) emphasizes the square planarity of the PtN_2S_2 unit (mean deviation within N_2S_2 plane of 0.0116 Å and Pt displacement from that plane of 0.0313 Å). The hinge at the bridging thiolate sulfurs is based on the intersection of the two best planes formed from the N(1)N(2)S(1)S(2) plane (without Zn) and the S(1)S(2)N(3)N(4) plane (without Pt) and calculated to be 107.2°.

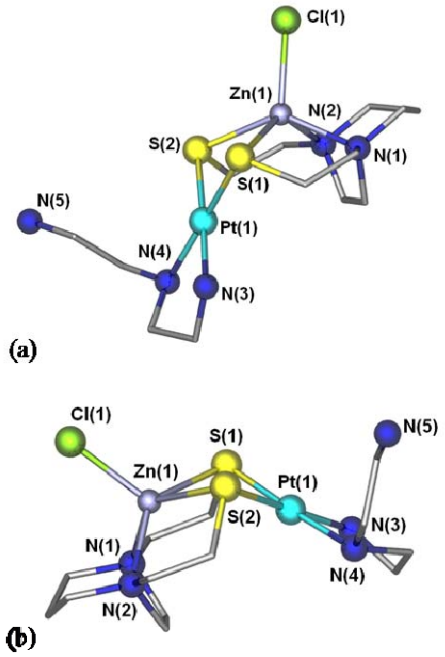

Figure II-6. (a) Ball and stick representation of the molecular structure of [(Zn(bme-dach)Cl)(Pt(dien))]Cl and (b) alternate view emphasizing the hinge angle of the dithiolate bridge.

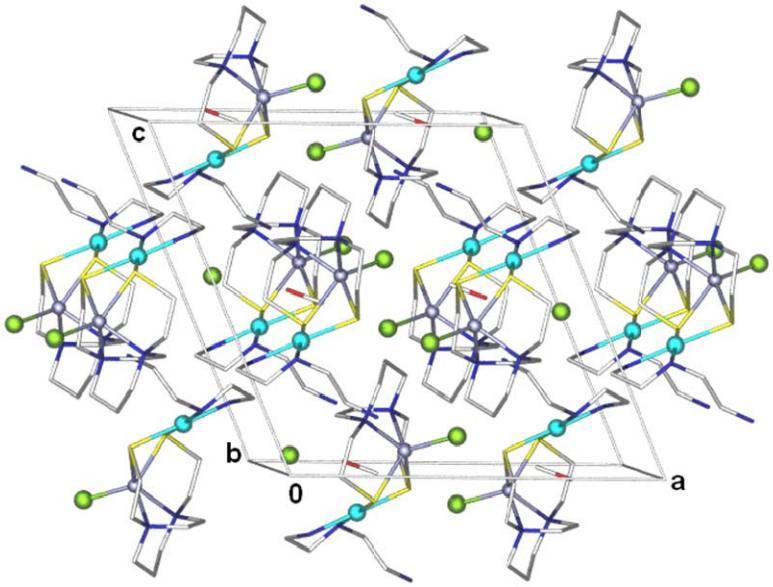

Figure II-7. Packing of [(Zn(bme-dach)Cl)(Pt(dien))]Cl, Complex **III**, displaying Cl^- ions and methanol packed within the unit cell.

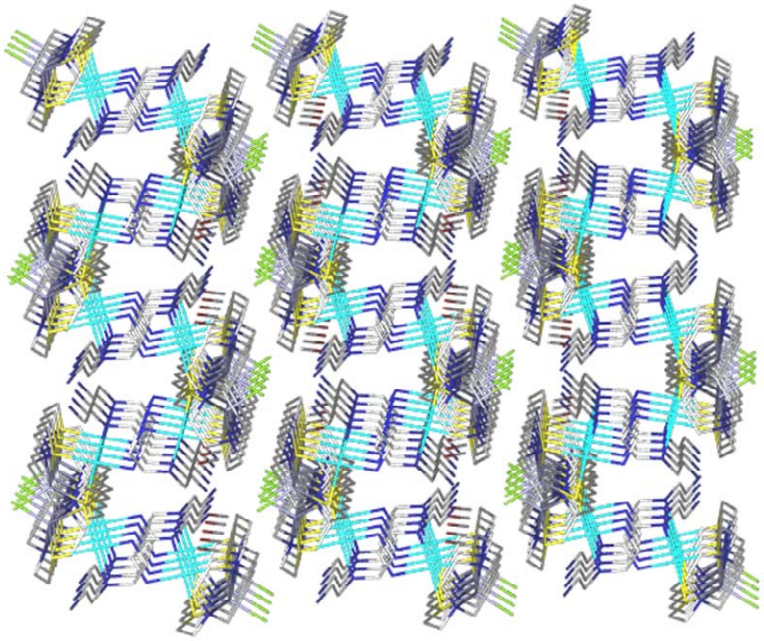

Figure II-8. Packing diagram of [(Zn(bme-dach)Cl)(Pt(dien))]Cl displaying the alternating arrangement of the free amine within the diethylenetriamine ligand.

The unit cell and the packing diagram of complex **III** are given in Figures II-7 and II-8. The dangling amine experiences long-range hydrogen bonding between the amine nitrogen and the hydrogen of methanol. Further hydrogen bonding between a hydrogen of the dangling amine and the Zn-bound chloride generates a dimer of dimers. In turn, the dimer of dimers utilizes the other hydrogen of the dangling amine to engage the free chloride, thus forming a three dimensional structure. Figure II-9 illustrates the dangling amine's hydrogen bonding partners and the dimer of dimers formed through this interaction.

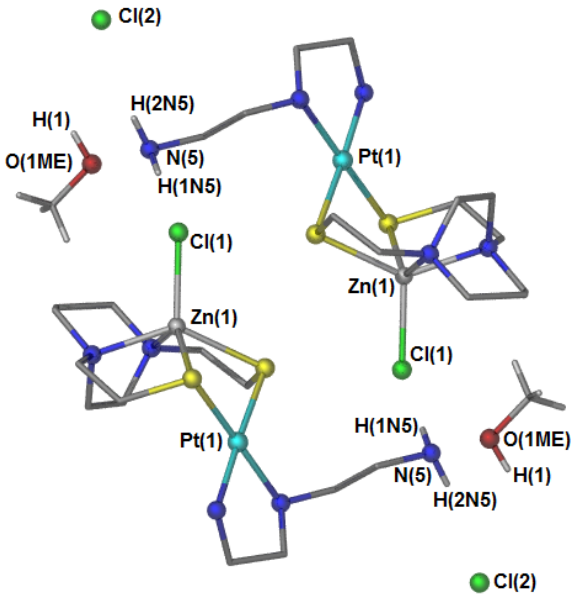

Figure II-9. Two [(Zn(bme-dach)Cl)(Pt(dien))]Cl molecules engaged in hydrogen bonding interactions via the dangling amine (N(5)). Selected distances (Å): H(1N5)-Cl(1), 2.690; H(2N5)-Cl(2), 2.536; N(5)-O(1ME), 2.753; N(5)-H(1), 2.923.

Structural Analyses. $[Zn(bme\text{-}dach)Cl]_2Pt$, Complex V. A trimetallic neutral species in which two $[Zn(bme\text{-}dach)Cl]^-$ units serve as bidentate metallodithiolato ligands to Pt^{2+} is the formulation of complex **V** shown in Figure II-10. This structure is analogous to the slant chair or stair-step complexes seen in such complexes as $[Ni(N_2S_2)]_2M^{2+}$ (M = Ni, Pd, Pt).[67, 68] It differs in that the center of the dithiolate ligand is a $ZnCl^+$ unit with the Zn^{2+} in a square pyramidal geometry, as described above. The metric parameters within the zinc coordination sphere are largely the same as those of complex **III**. These are compared in Table II-1. Similar to the previous Zn-Pt dithiolate-bridged species, the hinge angle formed between the best N(1)N(2)S(1)S(2) plane (without Zn) and the S(1)S(2)S(3)S(4) plane (without Pt) is calculated to be 104.5° and that of the N(3)N(4)S(3)S(4) and S(1)S(2)S(3)S(4) planes is calculated to be 99.0°.

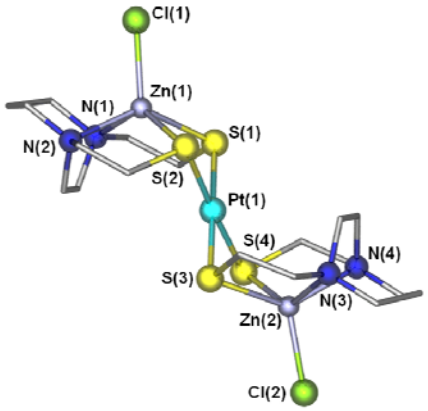

Figure II-10. Ball and stick presentation of the molecular structure of [Zn(bme-dach)Cl]$_2$Pt, Complex **V**.

Table II-1. Selected Bond Lengths (Å) and Bond Angles (°) for [(Zn(bme-dach)Cl)(Pt(dien))]Cl and [Zn(bme-dach)Cl]$_2$Pt.

	[(Zn(bme-dach)Cl)(Pt(dien))]Cl	**[Zn(bme-dach)Cl]$_2$Pt**
Zn(1) – S(1)	2.4567(10)	2.4390(16)
Zn(1) – S(2)	2.4210(10)	2.4159(17)
Zn(1) – N(1)	2.148(3)	2.178(5)
Zn(1) – N(2)	2.167(3)	2.196(5)
Zn(1) – Cl(1)	2.2575(9)	2.2520(17)
Pt(1) – S(1)	2.3078(9)	2.3401(14)
Pt(1) – S(2)	2.3107(9)	2.3407(15)
Zn disp. from N_2S_2 plane	0.8628	0.8755, 0.8668
∠ N(1) – Zn(1) – N(2)	75.1	74.9
∠ S(1) – Zn(1) – S(2)	82.3	82.6
∠ S(1) – Pt(1) – S(2)	88.0	86.4
∠ Cl(1) – Zn(1) – S(1)	115.9	114.5
∠ Cl(1) – Zn(1) – S(2)	114.4	116.6
[a]hinge ∠	107.2	104.5, 99.0

[a]defined in text

ESI-MS Analysis of the Reaction between [Pt(terpy)Cl]Cl and [Zn(bme-dach)]$_2$, Reaction 2: Evidence of Metal Exchange. To examine ligand effects on reactivity, the study was extended to [Pt(terpy)Cl]Cl, a square-planar complex in which the electronic and steric requirements of the rigid tridentate ligand contrasts with those of the diethylenetriamine (dien) chelate. The reactions were similarly designed at both Pt/Zn 1:1 and 2:1 nM stoichiometry and monitored by ESI-MS. Metal-containing species were indicated by matches of appropriate isotopic distributions. The reaction was significantly more complicated than that observed with $[Pt(dien)Cl]^+$. Figure II-11 displays the main species observed in the dissociation and recombination processes for these $[Pt(terpy)Cl]^+$ incubated reactions.

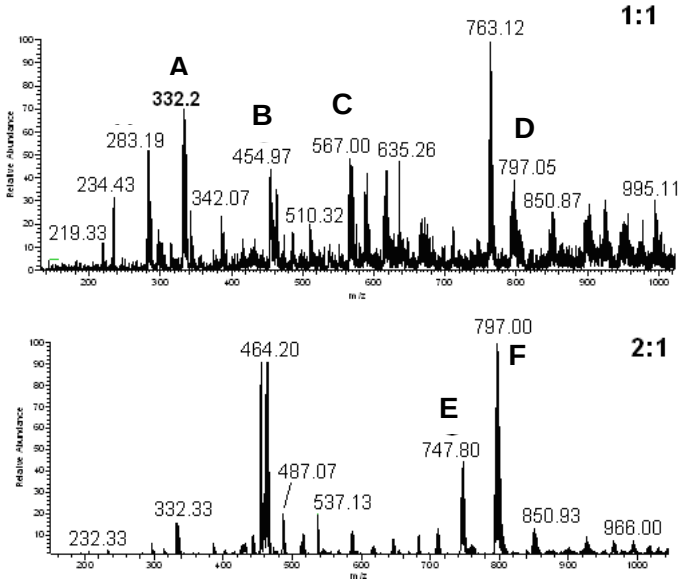

Figure II-11. ESI-MS spectra full scan (positive mode) of MeOH solution containing [Pt(terpy)Cl]Cl and [Zn(bme-dach)]$_2$ in a 1:1 (top) and 2:1 (bottom) molar ratio, after 2 hrs incubation at 37 °C. The 1:1 spectrum displays the formation of both metal exchanged products, $[Zn(terpy)Cl]^+$ (A) and $[Pt(bme\text{-}dach) + K]^+$ (B).

Examination of the first spectrum recorded after 5 min, following mixing of the reagents in a 1:1 Pt/Zn ratio, revealed a series of Zn – Pt species as well as a ligand – scrambling reaction. At this early reaction time, signals corresponding to reactants (species C, $[Zn(bme\text{-}dach)]_2$) and one corresponding to a metal-exchanged product $\{[Zn(terpy)Cl] - H^+\}^+$ (m/z = 335.2) were observed (species A in Figure II-11). Furthermore, the m/z envelope centered at 454.97, species B in Figure II-11, may be reasonably assigned to $[Pt(bme\text{-}dach) + K]^+$, as observed for the directly synthesized complex (see Experimental Details section). The 2:1 Pt/Zn reaction showed a few similar features to the 1:1, and contained the principal multi-metallic aggregate, $\{[(Zn(bme\text{-}dach))_2PtCl]^+ - H^+\}$ (m/z = 797.1, species D on top and F on bottom of Figure II-11). Again, this m/z envelope matched that observed in the ESI-MS analysis of the directly synthesized $[Zn(bme\text{-}dach)Cl]_2Pt$, Complex V (see Experimental Details section). At a Pt/Zn ratio of 2:1, the species corresponding to $\{[Zn(bme\text{-}dach)Pt(terpy)]^+ – H^+\}^+$ (m/z = 747.9, E) was observed. Spectra taken after 6 days also showed these major features to be maintained. In addition, a series of minor signals detected at lower abundance corresponding to Zn and Pt multi-metallic species was observed. In accordance with Jeffery *et al.*,[69] the formation of these adducts containing Zn and Pt is analogous to similar poly-metallic complexes employing transition metal N_2S_2 complexes, including $[Zn(bme\text{-}dach)]_2$, as metallo-dithiolate ligands.[67, 68, 70-72]

Discussion and Conclusions

Small-molecule models for biologically relevant ternary zinc finger/Pt/DNA protein adducts have been characterized using ^{195}Pt NMR spectroscopy and X-ray crystallography. The isolation of the Zn/Pt bi-metallics, **II** and **III**, is a major advance in this area, because, to our knowledge, there are no analogous structures. In fact, the Cambridge Crystallographic Data Centre (CCDC) finds only six crystallographic structures of Zn/Pt hetero-metallic compounds, and those are of multi-metallics with S^{2-} bridges rather than RS^-.[73-77] Scheme II-3 summarizes the reaction pathways in which the Zn/Pt adduct switches from a [PtN_3S] into a [PtN_2S_2] coordination (step 3), the Pt incorporates itself into the Zn model coordination sphere (and vice versa in the terpy case), and both reactions form multi-metallic aggregates. Zinc preservation of cysteine thiolate nucleophilicity renders the sulfur sufficiently reactive toward electrophilic platinum moieties to yield Zn-(μ-SR)-Pt-bridged, multi-metallic, and metal-exchanged species. In this respect, the chemistry is analogous to the formation of homo-dinuclear glutathionate (GS^-)- or cysteinate (Cys^-)- bridged Pt-RS-Pt species upon initial coordination of the thiol to a platinum center.[78-80] The tendency of coordinated Pt-GS species to form monothiolate-bridged dinuclear Pt-(μ-GS)-Pt species has been shown for $[Pt(dien)Cl]^+$, where the presence of only one leaving group in the mono-functional compound facilitated kinetic studies.[78] Crystallographic evidence for di-thiolate bridging *N*-acetylcysteine is seen for the compound [$Pt_2(\mu$-accys-$S)_2(bpy)_2$].[79] Likewise, a bridged species has been identified as the major product from the reaction of [$PtCl_2$(en)] with GSH.[80]

Scheme II-3. Reaction Pathways of the $[Zn(bme\text{-}dach)]_2$ with [Pt(dien)Cl]Cl and [Pt(terpy)Cl]Cl and the Formation of Thiolate-Bridged, Metal-Exchanged, and Multi-metallic Aggregate Species

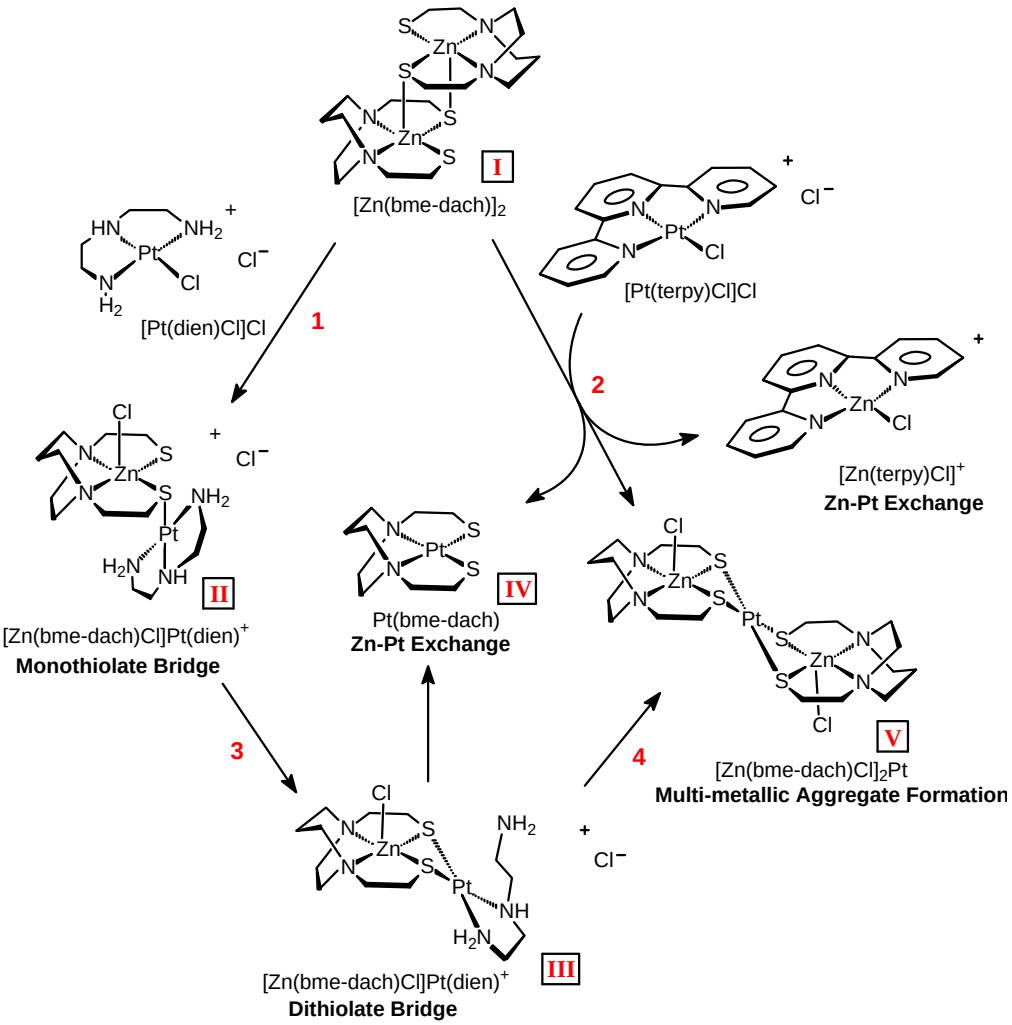

Specifically for $[Pt(dien)Cl]^+$, opening of the chelate ring (step 3) is a reflection of the strong *trans*- influence of cysteinate, even when modified by an interacting Zn^{2+} ion. Likewise, the formation of the tri-metallic aggregate **V** (step 4) may be explained as a consequence of further labilization of the chelate ring under the influence of the di-thiolate bridge in **III**. Note that the Pt-N bond that is broken in the tridentate dien is not

that of the "central" secondary amine, i.e., the one *trans* to Cys^-. While this would lead in principle to an initial formation of a large eight-membered ring, generally considered to be unfavorable, such an "opening" of the dien moiety has been previously reported through a complicated procedure involving reduction of Pt^{4+} to Pt^{2+}.[81] Should this have happened here, a rapid rearrangement to give the favored five-membered ethylenediamine ring must occur. Alternatively, complex **III** may more easily result from direct displacement of the bound terminal amine by the terminal Zn-thiolate sulfur.

In the case of terpyridine, the observed formation of $[Zn(terpy)Cl]^+$ and [Pt(bme-dach)] moieties demonstrates ligand scrambling or metal ion exchange. In contrast, no $[Zn(dien)Cl]^+$ species with concomitant zinc ejection is observed in the diethylenetriamine reaction, reflecting the different steric requirements around the Zn^{2+} ion. Interestingly, Zn^{2+} and Cu^{2+} (as their chloride salts) have been shown to cleave the Pt-S bond of thiolate–Pt–terpyridine to form [Pt(terpy)Cl]. A postulated mechanism involves the formation of a hetero-dinuclear thiolato-bridged species.[82] While these results represent a reaction in the "opposite" direction to that discussed here, nevertheless, the general system Pt(terpy)/thiolate/Cu^{2+}/Zn^{2+} appears quite reactive, supporting the possibility that the reactions reported from the mass spectrometric study can occur in solution. Furthermore, the mass spectrometry results on the $[Pt(dien)Cl]^+$ system also correlated well with the solution behavior. One goal of this project, indeed, was to provide support for the structural interpretation of the MS data, hence the direct synthesis complement.

The hetero-dinuclear thiolate-bridged structures described here may represent reasonable descriptions of intermediates in metal exchange on bio-ligands. The exact nature of the reaction is dependent upon the choice of the ligands in the coordination sphere of platinum. Some or all of these modes of binding may be involved in zinc ejection from zinc fingers by nucleobase compounds, such as *trans*-[PtCl(9-EtGua)$(pyr)_2]^+$ and *[SP-4-2]*-[PtCl(9-EtGua)(NH_3)(quin)]$^+$, or certainly by cisplatin itself.[37, 53] These features may be general. For example, the anti-arthritic gold compound, aurothiomalate, interacts with Cys_2His_2 zinc fingers of TFIIIA and Sp1 with subsequent inhibition of the DNA-binding activity of the protein.[83] Studies using a model peptide based on the third zinc finger of Sp1 confirmed that Au-binding triggered zinc release.[42] Indeed, the course of the reaction will depend upon not only the nature of the coordination sphere around platinum but also that around the zinc. The chemical composition of a zinc finger core, as well as the local protein environment, determine the reactivity of the zinc finger.[84] The groups of Lippard, Parkin, Carrano, etc. have developed structural models of tetrahedral active sites of zinc enzymes that have also proven to be functional in their alkylation reactivity.[5] Lippard utilized $[Zn(SC_6H_5)_4]^{2-}$ as a mimic of the *Escherichia coli* Ada protein, responsible for repair of DNA methylphosphotriesters by methyl transfer through a zinc-activated cysteine nucleophile from a $Zn(Cys)_4$ site.[27, 85, 86] Kinetic studies of this ZnS_4 model and various ZnS_xN_{4-x} species showed that the rate of methylation followed the trend: $[Zn(PhS)_4]^{2-}$ > $[Zn(PhS)_3(MeIm)]^-$ » $[Zn(PhS)_2(MeIm)_2]$. Studies by Darensbourg *et al.* have demonstrated zinc-sulfur methylation of tethered thiolates in the closely related

$[Zn(bme\text{-}daco)]_2$ complex and its Cd analogue.[29] Grapperhaus *et al*. have also investigated the reactivity of a similar monomeric $Zn(N_2S_2)$ complex toward alkylation and oxygenation, in which zinc-bound thiolates were alkylated by MeI and underwent oxygenation and release of Zn^{2+} in the presence of H_2O_2.[30, 31] These studies point to the capability of zinc-bound thiolates to serve as active nucleophiles toward carbon electrophiles. The platination with the $[Pt(dien)Cl]^+$ and $[Pt(terpy)Cl]^+$ moieties described above further strengthens the analogy between alkylation and platination of the Zn-thiolate bond. Whether such chemistry could occur with a platinated purine or pyrimidine moiety is under investigation.

The structures described in this paper also represent viable chemical descriptions for potential ternary Pt-DNA–protein complexes involving zinc fingers and platinated DNA. The labilization of the diethylenetriamine chelate by the $Zn\text{-}RS^-$ group further suggests a possible mode of chemical DNA repair. Glutathione has also been shown to chemically remove mono-functional Pt-DNA adducts.[87, 88] The molecular description of these events implies a labilization of GS-Pt-L axis, where L is a DNA base, usually guanine. The chemistry described here suggests that $Zn\text{-}Cys^-$ could easily replicate the features of the glutathione. Additional studies pursue this interesting possibility.

An additional relevant feature of the present study is the observation of several examples of five-coordinate zinc. The predictive power of bioinorganic chemistry lies to some extent in the use of model chemistry to suggest possible unexpected biological motifs. In this work, the formation of five-coordinate zinc complexes is a prevailing feature of N_2S_2Zn upon the reaction with platinum electrophiles. While it is true that the

nature of the tetradentate N_2S_2 ligand produces some constraints against the tetrahedral geometry, as also evidenced by the axial ligation in the Zn dimer precursor itself, it is provocative to think that zinc fingers may use a four- or five-coordinate "coordination switch" in exercising some of their biological functions. In previous studies, species corresponding to five-coordinate Zn-9-EtGua adducts were observed when the reactions of the C-terminal NCp7 zinc finger peptide from HIV nucleocapsid protein with *trans*-$[PtCl(9\text{-}EtGua)(pyr)_2]^+$ and 9-EtGua itself were followed by ESI-MS.[37] In further agreement, a species corresponding to an adduct analogous to complex **II** has been observed in the reaction of [Pt(dien)Cl]Cl with the same C-terminal zinc finger NCp7 peptide (Farrell, unpublished observations). The lack of a specific coordination number and geometry about zinc evidenced by this work undoubtedly relates to the metal-exchange properties of such biomimetic systems. This is consistent with Vahrenkamp's stated perspective on nature's use of zinc: "the non-properties of zinc are the basis of its success".[8] While these "non-properties" are well-known to coordination chemists, in biological chemistry, the usual view of zinc in zinc finger proteins is of a four-coordinate, tetrahedral complex. In this study, the binding of chloride, that generates a penta-coordinate anionic complex arguably increases the nucleophilicity of the thiolate sulfurs.[27] It is of interest to see if some of the biology exercised by zinc can be attributed to this facet of its coordination chemistry. These and other questions raised here present a rich area of yet to be explored bioinorganic chemistry.

CHAPTER III

SYNTHESIS OF Pd(II) AND Au(III) N_2S_2 COMPLEXES: STRUCTURAL COMPARISONS TO THE Pt(II) AND Ni(II) DERIVATIVES

Introduction

In terms of investigating small molecule models for further insight into Zn protein/Pt/DNA interactions, the expansion of such studies to other transition metal complexes may elucidate the effects of xenobiotic metal ions on ZnN_2S_2 systems. Thus the reactivity of a ZnN_2S_2 model complex, $[Zn(bme\text{-}dach)]_2$ with Pd^{2+} and Au^{3+} compounds has been investigated in pursuit of possible Zn^{2+}/Pd^{2+} and Zn^{2+}/Au^{3+} thiolate-bridged adducts or metal-exchanged products. The use of Pd^{2+} complexes may ensure a greater kinetic reactivity with a ZnN_2S_2 moiety than that of Pt^{2+}, while preserving the coordination number and geometry commonly associated with platinum species. Furthermore, a square planar Pd(II) bis(2-mercaptoethyl)-1,4-diazacyclooctane N_2S_2 complex, Pd(bme-daco), has been characterized and probed for its thiolate reactivity with small molecules.[89-91] The daco derivative contains one more carbon atom in the diazacyclo backbone than the H_2bme-dach (bis(2-mercaptoethyl)-1,4-diazacycloheptane) ligand system which has been used in this study, yielding in the former an additional conformation possibility in the metallo-diazacyclooctane ring. [89-91] The synthesis of the stable Pd(bme-daco) [89-91] and Pt(bme-dach) (Chapter II)[92] complexes demonstrates the likelihood of a Pd^{2+} ion to easily enter into and reside within the bme-dach chelate ligand.

Gold (I) compounds, containing thiolate and phosphine ligands, are commonly used in anti-rheumatic drug therapy.[93, 94] The anti-arthritic gold compound, aurothiomalate, has been discovered to interact with the Cys_2His_2 zinc fingers of TFIIIA and Sp1 transcription factors with subsequent inhibition of the DNA-binding activity of the protein.[95] Studies utilizing a model peptide based on the third zinc finger of Sp1 have confirmed that the binding of gold triggered zinc release. Gold (I) compounds play an important therapeutic role, and their mechanism of action is based on their direct interaction with Cys residues. It is found however that Au^{1+} aqua complexes are often unstable and may disproportionate to form Au^0 and Au^{3+} species.[93] It has been suggested that certain side effects brought about during gold (I) anti-arthritic therapy are due to the formation of Au^{3+} complexes. To explore Au^{3+} reactivity with the [Zn(bme-dach)]$_2$ model, the present work supports the possible products resulting from Zn^{2+}-S-Au^{3+} interactions.

The inspiration for this work stems from our continued collaboration with the N. Farrell research group (VCU) to obtain the directly synthesized products that match metal-exchanged products from Zn^{2+}/Pd^{2+} and Zn^{2+}/Au^{3+} reactions. As in the previous chapter, the collaborators have employed the [Zn-bme-dach]$_2$ dimeric complex as a zinc finger model in reactions with [Pd(L)Cl]Cl and [Au(L)Cl]Cl_2 (where L = terpyridine and diethylenetriamine). The preliminary evidence of the metal exchange and heavy metal thiolate bridged aggregates has been observed by the Farrell group via ESI-MS analysis and MS/MS experiments. Their initial interpretation of ESI-MS results suggest that zinc reacts with both [Pd(terpy)Cl]Cl and [Pd(dien)Cl]Cl to form a [Zn(bme-dach)Cl]$_2$Pd

aggregate. Furthermore, MS/MS experiments on the multi-metallic product obtained from the [Pd(terpy)Cl]Cl reaction indicated the formation of a metal-exchanged Pd(bme-dach) species. The ESI-MS monitored reactions with $[Au(terpy)Cl]Cl_2$ and $[Au(dien)Cl]Cl_2$ found immediate speciation of a monomeric $[Au(bme\text{-}dach)]^+$ *m/z* bundle, suggesting Zn^{2+}/Au^{3+} metal exchange.

As in Chapter II, the Pd(bme-dach) and $[Au(bme\text{-}dach)]BPh_4$ metal-exchanged products were directly synthesized on a large scale for the purpose of complementing the initial ESI-MS findings, and have thus provided solid evidence that the N_2S_2 ligand can hold Pd^{2+} and Au^{3+} within its chelate center. The dithiolate-bridged $[Zn(bme\text{-}dach)Cl]_2Pd$ aggregate was crystallized from the reaction of $[Zn(bme\text{-}dach)]_2$ with [Pd(terpy)Cl]Cl performed by the collaborators, and the single crystal was analyzed via X-ray diffraction at Texas A&M University. The present chapter will primarily focus on the structural characteristics of the new additions to the $M(N_2S_2)$, M(bme-dach), collection and how they compare to the known Pt(II) and Ni(II) analogues. In addition, comparisons of the $[Zn(bme\text{-}dach)Cl]_2Pd$ and $[Zn(bme\text{-}dach)Cl]_2Pt$ (from Chapter II)[92] molecular structures will be reviewed in detail.

Experimental Details

Methods and Materials. All solvents used were reagent grade and were dried and distilled under N_2 using standard techniques. All reagents and reactants were used without further purification. The bis(2-mercaptoethyl)-1,4-diazacycloheptane (H_2bme-

dach) ligand was prepared according to published procedures.[55] All reactions were carried out under inert atmosphere unless otherwise noted.

Physical Measurements. Elemental analyses were performed by Atlantic Microlab, Inc. Norcross, GA, USA. Electrospray ionization mass spectra (ESI-MS) on the directly synthesized Pd(bme-dach) and [Au(bme-dach)]BPh_4 were obtained in the Laboratory for Biological Mass Spectrometry at Texas A&M University.

Direct Synthesis of N, N'–Bis(2-mercaptoethyl)-1,4–diazacycloheptane palladium(II), Pd(bme-dach). This experimental procedure, including crystallization of Pd(bme-dach) product, was executed by Jason A. Denny. Under an inert atmosphere, a solution of NaOMe (0.470 g, 0.870 mmol) in 10 mL of MeOH was added to H_2bme-dach (0.188 g, 0.853 mmol) in 15 mL of MeOH and was stirred for 1.5 hrs at 22 °C. The $PdCl_2$ (0.151 g, 0.852 mmol) was dissolved in a mixture of 7 mL H_2O and 20 mL MeOH, and cannulated into the stirring ligand solution. After 2 d of stirring at 22 °C under an Ar blanket, the black precipitate was removed via filtration and the yellow solution was concentrated *in vacuo* and purified through silica column chromatography (5 cm x 25 cm) with MeOH as the eluent. The air-stable product was collected from the mobile pale yellow band and dried *in vacuo* to yield 0.100 g (0.309 mmol, 36.2 %) of Pd(bme-dach). Large, needle-shaped x-ray quality crystals were acquired by slow N_2 flow over a MeOH solution of product. ESI-Mass Spectrum in MeOH: $[M + H^+]^+$ m/z = 325 ; Elem. Anal. Calcd. (found) for $C_9H_{18}N_2Pd_1S_2$: C, 33.28 (31.98); H, 5.59 (5.29); N, 8.63 (7.57). The elemental analysis confirms the existence of Pd(bme-dach) oxygenated species, as observed previously with the Pd(bme-daco) derivative.[89-91] Calculation of

oxygenated Pd complexes more closely matched the elemental percentages found. Calcd. (found) for $C_9H_{18}N_2Pd_1S_2O_1$: C, 31.72 (31.98); H, 5.32 (5.29); N, 8.22 (7.57); $C_9H_{18}N_2Pd_1S_2O_2$: C, 30.30 (31.98); H, 5.08 (5.29); N, 7.85 (7.57).

Direct Synthesis of N, N'–Bis(2-mercaptoethyl)-1,4–diazacycloheptane gold(III) tetraphenylborate, [Au(bme-dach)]BPh_4. Under Ar, H_2bme-dach (0.096 g, 0.436 mmol) was dissolved in 15 mL MeOH, and KOH (0.050 g, 0.891 mmol) in 15 mL MeOH was slowly added. The solution was vigorously stirred for 1 h at 22°C. $KAuCl_4$ (0.166 g, 0.439 mmol) dissolved in a mixture of 5 mL deionized H_2O and 10 mL MeOH was rapidly added to the stirring ligand solution, immediately forming a cloudy, peach suspension. After 18 h of stirring under an Ar blanket, the white solid was anaerobically filtered to yield a clear, light yellow-orange solution. The solution was reduced in volume and ether added to precipitate a peach colored solid. The isolated solid was washed three times each with MeOH and ether and dried under an Ar flow to yield 0.161 g [Au(bme-dach)]Cl (0.356 mmol, 81.1 % yield).

Counterion Exchange. A solution of $NaBPh_4$ (0.122 g, 0.356 mmol) in 15 mL of MeOH was added to a yellow-orange solution of [Au(bme-dach)]Cl (0.161 g, 0.356 mmol) in 25 mL of MeOH, and allowed to stir at 22 °C for 16 h. The resulting reaction mixture was anaerobically filtered to separate the peach solid from the clear, colorless solution. The solid was redissolved in MeCN, filtered to remove residual NaCl, and ether added to precipitate solid product, [Au(bme-dach)]BPh_4. The solid was washed three times each with MeOH and ether before drying *in vacuo* to yield 0.122 g (0.166 mmol, 37.8 % yield). X-ray quality crystals were obtained by slow evaporation from a

MeCN solution. ESI-Mass Spectrum in MeCN: $[M]^+$ *m/z* = 415; . Elem. Anal. Calcd. (found) for $C_{33}H_{38}Au_1N_2S_2$: C, 54.76 (55.61); H, 5.29 (5.77); N, 3.87 (4.15).

Isolation of [Zn(bme-dach)Cl]$_2$Pd. This reaction and subsequent isolation of the [Zn(bme-dach)Cl]$_2$Pd multi-metallic aggregate was performed by Quiete de Paula (VCU), and crystals were sent to TAMU for X-ray diffraction studies. The [Zn(bme-dach)]$_2$ (0.006 g, 0.010 mmol) was partially dissolved in 10 mL of MeOH and was heated for 10 min at 90° C. The [Pd(terpy)Cl]Cl complex was dissolved in MeOH in accordance with 1Pd:1Zn (0.004 g Pd, 0.010 mmol) and 2Pd:1Zn (0.008 g Pd, 0.020 mmol) ratios. Upon slow addition of the Pd solution to the [Zn(bme-dach)]$_2$ solution, a yellow precipitate appeared immediately. The yellow solid was partially soluble in CH_3CN and $CHCl_3$, and was completely soluble in DMSO. The crystals of the [Zn(bme-dach)Cl]$_2$Pd were obtained by layering of a $CHCl_3$ solution with diethyl ether. Elem. Anal. Calcd. (found) for $C_{18}H_{36}N_4Cl_2S_4Zn_2Pd_1$: C, 29.02 (29.47); H, 4.87 (4.83); N, 7.52 (7.24).

X-ray Structure Analysis (TAMU). The final structural solutions for the three structures presented in this chapter were finalized and prepared for publication by Dr. N. Bhuvanesh, X-ray Diffraction Laboratory at Texas A&M University. Data for [Au(bme-dach)]BPh_4 and [Zn(bme-dach)Cl]$_2$Pd were collected on a Bruker D8 GADDS general-purpose three-circle x-ray diffractometer (Cu Kα radiation, λ = 1.54178 Å) operating at 110 K. The Pd(bme-dach) single crystal data were collected on a Bruker SMART 1000 CCD based diffractometer [56] (Mo Kα radiation, λ = 0.71073 Å), also at 110 K. The structures were solved by direct methods. H atoms were added at idealized positions and

refined with fixed isotropic displacement parameters equal to 1.2 times the isotropic displacement parameters of the atoms to which they were attached. Anisotropic displacement parameters were established for all non-H atoms. The following programs were employed: data collection and cell refinement for [Au(bme-dach)]BPh_4 and [Zn(bme-dach)Cl]$_2$Pd, Bruker FRAMBO, CELL-NOW, and SAINT[96-98]; data collection and cell refinement for Pd(bme-dach), APEX-II[99]; absorption correction, SADABS[100]; structure solution and structure refinement for all structures, SHELXS-97 and SHELXL-97[101]; and molecular graphics and preparation of material for publication, SHELXTL-PLUS, version 6.14[101] . X-seed was used for the final data presentation and structure plots[60]. The crystallographic data reports for the three compounds included in this report are listed in the Appendix.

Results and Discussion

Molecular Structures of Pd(bme-dach) and [Au(bme-dach)]BPh_4. The direct syntheses of Pd(bme-dach) and [Au(bme-dach)]BPh_4 were executed to support the Zn/Pd and Zn/Au adduct-forming and metal-exchange reactions from the aforementioned ESI-MS monitored reactions and MS/MS fragmentations (VCU). X-ray quality crystals were obtained from slow evaporation of a MeOH solution to produce the Pd(bme-dach) crystals, and an MeCN solution to yield the [Au(bme-dach)]BPh_4 crystals. Figure III-1 displays the ball and stick representations of the Pd(bme-dach) (a) and [Au(bme-dach)]$^+$ (c) molecular structures, with selected bond distances and angles denoted within the figure. The Pt(bme-dach) structure (b), previously described in Chapter II, is also

included in Figure III-1 for comparison. The Pd(bme-dach) and $[Au(bme\text{-}dach)]^+$ complexes are highly regular square planes and contain similar metric parameters to that of the Pt(bme-dach) derivative.[92] Reminiscent of the Pt(II) analogue, the Pd(bme-dach) is comprised of a perfect N_2S_2 plane, where one half of the molecule is the symmetry-generated product of the other. Furthermore, the Pd(II) is displaced from the perfect N_2S_2 plane by 0.0176 Å, whereas the Pt(II) resides within the same ligand set with a lesser deviation (0.0003 Å).

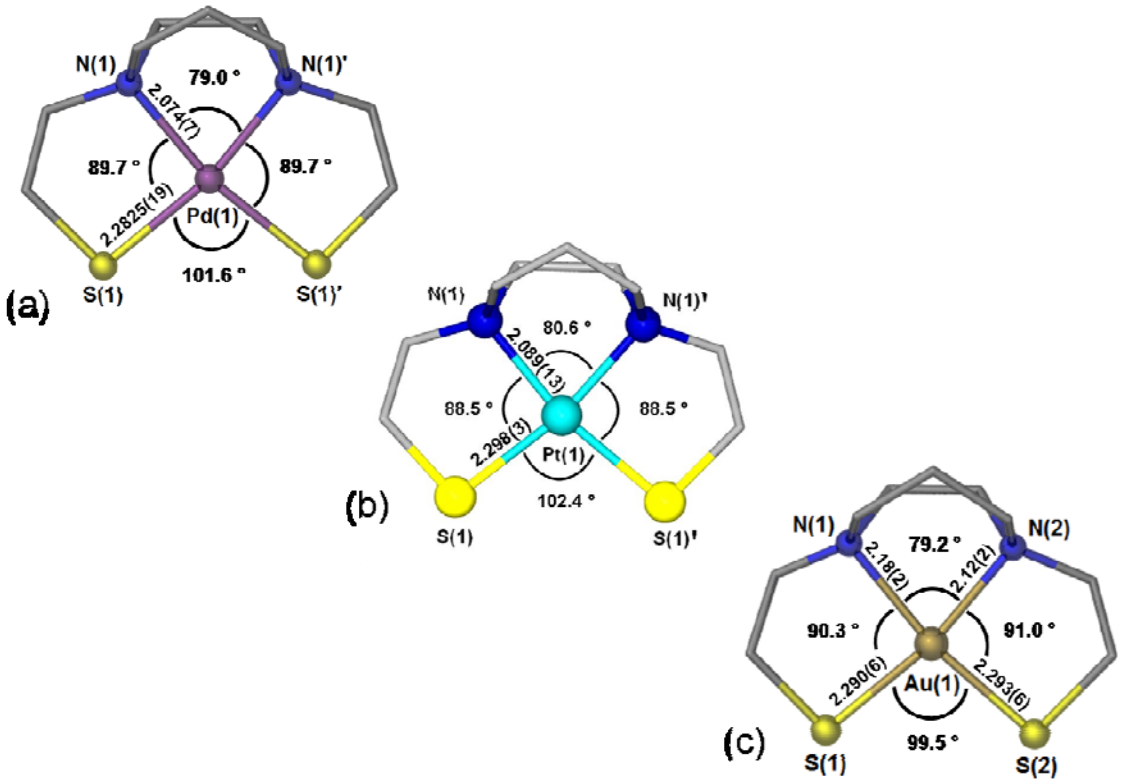

Figure III-1. Ball and stick illustrations of the bird's eye views of: (a) Pd(bme-dach), (b) Pt(bme-dach), and (c) $[Au(bme\text{-}dach)]^+$, with the BPh_4 counterion omitted for clarity.

The crystal packing of the Pd(bme-dach) molecule exhibits disorder of the C(2) atom (and the symmetry-generated C(2)'atom) within the pendant thiolate arms. Figure III-2 displays two views of the Pd(bme-dach) molecule, in which the structural disorder at C(2) is highlighted in red text. Within the series of M(bme-dach) complexes discussed within this chapter, the Pd(bme-dach) is the only structure to experience such disorder within the pendant thiolate arms.

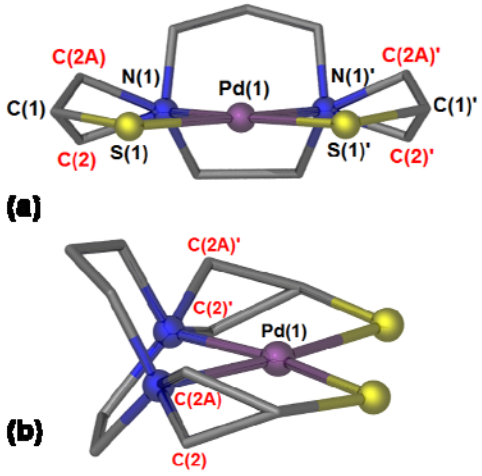

Figure III-2. Ball and stick images of the Pd(bme-dach) structural disorder at C(2) (Occ = 0.69355) and C(2A) (Occ = 0.30645), labeled in red. (a) end-on view and (b) side view.

The $[Au(bme\text{-}dach)]^+$ structure contains an N(1)N(2)S(1)S(2) plane with a mean atom deviation of 0.0228 Å, and the Au(III) shifted only 0.0016 Å outside of this plane. As previously mentioned, the bond distances and angles closely parallel those found within the Pt(bme-dach), displayed in Table III-1 along with comparisons to the Ni(II) analogue.[92, 55] As revealed in Table III-1, the development of the Pd(II) and Au(III)

derivatives adds to the library of existing M(bme-dach) compounds. The Zn/Au metal exchange reported in the ESI-MS monitored reactions by the N. Farrell group rendered the first indication of possible formation of a Au(III) derivative to exist in this bme-dach collection. Thus, the direct synthesis and structural determination of the complex served as solid evidence that Au(III) may securely reside within the N_2S_2 donor set.

Table III-1. Comparison of Selected Bond Angles and Distances Within M(bme-dach) Structures, Where M = Ni(II), Pd(II), Pt(II), and Au(III).

[M(bme-dach)], M =	Ni(bme-dach)	Pd(bme-dach)	Pt(bme-dach)	[Au(bme-dach)]$^+$
M – N (Å)	1.940(4)	2.074(7)	2.089(13)	2.18(2), 2.12(2)
M – S (Å)	2.164(1)	2.283(2)	2.298(3)	2.290(6), 2.293(6)
∠ N – M – N (°)	82.5(2)	79.0(4)	80.6(8)	79.2(8)
∠ S – M – S (°)	95.4(1)	101.7(1)	102.4(2)	99.5(2)
M displacement from N_2S_2 plane (Å)	n/a	0.0176	0.0003	0.0016
Pendant thiolate arm confirmation	Eclipsed	Eclipsed	Eclipsed	Eclipsed

As expected, the M – N and M – S bond distances lengthen as the central metal ion descends from a first to second to third row transition metal. In terms of the ∠ N – M – N and ∠ S – M – S, both the size of the central metal ion and the flexibility of the ligand play a role in the angles ultimately observed. With regard to the metal ion, as the size increases, the ∠ S – M – S normally increases within this tetradentate ligand set. Such an "opening" of the ∠ S – M – S is associated with a concurrent "pinching" or decrease in the ∠ N – M – N. This trend is observed between the Ni(II), Pd(II), and

Pt(II) complexes. The Au(III) complex, however, does not continue to show an increase in ∠ S – M – S with a corresponding decrease in ∠ N – M – N. Although it is a third row transition metal, the higher oxidation state and thus decrease in ionic radii may contribute to angles being more comparable to those found within the Pd(II) complex.

Structural Analysis of the [Zn(bme-dach)Cl]$_2$Pd Complex. The [Zn(bme-dach)Cl]$_2$Pd tri-metallic aggregate was isolated by the N. Farrell research group as a yellow solid that readily precipitated out of the reactions of [Zn(bme-dach)]$_2$ and [Pd(terpy)Cl]Cl. In compliance with the Zn/Pt tri-metallic product reported in Chapter II,[92] this Pd analogue was confirmed by elemental analysis and x-ray diffraction of a single crystal. The ball and stick representation of the molecular structure, Figure III-3(a), illustrates the Zn_2Pd stair-step product resulting from the 2Pd:1Zn reaction. The molecular structure of [Zn(bme-dach)Cl]$_2$Pd displays each zinc center coordinated to two sulfurs, two nitrogens and an apical chloride in a penta-coordinate geometry. The N_2S_2 atoms (without Zn) form a plane with a mean atom deviation of 0.0120Å.

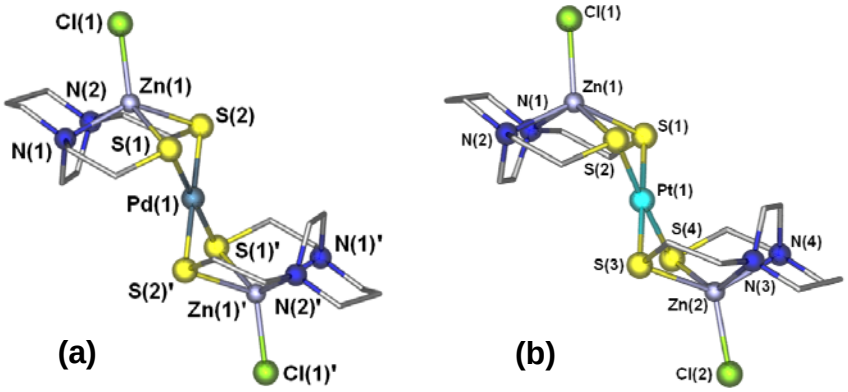

Figure III-3. The molecular structure representations of: (a) $[Zn(bme\text{-}dach)Cl]_2Pd$ and (b) $[Zn(bme\text{-}dach)Cl]_2Pt$ tri-metallic aggregates.

An interesting feature of this structure is the distance at which the zinc center is raised above the N_2S_2 plane towards the apical chloride by 0.8707 Å. The palladium forms a perfectly square planar bridge between the two sulfurs from each $Zn(N_2S_2Cl)$ moiety, with the Pd atom acting as the center of symmetry. The hinge angle of the stair-step structure, represented by the angle formed between the N(1)N(2)S(1)S(2) best plane and the S(1)S(2)S(1)'S(2)' plane, is 81.9°. The Pt(II) derivative (Figure III-3(b)), presented in Chapter II, contains Pt(II) as the bridging metal ion between the two $Zn(N_2S_2Cl)$ moieties and has very similar metric parameters to the Pd(II) trimetallic complex (Figure III-3(a)). Each of the Zn centers within the Pt(II) tri-metallic is held above their respective N_2S_2 planes by 0.8755 and 0.8668 Å. The $[Zn(bme\text{-}dach)Cl]_2Pd$ complex is not as symmetrical as the $[Zn(bme\text{-}dach)Cl]_2Pt$ structure; it does not possess half of its molecule as a symmetrically-generated duplicate of the other half. The Pt(II) derivative contains hinge angles, as previously defined, of 104.5° and 99.0°. Table III-2 below lists pertinent bond distances and angles for the Pd and Pt trimetallic complexes.

Table III-2. Selected Bond Lengths (Å) and Bond Angles (°) for $[Zn(bme\text{-}dach)Cl]_2Pd$ and $[Zn(bme\text{-}dach)Cl]_2Pt$.

	$[Zn(bme\text{-}dach)Cl]_2Pd$	**$[Zn(bme\text{-}dach)Cl]_2Pt$**
Zn(1) – S(1)	2.4373(9)	2.4390(16)
Zn(1) – S(2)	2.4219(9)	2.4159(17)
Zn(1) – N(1)	2.157(2)	2.178(5)
Zn(1) – N(2)	2.185(2)	2.196(5)
Zn(1) – Cl(1)	2.2415(9)	2.2520(17)
Pd(1) – S(1) / Pt(1) – S(1)	2.3510(8)	2.3401(14)
Pd(1) – S(2) / Pt(1) – S(2)	2.3543(8)	2.3407(15)
Zn disp. from N_2S_2 plane	0.8707	0.8755, 0.8668
∠ N(1) – Zn(1) – N(2)	74.8	74.9
∠ S(1) – Zn(1) – S(2)	83.0	82.6
∠ S(1) – Pd / Pt (1) – S(2)	86.3	86.4
∠ Cl(1) – Zn(1) – S(1)	116.1	114.5
∠ Cl(1) – Zn(1) – S(2)	116.7	116.6
[a]hinge ∠	81.9	104.5, 99.0

[a]defined in text

Comments and Conclusions

Within the present work and previous collaborative efforts, the interactions of $[Zn(bme\text{-}dach)]_2$ with Pt(II), Pd(II), and Au(III) complexes have amply demonstrated the capability of such species to form stable thiolate-bridged heteronuclear aggregates as well as metal-exchanged products. The corresponding direct synthesis of products has verified the occurrence of metal exchange between such biomimetic compounds. The large scale synthesis and structural determination of the monomeric Pd(bme-dach) and $[Au(bme\text{-}dach)]BPh_4$ complexes has added to the collection of well-studied $M(N_2S_2)$ structures, and has also supported the initial ESI-MS and MS/MS findings.

The molecular structure of the isolated Zn/Pd trimetallic product confirms the reactivity of the Zn-bound thiolates to form stable bridges to Pd(II), while retaining the Zn-S bond. This Zn-(μ-SR)$_2$-Pd complex may be relevant to possible adduct formation between heavy metal compounds and zinc finger proteins. Interestingly, the collaborator's ESI-MS results for the Zn/Pd model systems did not indicate formation of any dinuclear thiolate bridged Zn/Pd adducts, as observed in the Zn/Pt reactions to form [(Zn(bme-dach)Cl)(Pt(dien))]Cl, discussed in Chapter II.[92] The faster rate of reactivity expected for Pd(II) over Pt(II) may be the reason for the lack of observed Zn(μ-SR)Pd dinuclear species. Thus, the only thiolate bridged adduct observed is that in which the Pd(II) has lost its terpyridine or dien chelate and directly mediates between two [ZnN_2S_2Cl] moieties. Each of the products obtained from these model studies may provide new insight into the possible bonding arrangements and interactions amongst the Zn-S sites with exogenous heavy metal ions.

CHAPTER IV

THE DEVELOPMENT OF PENTA–COORDINATE ZINC MONO– AND DI–THIOLATES AS METALLO–S– DONOR LIGANDS: FORMATION OF A Zn-W COORDINATION POLYMER*

The synthesis and isolation of mono- and di-thiolate bridged Zn-(μ-SR)$_n$-W(CO)$_m$ (where n = 1, m = 5; n = 2, m = 4) species from the dimeric N, N'–bis(2-mercaptoethyl)-1,4–diazacycloheptanezinc(II), [Zn-1']$_2$, and the monomeric (N-(3-Thiabutyl)-N'-(3-thiapentaneoate)-1,4-diazacycloheptane)zinc(II), **Zn-1'-Ac**, are described. Upon cleavage of the dimeric [Zn-1']$_2$ with $Na^+[ICH_2CO_2]^-$, the resulting **Zn-1'-Ac** product is isolated as a monomeric, five-coordinate Zn(N_2SS'O) complex equipped with one available Zn-bound thiolate for further reactivity. Cleavage of [Zn-1']$_2$ with $[Et_4N]^+Cl^-$ afforded a monomeric intermediate, [Zn-1'-Cl]$^-$, containing two Zn-bound thiolates. The Zn mono- and dithiolato complexes demonstrated reactivity towards labile-ligand tungsten carbonyl species, (THF)W(CO)$_5$ and (pip)$_2$W(CO)$_4$, to yield, respectively, **[(Zn-1'-Ac)W(CO)$_5$]$_x$** and **[(Zn-1'-Cl)W(CO)$_4$]$^-$** complexes that were isolated and characterized spectroscopically and via X-ray diffraction. Upon binding to W(CO)$_5$, the five-coordinate Zn(N_2S_2O) complex becomes six-coordinate within the coordination polymer **[(Zn-1'-Ac)W(CO)$_5$]$_x$**, in which the acetate tether of

---

*Reproduced with permission from: "The Development of Penta-Coordinate Zinc Mono- and Di-Thiolates as Metallo-S-Donor Ligands: Formation of a Zn-W Coordination Polymer" Almaraz, E.; Foley, W. S.; Denny, J. A.; Reibenspies, J. H.; Darensbourg, M. Y. *Inorg. Chem.*, accepted.

each molecule provides an O- donor to occupy the octahedral axial position of each neighboring moiety. The **[(Zn- 1'-Cl)W(CO)$_4$]$^-$** dithiolate bridged complex maintains a five-coordinate, square pyramidal [Zn(N_2S_2Cl)]$^-$ center, utilizing a chloride as the apical donor and resulting in an overall anionic complex. The addition of $CO_{(g)}$ to the **[(Zn-1'-Cl)W(CO)$_4$]$^-$** complex was monitored by IR spectroscopy, which showed the emergence of [(Zn-1'-Cl)W(CO)$_5$]$^-$.

Introduction

Zinc(II), a ubiquitous ion that is essential for all life forms, has established its importance in biology through both structural and catalytic purposes.[2, 40] As a borderline hard/soft metal ion with no strong geometrical preferences, N-, S-, and O- donor sets are commonly observed in biological systems.[102, 103] Zinc-thiolate reactivity, such as cysteine S-alkylation, plays a significant role in the function of proteins such as cobalamin-independent and cobalamin-dependent methionine synthase, farnesyl transferase, and the Ada repair protein.[104-106] The exploration of Zn-thiolates encompasses a wide range of synthetic models which seek to elucidate the reactivity of such spectroscopically silent species. There is an established library of known synthetic models for these sites, especially for the Zn site within the *E. coli* Ada protein, which is responsible for repair of DNA alkyl phosphotriester lesions through alkyl group transfer to the S- of a Zn-bound thiolate. Small molecule analogs, such as [Zn(SC_6H_5)$_4$]$^{2-}$ and zinc tripodal complexes, have been examined for their SR$^-$ reactivity via alkylation studies.[5, 8, 27] Other Zn-containing models have developed tetradentate N_2S_2 ligands that

position Zn in a secure square pyramidal or distorted tetrahedral environment for investigations on reactivity of their Zn-S sites.[29-31]

The pre-organization of multi-dentate N_2S_2 ligands, as implemented in the present study, maintains the structural integrity of the coordination complex and allows for modification of the terminal thiolate S-atoms by metallation or oxygenation while remaining Zn-bound. Certain metalloenzyme active sites containing cysteinyl thiolates are known to be post-translationally modified by oxygenation (Nitrile Hydratase) or metallation (Acetyl coA Synthase).[107, 108] While post-translational modifications have not yet been discovered for biomolecules containing Zn-thiolates, S-metallation has been proposed to be involved in ternary complexes of Zn-finger proteins and platinum-bound DNA.[37] Explorations of the possible molecular interactions have employed the $[Zn\text{-}1']_2$ as a biomimetic for cysteine-rich Zn-finger sites and $[Pt(N_3Cl)]^+$ complexes as models of Pt-bound DNA to yield discrete complexes containing Zn(μ-SR)Pt bridges, along with Zn/Pt metal exchanged products.[53, 92] These investigations have been based on the notion that modification of the Zn-S sites, whether by alkylation, oxidation or metallation, may disrupt the overall structure of the Zn-proteins, thus altering and/or inhibiting their critical biological functions.[19] Furthermore, this hindering of Zn-protein structure and function by chemical modification has led to drug targeting of such metalloproteins in cancer and HIV treatment.[109-112]

Figure IV-1 (a) and (b) display the mono- and di-thiolate bridged Zn-(μ-SR)-Pt products that resulted from the reaction of $[Zn\text{-}1']_2$ and [Pt(dien)Cl]Cl at 22 °C. Through ^{195}Pt NMR spectroscopy, 1(a) and 1(b) were observed to exist in equilibrium in

the reaction solution (MeOH), yet the di-thiolate bridged species (b) was the sole product detected from X-ray diffraction on a single crystal of the product solution.[92] To

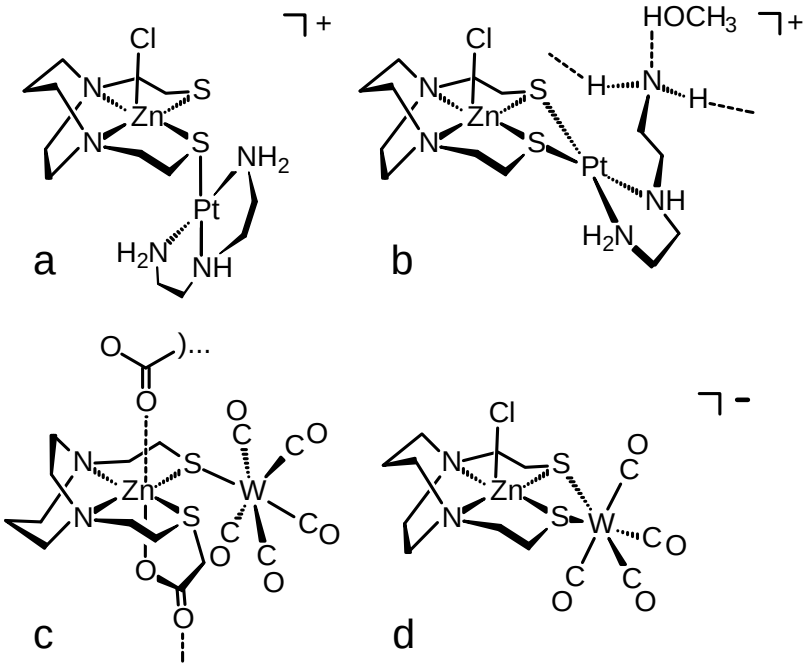

Figure IV-1. Zn-Pt and Zn-W mono- and di-thiolate bridged complexes. (a) [(Zn(bme-dach)Cl)(Pt(dien))]$^{+}$ mono-thiolate bridged adduct, supported by ^{195}Pt NMR spectroscopy, (b) [(Zn(bme-dach)Cl)(Pt(dien))]$^{+}$ di-thiolate bridged adduct with dangling amine stabilized by a network of hydrogen bonding, confirmed by ^{195}Pt NMR spectroscopy and X-ray crystallography, (c) **(Zn-1'-Ac)W(CO)$_5$** mono-thiolate bridged unit within a coordination polymer, and (d) **[(Zn-1'-Cl)W(CO)$_4$]**$^{-}$ di-thiolate bridged complex.

our knowledge, this Zn-(μ-SR)-Pt-bridged species, [(Zn(bme-dach)Cl)(Pt(dien))]Cl, has been the first structurally isolated Zn-Pt bimetallic thiolate-bridged model that demonstrates the interaction between Zn-bound thiolates and Pt^{2+}.

To provide a broader base of Zn(μ-SR)M interaction possibilities and to further the understanding of Zn-thiolates as S-donor ligands to heavy metals, the present study

(1) implements similar Zn-S complexes and S-modified derivatives; (2) employs an exogenous heavy metal, tungsten, that is not likely to replace zinc within the ligand chelate; and (3) incorporates carbonyl ligands about the tungsten to allow for IR spectral reporting via ν(CO) stretching frequencies. Figure IV-1 (c) and (d) show the mono- and di-thiolate bridged Zn-W complexes to be discussed within the present paper. To target and isolate a mono-thiolate bridged complex (c), the cleaved product of $[Zn\text{-}1']_2$ and $Na^+[ICH_2CO_2]^-$, the $Zn(N_2SS'O)$ complex (where S = thiolate and S' = thioether), was used as the metallo-ligand for bridging to the tungsten carbonyl moiety via one thiolate. Herein, the synthesis, characterization, and spectral and structural properties of the $Zn(N_2SS'O)$, or **Zn-1'-Ac**, and $Zn\text{-}(\mu\text{-}SR)_n\text{-}W(CO)_m$ (where n = 1, m = 5; n = 2, m = 4) adducts will be described in detail.

Experimental Details

Methods and Materials. All solvents used were reagent grade and were dried and distilled under N_2 using standard techniques. The N, N'–bis(2-mercaptoethyl)-1,4–diazacycloheptanezinc(II) dimer [92] (Chapter II Experimental Details section) and *cis*-$(pip)_2W(CO)_4$ (pip = piperidine)[113] were prepared according to published procedures. All reactions were carried out under inert atmosphere unless otherwise noted.

Physical Measurements. Elemental analyses were performed by Canadian Microanalytical Services, Ltd., Delta, British Columbia, Canada (**(Zn-1'-Ac)W(CO)$_5$**) and Atlantic Microlab, Inc. Norcross, GA, USA. Electrospray ionization mass spectra (ESI-MS) were obtained in the Laboratory for Biological Mass Spectrometry at Texas

A&M University. Infrared spectra were recorded on a Bruker Tensor 37 Fourier Transform – IR spectrometer, using a CaF_2 cell with 0.1 mm path length for solution analysis and an Attenuated Total Reflectance (ATR) attachment equipped with a ZnSe crystal for solid sample analysis. Photolysis experiments were performed using a Newport Oriel Apex Illuminator 100W Hg UV lamp. Thermogravimetric Analysis (TGA) was performed on an Instrument Specialists Inc. TGA 1000 Thermogravimetric Analyzer, and monitored over a range of 22 – 300 °C at 1 °C increase per min.

Synthesis of (N-(3-Thiabutyl)-N'-(3-thiapentaneoate)-1,4-diazacycloheptane) zinc(II), Zn(tbtp-dach), Zn-1'-Ac. A portion of $[Zn\text{-}1']_2$ (0.171 g, 0.301 mmol) was placed in a degassed 500 mL Schlenk flask equipped with a reflux condenser, followed by addition of 200 mL CH_3OH. As the suspension was stirred at room temperature, a solution of $Na^+[ICH_2CO_2]^-$ (0.134 g, 0.644 mmol) dissolved in 25 mL of CH_3OH was added via cannula. The reaction mixture was refluxed in an oil bath held at 80 °C overnight under N_2. After cooling to 22 °C, the solution was filtered to remove solids and the filtrate was placed in a rotary evaporator for solvent removal. The resulting white solid was purified by silica gel chromatography column (5 cm x 20 cm) with CH_3OH as the eluent to remove NaI. The product was dried to yield 0.172 g (0.504 mmol, 83.6 %) and recrystallized by vapor diffusion of diethyl ether into a CH_3OH solution. ESI-mass spectrum: $[M + Na]^+$ *m/z* = 363. IR (in CH_3CN, cm^{-1}): 1636 (s, br), 1445 (vs), 1420 (shoulder), 1375 (vs, sharp). Elem. Anal. Calcd. (found) for $C_{11}H_{20}N_2S_2O_2Zn_1$: C, 38.65 (38.56); H, 5.90 (6.04); N, 8.20 (7.86). m. p.: 126-127 °C.

Synthesis of N,N'-Bis(2-mercaptoethyl)-1,4-diazacycloheptanezinc(II)acetate tungsten pentacarbonyl coordination polymer, $[(Zn\text{-}1'\text{-}Ac)W(CO)_5]_x$. A suspension of $W(CO)_6$ (0.074 g, 0.211 mmol) in 65 mL of THF was photolyzed for 2 h under an Ar flow to produce a clear, golden solution of $(THF)W(CO)_5$ (2075 (vw), 1930 (s), 1891(w) cm^{-1}). The solution was transferred by cannula to a stirring suspension of **Zn-1'-Ac** (0.072 g, 0.211 mmol) in 5 mL of THF. The mixture was allowed to stir for 3.5 h at 22 °C, and the reaction was monitored via IR spectroscopy. The resulting clear, bright-yellow solution, with ν(CO) IR bands as listed below, was filtered anaerobically. Hexanes were added to the filtrate to precipitate a yellow powder. The flask was placed in the freezer (- 20 °C) to assist in further precipitation of product. The solid was isolated via anaerobic filtration, washed three times with hexane, and dried under an Ar flow to yield 0.040 g (0.061 mmol, 28.8 %). The product was re-dissolved in THF and layered with hexanes to yield yellow X-ray quality crystals. IR (in THF, cm^{-1}): acetate, 1653 (s, br), 1460 (vs, sharp), 1365 (m); ν(CO), 2065(vw), 1925(s), 1888(w). (in DMF, cm^{-1}): ν(CO), 2065(vw), 1921(s), 1871(w). (in solid state, cm^{-1}): acetate, 1592 (s), 1462 (m, sharp), 1365 (m); ν(CO), 2059(vw), 1910(s), 1867(w), 1807 (shoulder). m.p. / decomposition range: 240 °C - 280 °C. Elem. Anal.: Samples from two preparations both showed better matches with CO loss as displayed below in Table IV-1.

Table IV-1. Elemental Analyses of **$[(Zn\text{-}1'\text{-}Ac)W(CO)_5]_x$**.

Calculated				Found	
$C_{16}H_{20}N_2S_2O_7W_1Zn_1$	– CO	– 2 CO		Sample **1**	Sample **2**
C	28.87	28.25	27.58	27.88	27.40
H	3.03	3.16	3.31	3.57	3.15
N	4.21	4.39	4.59	4.74	3.95

Thermogravimetric analysis of the **$[(Zn\text{-}1'\text{-}Ac)W(CO)_5]_x$** solid indicated 4.6 % weight loss at 42 – 140 °C (loss of one CO ligand = 4.2 % mass). Above 140 °C, the thermal decomposition curve displays a steady decrease in mass with no stability plateaus.

Synthesis of [Tetraethyl ammonium][N,N'-Bis-2-mercaptoethyl-N,N'-diazacycloheptane]zinc(II)chloro tungsten tetracarbonyl, $[Et_4N][(Zn\text{-}1'\text{-}Cl)W(CO)_4]$. The synthesis of the **$[Et_4N][(Zn\text{-}1'\text{-}Cl)W(CO)_4]$** powder was performed by William S. Foley. In a 100 mL Schlenk flask, a sample of $[Zn\text{-}1']_2$ (0.154 g, 0.271 mmol) and Et_4NCl (0.101 g, 0.610 mmol) were degassed prior to addition of 25 mL of dry CH_2Cl_2. The cloudy suspension was stirred for 10 min, upon which time it became clear and colorless. A solution of *cis*-$(pip)_2W(CO)_4$ (0.265 g, 0.570 mmol) in 35 mL CH_2Cl_2 was slowly cannulated into the stirring Zn solution. After 3 h, the solution was filtered anaerobically and hexanes were added to the filtrate to precipitate a yellow powder. The yellow product was isolated via anaerobic filtration, washed twice with benzene, and dried under an N_2 flow to yield 0.298g (0.399 mmol, 73.7%). The product was dissolved in CH_2Cl_2 and layered with hexanes to yield yellow X-ray quality crystals. ν(CO) IR (in DMF, cm^{-1}): 1988 (w), 1861 (s), 1836 (m), 1801 (m); (in CH_2Cl_2, cm^{-1}):

1990 (w), 1863 (s), 1845 (m), 1800 (m). Elem. Anal. Calcd. (found) for $C_{21}H_{38}N_3S_2Cl_1W_1Zn_1$: C, 33.84 (33.04); H, 5.14 (5.38); N, 5.64 (5.44). decomposition range: 70 – 115 °C color change to brown; 215 °C color change to black.

X-ray Structure Analysis. The final structural solutions for the three structures presented in this chapter were finalized and prepared for publication by Dr. J. H. Reibenspies, X-ray Diffraction Laboratory at Texas A&M University. Low-temperature (110 K) X-ray diffraction data were collected on a Bruker SMART 1000 CCD based diffractometer (Mo Kα radiation, λ = 0.71073 Å) for **Zn-1'-Ac**.[56] The data for **[Et$_4$N][(Zn-1'-Cl)W(CO)$_4$]** were collected on the Bruker-AXS APEX-II CCD three-circle X-ray diffractometer under the same conditions. For the **[(Zn-1'-Ac)W(CO)$_5$]$_x$** crystal, data were obtained on a Bruker D8 GADDS/MWPC three-circle X-ray diffractometer (Cu Kα radiation, λ = 1.54184 Å), also operating at 110 K. The structures were solved by direct methods. H atoms were added at idealized positions and refined with fixed isotropic displacement parameters equal to 1.2 times the isotropic displacement parameters of the atoms to which they were attached. Anisotropic displacement parameters were determined for all non-H atoms. The programs utilized were as follows: data collection and cell refinement for **Zn-1'-Ac**, *SHELXTL*[101]; data collection and cell refinement for **[Et$_4$N][(Zn-1'-Cl)W(CO)$_4$] ,** *APEX-II*[99]; data collection and cell refinement for **[(Zn-1'-Ac)W(CO)$_5$]$_x$**, Bruker *FRAMBO*[96]; data reduction, *SAINT* [98]; absorption correction, *SADABS* [100]; structure solution and structure refinement for all structures, *SHELXS-97* and *SHELXL-97*[101]; and molecular graphics and preparation of material for publication, *SHELXTL-PLUS*, version 6.14 [101] . The final

data presentation and structure plots were performed using X-Seed.[60] Cambridge Crystallographic Data Centre (CCDC) 718636, 718637, and 718638 contain the supplementary crystallographic data for this report. These data can be obtained free of charge via www.ccdc.cam.ac.uk/data_request/cif, by e-mailing, or by contacting The Cambridge Crystallographic Data Centre, 12, Union Road, Cambridge CB2 1EZ, U.K.; fax, +44-1223-336033. Additionally, the crystallographic data for the three compounds included in this chapter are listed in the Appendix.

Results and Discussion

Scheme IV-1. Synthesis and Products

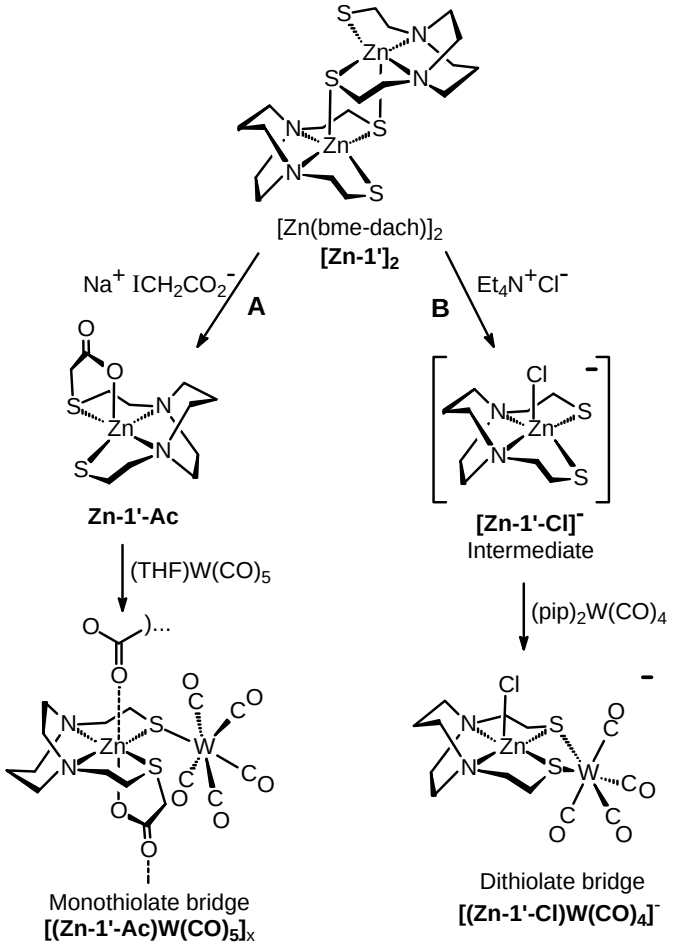

Scheme IV-1 displays the synthetic approach to monomeric zinc thiolates derived from the dimeric precursor $[Zn\text{-}1']_2$. As the $[Zn\text{-}1']_2$ and the monomeric **Zn-1'-Ac** product are colorless, the cleavage reaction by path A was first monitored by thin layer chromatography (tlc) on silica plates via iodine staining. Product separation was accomplished by silica column chromatography using MeOH as eluent and the retention factor from tlc plates to identify product-containing fractions. The solvent was removed from the consolidated product fractions and the white powder, **Zn-1'-Ac**, was recrystallized for characterization and use in further reactions. The complex, with m.p. of 172 °C, is hygroscopic yet stable in air.

The photolytic conversion of the $W(CO)_6$ to $(THF)W(CO)_5$ was monitored by FT-IR spectroscopy following the disappearance of the T_{1u} band of $W(CO)_6$ at 1974 cm^{-1} and the growth of the 1930 cm^{-1} band of $(THF)W(CO)_5$. This golden solution was added to a **Zn-1'-Ac** suspension in THF. Following overnight stirring, all of the **Zn-1'-Ac** solid was pulled into solution and the ν(CO) IR bands indicated conversion to a new species with absorptions as seen in Figure IV-2 (top). Yellow x-ray quality crystals were obtained by layering a THF solution with hexane. This product was typically protected from air and moisture as it is more sensitive than the **Zn-1'-Ac** metalloligand. Nevertheless, the **$[(Zn\text{-}1'\text{-}Ac)W(CO)_5]_x$** product is stable to $CO_{(g)}$ as was demonstrated by exposure to bubbling $CO_{(g)}$ for extensive time periods at 22 °C in THF. Over the course of 6 days, approximately 30 % conversion to $W(CO)_6$ was observed.

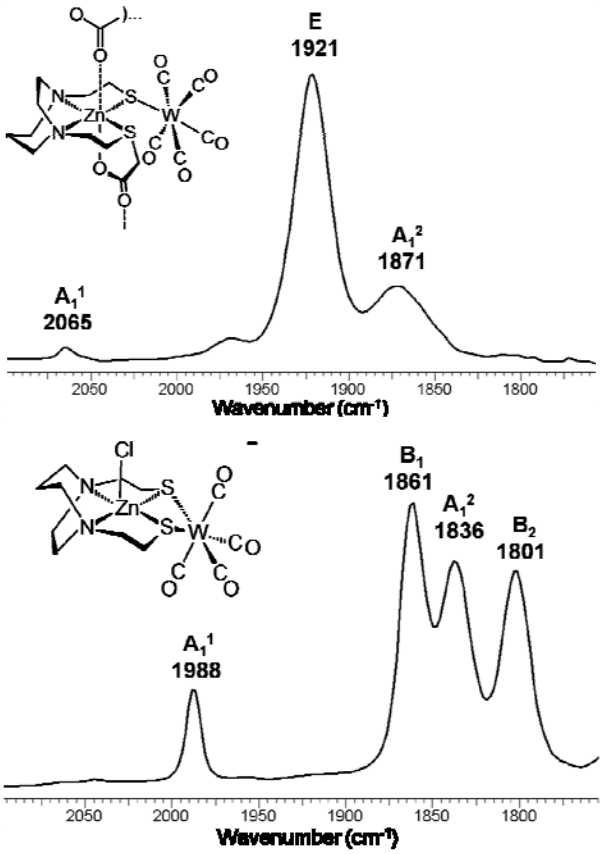

Figure IV-2. DMF solution Infrared Spectra ν(CO) region. Top: **[(Zn-1'-Ac)W(CO)$_5$]$_x$**; Bottom: **[(Zn-1'-Cl)W(CO)$_4$]$^-$**.

The [Zn-1'-Cl]$^-$ intermediate, shown in pathway B of Scheme IV-1, was produced by [Et$_4$N]$^+$Cl$^-$ cleavage of the insoluble [Zn-1']$_2$ dimer, drawing the Zn complex into solution as the reaction proceeded. Unlike the **Zn-1'-Ac** complex, the chloride-cleaved mono-zinc product [Zn-1'-Cl]$^-$, intermediate in Scheme IV-1, could not be isolated, but was used *in situ* for the synthesis of **[(Zn-1'-Cl)W(CO)$_4$]$^-$**. Addition of the (pip)$_2$W(CO)$_4$ complex as a CH_2Cl_2 solution to the [Zn-1'-Cl]$^-$ resulted in a clear golden solution. The air stable yellow solid obtained from this solution by hexane precipitation was washed with benzene and recrystallized by layering of a CH_2Cl_2

solution with hexane. The purified compound was re-dissolved in DMF to yield the IR spectra of the ν(CO) region given in Figure IV-2 (bottom).

Molecular Structure Analyses of Zn-1'-Ac. X-ray diffraction studies on the single crystals of **Zn-1'-Ac**, **[(Zn-1'-Ac)W(CO)$_5$]$_x$**, and **[(Zn-1'-Cl)W(CO)$_4$]$^-$** yielded the molecular structures shown in Figures IV-3 – IV-9. Figure IV-3 displays the **Zn-1'-Ac** monomeric complex as a ball-and-stick graphic and the [Zn-1']$_2$ precursor[92] is also shown for comparison. Views a and b highlight the diazacycle scaffolds and the flexibility of the pendant mercaptoethylene arms, which lead to irregular geometries. The 3-carbon N to N linker of the diazacycloheptane ring in the **Zn-1'-Ac** lies on the same side of the N_2S_2 donor set as does the acetate arm. Note that the pendant arms in both the **Zn-1'-Ac** and the [Zn-1']$_2$ structures are staggered across the N_2S_2 planes. Both compounds contain penta-coordinate Zn-centers with similar ∠ N(1)-Zn(1)-N(2) (72 – 75º) and ∠ S(1)-Zn(1)-S(2) (108º) within the bme-dach portion of the ligand. For both, the Zn-S(2)$_{terminal}$ distance is shorter than the remaining Zn-S(1) distance (the μ-S in [Zn-1']$_2$ and the thioether S- in **Zn-1'-Ac**). The N_2S_2 donor set within the **Zn-1'-Ac** complex (without zinc) forms an irregular "plane" with an average atom deviation of 0.306 Å. Analysis of the bond angles according to ideal square pyramidal (τ = 0) versus ideal trigonal bipyramidal (τ = 1) geometries yields a τ value of 0.36 for **Zn-1'-Ac**. According to Addison, *et al*., this value more closely approaches square pyramidal geometry, while that for the [Zn-1']$_2$ structure (τ = 0.47) is an exact intermediate between square pyramidal and trigonal bipyramidal geometries.[63, 92]

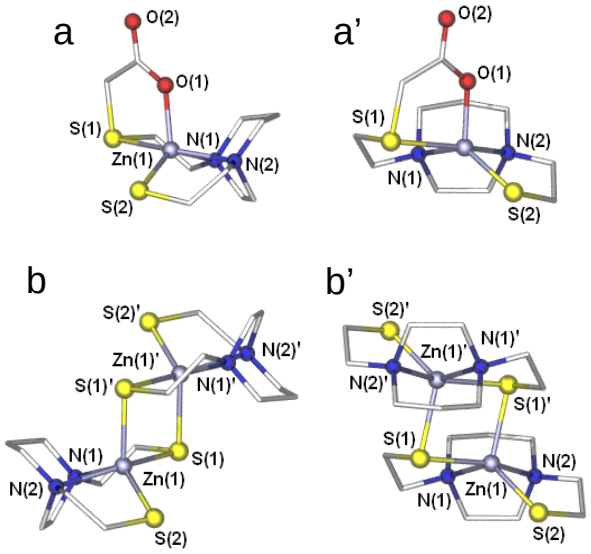

Figure IV-3. Ball-and-stick displays of the **Zn-1'-Ac** (a and a') and the $[Zn\text{-}1']_2$ precursor (b and b'). Selected metric parameters for **Zn-1'-Ac** (*$[Zn\text{-}1']_2$ italics*). Bond lengths (Å): Zn(1) – S(1), 2.587(3) (*2.496(2)*); Zn(1) – S(2), 2.263(2) (*2.308(2)*); Zn(1) – N(1), 2.159(3) (*2.181(6)*); Zn(1) – N(2), 2.171(3) (*2.274(5)*); Zn(1) – O(1), 1.983(2); Zn(1) – S(1)', 2.417(2). Bond angles (deg): N(1) – Zn(1) – N(2), 75.21(10) (*71.94(19)*); S(1) – Zn(1) – S(2), 107.72(4) (*108.28(6)*).

As the sizeable collection of reported NiN_2S_2 complexes have demonstrated the ideal use of the N_2S_2 diazacycle ligand systems for nearly perfect square planar geometry,[55, 114] the structures reported here add to the examples in which these systems demonstrate flexibility and positive response to the geometrical preferences of the central metal ion. Nevertheless, the hydrocarbon backbone portion of the N_2S_2 ligands has important effects on the overall geometry as well. For example, the penta-coordinate **Zn-1'-Ac** is analogous to the product of the cleavage reaction of $[Zn(bme\text{-}daco)]_2$, $[Zn\text{-}1]_2$, with $ClCH_2CO_2H$.[115] The resulting penta-coordinate Zn-1-Ac complex has a τ value of 0.12, i.e., substantially square pyramidal in geometry. It should be noted that the

packing diagram of the Zn-1-Ac analogue contains H_2O molecules hydrogen bonded to the carboxylate O-atoms within its crystallographic unit cell.

As shown in Figure IV-4, the packing of **Zn-1'-Ac** molecules results in a regular array that places Zn and the free acetate oxygen from an adjacent molecule at a distance of 4.419 Å, i.e., beyond bonding. The next closest atoms are at 6.094 and 6.835 Å. Thus, the packing diagram shows no intermolecular interactions that might indicate acetate bridging to neighboring zinc centers. In contrast, interactions between **Zn-1'-Ac** units are extensive in the **$[(Zn\text{-}1'\text{-}Ac)W(CO)_5]_x$** complex described next.

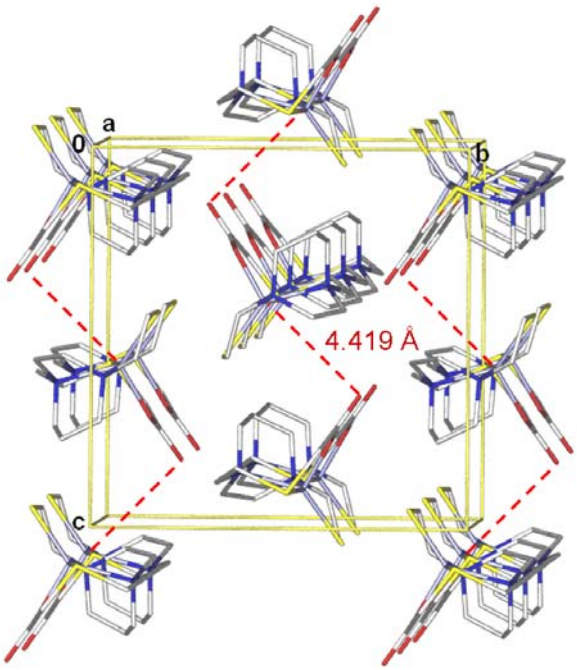

Figure IV-4. The **Zn-1'-Ac** unit cell displaying the closest intermolecular Zn-O distances in the bc plane. All other Zn---O intermolecular distances are > 6 Å.

Molecular Structure Analyses of $[(Zn\text{-}1'\text{-}Ac)W(CO)_5]_x$. As illustrated in Figure IV-5, the structure of **$[(Zn\text{-}1'\text{-}Ac)W(CO)_5]_x$** is that of a coordination polymer involving the **Zn-1'-Ac** unit, in which the acetate group serves as a bridging ligand between Zn atoms in adjacent molecules, utilizing both oxygen atoms, and resulting in six-coordinate Zn centers.

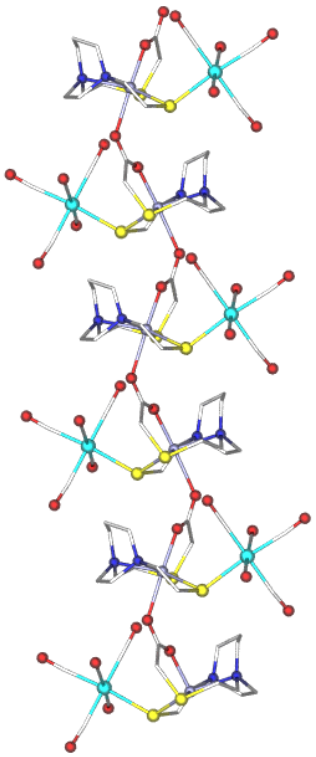

Figure IV-5. A ball-and-stick representation of the molecular structure of **$[(Zn\text{-}1'\text{-}Ac)W(CO)_5]_x$**, a coordination polymer.

As pictured in Figure IV-6 below, the repeating units propagate along the b axis of the crystal lattice. The intra- and intermolecular Zn-O distances are 2.074(18) and 2.265(17) Å, respectively.

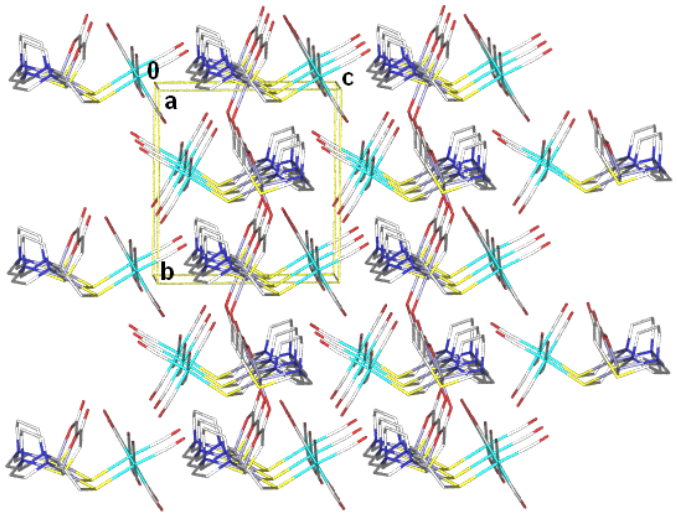

Figure IV-6. Packing diagram of **[(Zn-1'-Ac)W(CO)$_5$]$_x$**, illustrating the extended linear chains propagating along the b-axis of the crystal lattice. The unit cell is highlighted in gold with labeled axes.

Figure IV-7 presents two views which emphasize the orientation of the W(CO)$_5$ with respect to the **Zn-1'-Ac** metalloligand of the coordination polymer repeat unit. Notably, the W(CO)$_5$ resides on the same side as the acetate arm which emanates from S(2) as the μ-S bridge is created from S(1). In terms of the extended structure of the coordination polymer, this results in an alternation of W(CO)$_5$ units along the Zn-acetate chain. The ∠ Zn(1)-S(1)-W(1) of 120.0(3)° places the W(CO)$_5$ moiety beyond steric interactions, which is consistent with the regular C_{4v} LW(CO)$_5$ geometry suggested by the ν(CO) IR spectrum, Figure IV-2. The W(CO)$_5$ moiety is bound by the single S(1) thiolate of **Zn-1'-Ac** at S(1)-W(1) distance of 2.591(7)Å. The Zn-$S_{thiolate}$ distance of 2.403(7) is approx. 0.15 Å longer than in the free **Zn-1'-Ac** compound. As expected, the

$Zn\text{-}S_{thioether}$ distance of 2.548(7) Å in $[(Zn\text{-}1'\text{-}Ac)W(CO)_5]_x$ is largely the same as in the free **Zn-1'-Ac**, 2.587(3) Å.

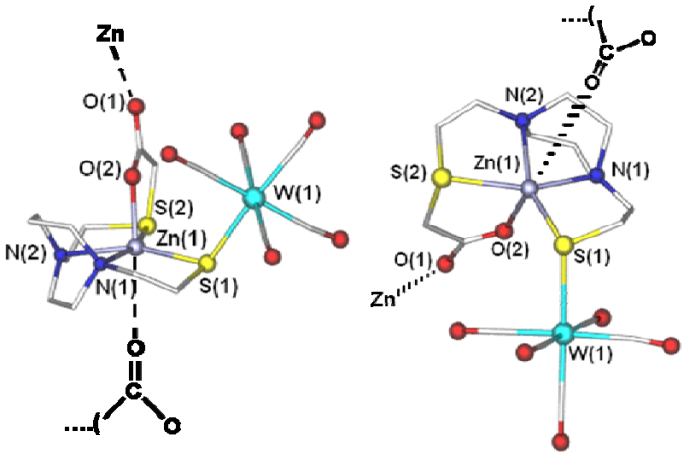

Figure IV-7. Two views of the repeat unit in the Zn(μ-SR)W coordination polymer. In each case, a dashed line represents the intermolecular Zn---O contact to an adjacent unit.

The Zn(1)-O(2) distance for the **Zn-1'-Ac** unit within the coordination polymer is approx. 0.1 Å longer than the $Zn\text{-}O_{intramolecular}$ distance in the free **Zn-1'-Ac**.

Molecular Structure Analyses of $[(Zn\text{-}1'\text{-}Cl)W(CO)_4]^-$. The Et_4N^+ salt of **$[(Zn\text{-}1'\text{-}Cl)W(CO)_4]^-$** was prepared according to the procedure outlined as route B in Scheme IV-1 and isolated from a CH_2Cl_2 solution layered with hexane. The structure of the anion is given in Figure IV-8 in ball-and-stick form. It consists of a square pyramidal $ZnN_2S_2Cl^-$ unit serving as a bidentate ligand to $W(CO)_4$. In contrast to the pentacoordinate **Zn-1'-Ac** structures, the $ZnN_2S_2Cl^-$ portion of the adduct finds the N_2S_2 donor set as a nearly ideal square plane with mean deviation of 0.0046 Å. The Zn atom is displaced from the N_2S_2 plane by 0.7436 Å towards the apical chloride with a Zn(1)-Cl(1) distance of 2.2902(12) Å. The angulation of a metal dithiolate to exogenous ion or

species interaction is expressed as a "hinge" angle. In this case, it is defined as the angle between the N(1)N(2)S(1)S(2) best plane (without Zn) and the S(1)S(2)C(11)C(12) (without W) plane, 125.9°. If defined by the Zn(1)S(1)S(2) and W(1)S(1)S(2) plane intersection, the angle is 150.4°.

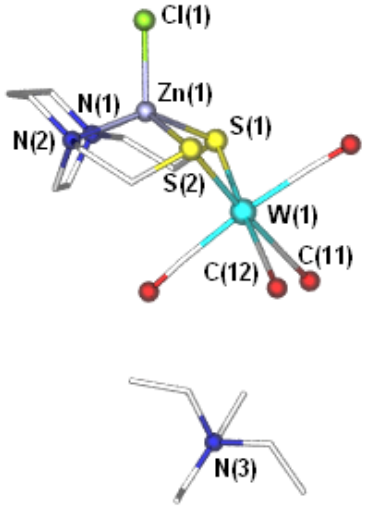

Figure IV-8. Ball-and-stick graphic of **[Et_4N][(Zn-1'-Cl)$W(CO)_4$]**. The H_2O and CH_2Cl_2 molecules found within the crystal lattice are removed from this illustration for clarity. Selected metric parameters: Bond lengths (Å): Zn(1)–S(1), 2.3845(11); Zn(1)–S(2), 2.4055(12); Zn(1)–N(1), 2.232(4); Zn(1)–N(2), 2.182(3); Zn(1)–Cl(1), 2.2902(12); W(1)–S(1), 2.5915(11); W(1)–S(2), 2.5912(11). Bond angles (deg): N(1)–Zn(1)–N(2), 73.21(13); S(1) –Zn(1) –S(2), 90.84(4); S(1) –W(1) –S(2), 82.34(3).

Both thiolate sulfur atoms are bound to the $W(CO)_4$ at S(1)-W(1) and S(2)-W(1) distances of 2.5915(11) and 2.5912(11) Å. The S-W distance within the **[(Zn-1'-Cl)$W(CO)_4$]$^-$** is identical to that found within the **[(Zn-1'-Ac)$W(CO)_5$]$_x$** described above. Furthermore, Zn(1)-S(1) and Zn(1)-S(2) distances of 2.3845(11) and 2.4055(12) Å are not significantly different from the Zn-$S_{thiolate}$ distance (2.403(7) Å) in **[(Zn-1'-**

Ac)W(CO)$_5$]$_x$. Figure IV-9 displays the extended molecular packing of **[Et$_4$N][(Zn-1'-Cl)W(CO)$_4$]**, including solvent molecules packed within the crystal lattice.

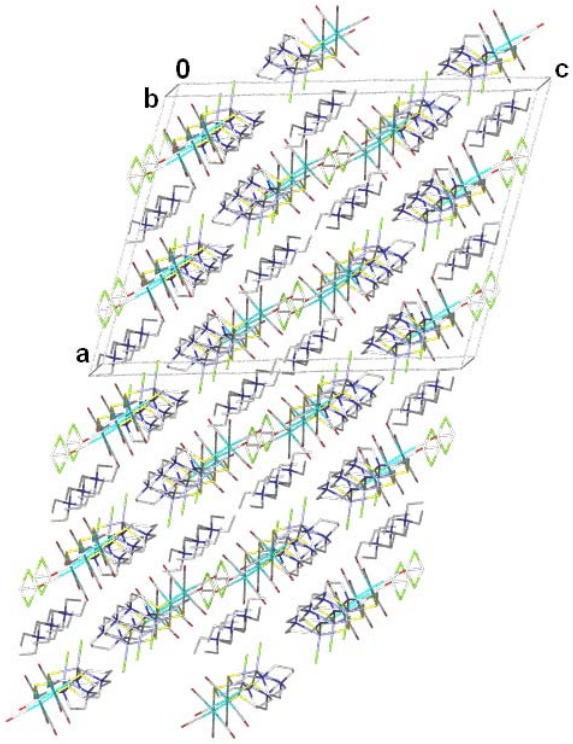

Figure IV-9. Packing diagram of **[Et$_4$N][(Zn-1'-Cl)W(CO)$_4$]**, displaying the H_2O and CH_2Cl_2 molecules packed within the crystal lattice. The unit cell is highlighted in silver with labeled axes.

The **[(Zn-1'-Cl)W(CO)$_4$]$^-$** di-thiolate bridged complex contains several structural features comparable to that of the Pt(II) adduct, [(Zn(bme-dach)Cl)(Pt(dien))]$^+$, shown in Figure IV-1 as (b) and (d). The Zn displacement of 0.7436 Å from the N_2S_2 best plane within **[(Zn-1'-Cl)W(CO)$_4$]$^-$** is similar to that found in the [Zn-1'-Cl]$^-$ unit of [(Zn(bme-dach)Cl)(Pt(dien))]$^+$, 0.8628 Å.[92] The di-thiolate bridge Zn-S bond distances in **[(Zn-1'-Cl)W(CO)$_4$]$^-$** are slightly shorter than those found within the Pt(II) adduct

(2.4567(10) and 2.4210(10) Å). Comparison of hinge angles, defined above (without Zn or Pt centers), finds a more acute angle of 107.2° for the Pt derivative. The hinge angles have also been established in a series of $(NiN_2S_2)W(CO)_4$ complexes to range between 107 to 136°, depending largely on the intramolecular steric interactions.[114, 116] Comparisons to selected Ni derivatives are also presented in the IR spectroscopy discussion below.

Infrared Spectroscopy. As the Zn-Pt thiolate bridging derivatives allow for ample structural investigations of heavy metal adducts, the CO ligand incorporation into the Zn-W adducts permits spectral identification of the complexes via IR spectroscopy. The $LW(CO)_5$ complexes have three ν(CO) IR active bands as seen at the bottom of Figure IV-2, shifted to higher wavenumbers from those observed from the $L_2W(CO)_4$ analogues. Interestingly, there is little difference in ν(CO) values between the anionic $[Zn\text{-}1'\text{-}Cl]^-$ as a mono-dentate donor and the neutral **Zn-1'-Ac** S-donor metallo-ligand, Table IV-2. We conclude that in the latter the modification of the thiolate to a thioether is compensated by the addition of the O-donor to Zn, rendering the available thiolate S-donor nearly as electron-rich as in the anionic chloro-Zn ligand.

The ν(CO) IR spectra of the tungsten carbonyl derivatives, $M(\mu\text{-}SR)_2W(CO)_4$ and $M(\mu\text{-}SR)W(CO)_5$, display the requisite number of bands as predicted for idealized C_{2v} and C_{4v} symmetry, respectively.[117] Despite the severe asymmetry of the complex in which $[Zn\text{-}1'\text{-}Cl]^-$ serves as a monodentate ligand to $W(CO)_5$ and also in the **[(Zn-1'-**

Ac)W(CO)$_5$]$_x$ complex, the ν(CO) IR spectra are not distorted from those of typical $LW(CO)_5$ in which L is a symmetrical ligand.

Table IV-2. CO Stretching Frequencies (cm^{-1}) and Assignments for $W(CO)_4$ (pseudo-C_{2v}) and $W(CO)_5$ (pseudo-C_{4v}) Derivatives of Zn(II) and Ni(II) Metallo Thiolate Ligands.

L⌒LW(CO)$_4$	Solvent	A_1^1	B_1	A_1^2	B_2
[Zn-1'Cl]$^-$	DMF	1988	1861	1836	1801
[Zn-1'Cl]$^-$	CH_2Cl_2	1990	1863	1845	1800
[Ni-1']^a	DMF	1996	1873	1852	1817
[Ni-1*]^b	DMF	1996	1871	1857	1816
[Ni-ema]$^{2-}$ ^{c}	DMF	1986	1853	1837	1791
LW(CO)$_5$	**Solvent**	**A_1^1**	**E**	**A_1^2**	
THF	THF	2075	1930	1891	
Zn-1'-Ac	THF	2065	1925	1888	
Zn-1'-Ac	DMF	2065	1921	1871	
Zn-1'-Ac	solid	2059	1910	1867 (sh 1807)	
[Zn-1'Cl]$^-$	DMF	2063	1920	1869	
[Zn-1'Cl]$^-$	CH_2Cl_2	2064	1921	1863	
[Ni-1*]	DMF	2061	1920	1874	

^{a}[Ni-1'] = (N, N'– bis – 2 – mercaptoethyl – N, N'– diazacycloheptane) nickel (II). ^{b}[Ni-1*] = (N, N'– bis – 2 – mercapto – 2 – methylpropane – N, N' – diazacyclooctane) nickel (II). ^{c}[Ni-ema]$^{2-}$ = (N, N'-ethylenebis-2-mercaptoacetamide) nickel(II) [67, 114, 116]

As listed in Table IV-2, the observed ν(CO) frequencies for **[(Zn-1'-Ac)W(CO)$_5$]$_x$** remained relatively consistent in various solvents, and the ν(CO) solid state values showed more complexities as expected, but are nevertheless quite similar. As the $W(CO)_5$ unit does not report on the degree of aggregation in solution versus solid state, the carboxylate region was examined for possible insight into the intramolecular interactions between **(Zn-1'-Ac)W(CO)$_5$** units. The IR spectra of the acetate region in the free **Zn-1'-Ac** and in the **[(Zn-1'-Ac)W(CO)$_5$]$_x$** illustrated multiple bands in the 1400 cm^{-1} range, which have not been assigned, and a high frequency band in the 1590 –

1650 cm^{-1} range, indicative of uni-dentate carboxylate coordination, as observed in classical metal-acetate complexes.[118] The higher frequency band of **[(Zn-1'-Ac)W(CO)$_5$]$_x$** at 1592 cm^{-1} in the solid state spectrum shifts to 1653 cm^{-1} when dissolved in THF, a value consistent with the free **Zn-1'-Ac** (1636 cm^{-1} in CH_3CN), and suggests dissociation into discrete **(Zn-1'-Ac)W(CO)$_5$** units in solution.

A wide range of Ni(N_2S_2) complexes have been well-studied as metallo-ligands to tungsten carbonyl complexes, and their ν(CO) frequencies used to indicate their electronic donating abilities.[67, 114, 116] Data points from these studies are included for comparison to the [Zn-1'-Cl]$^-$ and the **Zn-1'-Ac** metallo-ligands in Table IV-2. The four ν(CO) values for the anionic **[(Zn-1'-Cl)W(CO)$_4$]$^-$** are positioned 8 to 16 cm^{-1} lower than the neutral [(Ni-1')(μ-SR)$_2$W(CO)$_4$] analogue. This result is consistent with overall charge on the hetero-bimetallic as the dianionic [(Ni-ema)W(CO)$_4$]$^{2-}$ (ema = N, N'-ethylenebis-2-mercaptoacetamide) has ν(CO) IR bands some 10 cm^{-1} lower.

Zn-W Di-thiolate to Mono-thiolate Bridging Adducts: $CO_{(g)}$ Addition. In addition to the IR spectral comparisons to Ni(II) thiolate analogues above, the **[(Zn-1'-Cl)W(CO)$_4$]$^-$** complex was probed for its Zn(μ-SR)$_2$W bridge stability under $CO_{(g)}$ purging, as was carried out for [Ni-1*]W(CO)$_4$.[114, 116] The di-thiolate bridged [Ni-1*]W(CO)$_4$ ((N, N'–bis– 2 – mercapto – 2 – methylpropane – N, N' – diazacyclooctane) nickel (II)) complex listed at the top of Table IV-2 was placed under a $CO_{(g)}$ atmosphere to monitor its conversion to the mono-thiolate adduct (listed at the bottom of Table IV-2). The Ni complex in a DMF solution was pressurized with 400 – 1400 psi of $CO_{(g)}$ (at variable temperatures) in a stainless steel Parr reactor, and the ν(CO) region monitored

by IR spectroscopy. These studies concluded that the [Ni-1*]$W(CO)_4$ di-thiolate adduct was readily converted to the [Ni-1*]$W(CO)_5$ mono-thiolate bridge via a ring-opening process. However, the [Ni-1*]$W(CO)_5$ species was extremely stable toward further W-S bond cleavage and CO ligand substitution.

Scheme IV-2. The Addition of $CO_{(g)}$ to **[(Zn-1'-Cl)W(CO)$_4$]$^-$** to Form the Mono-thiolate Bridge

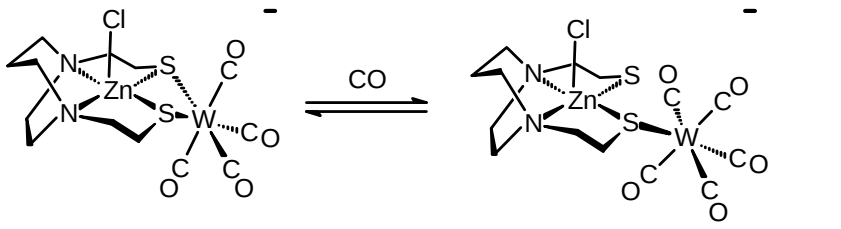

1988 (A_1^1), 1861 (B_1), 1836 (A_1^2), 1801 (B_2) **2063 (A_1^1), 1920 (E), 1869 (A_1^2)**

As shown in Scheme IV-2, the ν(CO) frequencies of the **[(Zn-1'-Cl)W(CO)$_4$]$^-$** complex were examined under 1 atm of $CO_{(g)}$ atmosphere in DMF solution (at 22 °C). Consistent with the Ni(II) complex, the di-thiolate bridged **[(Zn-1'-Cl)W(CO)$_4$]$^-$** readily formed the mono-thiolate adduct under these conditions. Furthermore, the addition of $CO_{(g)}$ for over a period of 6 days showed minimal formation of $W(CO)_6$ (at 1972 cm^{-1}), suggesting the great stability of the mono-thiolate metallo-ligand toward loss and CO exchange. IR spectral overlays of the ν(CO) frequencies during $CO_{(g)}$ bubbling in DMF and CH_2Cl_2 solutions are shown in Figures IV-10 and IV-11, respectively.

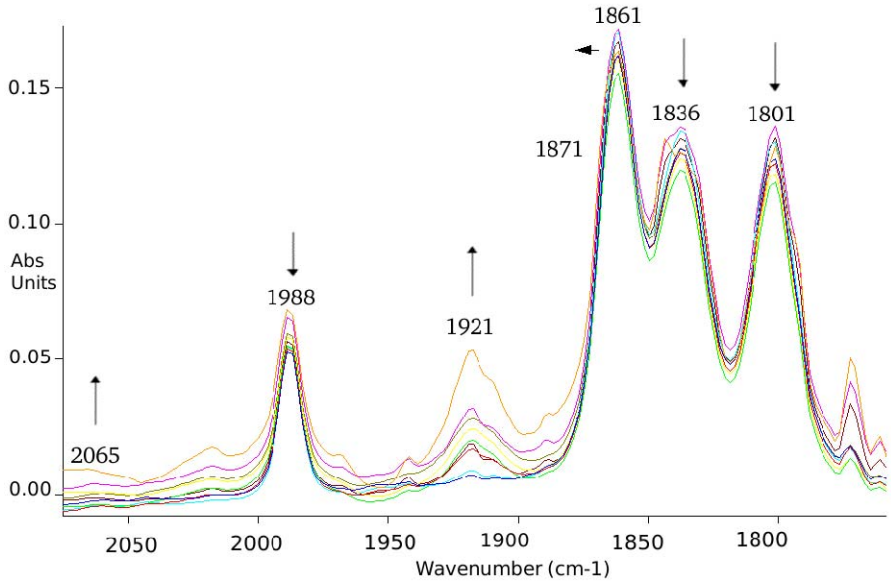

Figure IV-10. DMF solution IR spectra ν(CO) region of **[Et$_4$N][(Zn-1'-Cl)W(CO)$_4$]** during 1 atm CO gas addition over the course of 1 day at 22 ºC. Monitored conversion from **[(Zn-1'-Cl)W(CO)$_4$]$^-$** (1988, 1861, 1836, 1801 cm^{-1}) to [(Zn-1'-Cl)W(CO)$_5$]$^-$ (2065, 1921, 1871 cm^{-1}). The reaction was executed and the figure generated by William S. Foley.

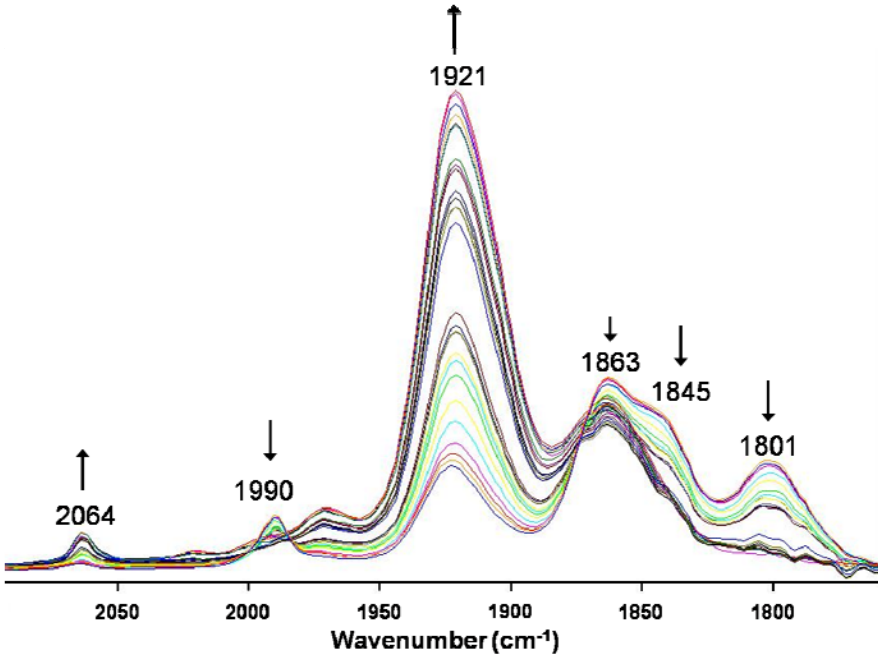

Figure IV-11. CH_2Cl_2 solution IR spectra ν(CO) region of **[Et$_4$N][(Zn-1'-Cl)W(CO)$_4$]** during 1 atm CO gas addition over the course of 3 days at 22 ºC. Monitored conversion from **[(Zn-1'-Cl)W(CO)$_4$]$^-$** (1990, 1863, 1845, 1800 cm^{-1}) to [(Zn-1'-Cl)W(CO)$_5$]$^-$ (2064, 1921, 1863 cm^{-1}).

Comments and Conclusions

The bme-dach ligand, known for its square planar N_2S_2 donor set in d^8 transition metal complexes, displays considerable flexibility according to the geometrical preferences of zinc(II) in the compounds characterized herein. A square pyramid is observed in the **[(Zn-1'-Cl)W(CO)$_4$]$^-$** complex where Zn is significantly displaced out of the N_2S_2 plane and towards the apical chloride. In contrast, the [Zn-1']$_2$ and **Zn-1'-Ac** complexes are penta-coordinate and exhibit seriously distorted geometries, with the latter significantly rearranging in the $W(CO)_5$ adduct. The **[(Zn-1'-Ac)W(CO)$_5$]$_x$** utilizes an additional O-atom interaction at the Zn, which generates an octahedral $ZnN_2SS'O_2$ structure, defining a coordination polymer, with the $W(CO)_5$ units decorating the [Zn-1'Ac]$_n$ chain. The role of the $W(CO)_5$ in inducing the bridging carboxylate interaction that defines the coordination polymer would appear to be electronic. The W-S interaction reduces the electron donor character of the thiolate, enhancing the electrophilicity of the Zn within the **Zn-1'-Ac**, and thus results in the attraction of an adjacent carboxylate.

Such a coordination polymer is not without precedent. In fact, S-modification of a similar N_2S_2 complex of nickel (II), Ni(bme-daco), by methylation of one thiolate S, allowed for the remaining S to react with a single iodoacetate, producing a paramagnetic NiN_2S_2OO' coordination polymer, Figure IV-12.[119] Reminiscent of the Zn polymer, the Ni compound contains an oxygen atom of a neighboring cation which occupies the sixth coordination site on the central Ni(II). This result again demonstrates that S-modification may have a major effect on structural diversity. As the nickel complex

forms a coordination polymer after S-methylation, the Zn analogue does so as a result of S-bridging to tungsten. This also points to the connection between S-alkylation and S-metallation, as noted in the introduction, for the interactions of Zn-bound thiolates with methyl (Ada protein) and platinum (chemotherapeutic) species.

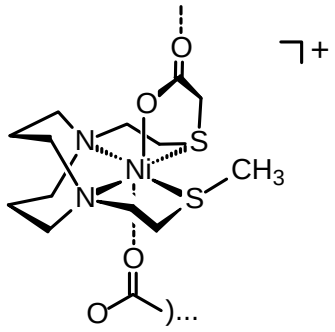

Figure IV-12. The NiN_2S_2OO' subunit within the Ni^{2+} coordination polymer, (N- (3-thiabutyl)- N'- (3- thiapentaneoate)- 1, 5- diazacyclooctane) nickel(II) iodide. Adapted from [119].

Grapperhaus *et al.* have reported two unique studies in which nickel and zinc are compared in precisely the same N_2S_2 ligand donor set.[30, 31] The studies of S-oxygenation and S-alkylation concluded that the effects of electrostatic interactions prevalent in the Zn^{2+} derivative and the π anti-bonding interactions in the Ni^{2+} complexes served in the former to protect the thiolate while the latter activated the thiolate. Our studies of alkylation and metallation suggest that both Ni and Zn thiolates may show similar reactivity, electronic effects as metallo-ligand donors, and templating effects toward ligand modification.

The distorted N_2S_2 "plane" (average atom deviation of 0.306 Å) within the **Zn-1'-Ac** holds the central Zn displaced by 0.447 Å from the irregular plane. With

formation of the coordination polymer, the N_2S_2 best plane transforms to an average atom deviation of only 0.131 Å and the Zn is displaced by only 0.146 Å. Such metric shifts resulting from penta- to hexacoordinate geometries may occur in macromolecules, and possibly in proteins, in which long range structural consequences could be considerable. As the coordination environments about Zn in many Zn-bearing biomolecules are uncertain, we merely note the possible interactions, geometries and coordination spheres that the small ion is amenable to accommodate and shift between.

Zinc is shown to template the bme-dach ligand into a *cis*-dithiolato and mono-thiolato S-donor ligand to heavy metal tungsten carbonyl derivatives. There is considerable significance to this finding, as metal carbonyls are well-known as bio-markers through the sensitivity of their IR active, isolated CO stretching vibrations.[120, 121] The stability of the $Zn(\mu\text{-}SR)W(CO)_x$ bond suggests promise for application of such bio-markers toward the notoriously silent zinc in S-cysteinyl environments.

CHAPTER V

DISPLACEMENT OF Zn(II) BY Ni(II) UTILIZING PENTA- AND HEXA- COORDINATE Zn(II) COMPLEXES AS METAL EXCHANGE SITES

Introduction

There are multiple reasons for exploring the coordination chemistry of zinc as may pertain to its myriad roles in biology. Zinc is readily available throughout nature, and its concentration within biological cells varies some six orders of magnitude (estimated from 10^{-3} to 10^{-9} M).[10, 11] Biochemistry's view of the importance of zinc as a structural metal, involved in the organization of protein structures such as zinc fingers, has expanded into the realm of allosteric effects on regulatory protein/DNA interactions, as well as into establishing its vital role in numerous catalytic enzymes. As a "silent" d^{10} metal ion, many investigations on structural and catalytic Zn^{2+} sites have implemented replacement of zinc with redox active metal ions to spectroscopically monitor structural and functional activity.[9] For example, zinc finger proteins and peptides corresponding to the Zn^{2+} binding domain have been examined for their binding affinities towards various transition metal ions such as Mn^{2+}, Cu^{2+}, Cd^{2+}, Hg^{2+}, Ni^{2+}, Co^{2+} and Fe^{2+}.[12, 14, 18-20] These studies have investigated the binding preference of the natural protein or peptide sequence for Zn^{2+} and the effects of the different metal ions on the coordination within the binding site and the overall structure of the protein/peptide. The main consensus of these studies suggests that the selectivity for Zn^{2+} over other transition metal ions is

largely due to the available coordination environment (Cys_2His_2, Cys_3His, and Cys_4) and the metal ion geometrical preferences, i.e., between being bound tetrahedrally within the protein versus the typical hexa-aqua coordination outside of the protein.[12, 14, 18-20] Small molecule synthetic models of zinc-containing protein and enzyme binding sites have also been compared to their Co^{2+}, Cd^{2+}, Fe^{2+}, and Ni^{2+} counterparts to determine the first coordination sphere effects, as well as spectroscopic investigations.[21-26]

The total amount of Ni^{2+} in the average human body has been stated to be between 10 to 15 milligrams, and has been linked to growth / growth depression via an unidentified mechanism.[3, 122] However, it is well-known to be toxic in excess, resulting in ailments such as dermatitis, cancer, and even death.[3, 122] In cases of solution exposure in excess, 2,3-dimercapto-1-propanol (dimercaprol or British anti-Lewisite, BAL) has been used as a chelate ligand for detoxification after Ni^{2+} poisoning.[3] This form of "bioinorganic chelate therapy" utilizes multi-dentate ligands to bind toxic metal ions such as Ni^{2+}, Hg^{2+}, Cu^{2+}, Pb^{2+}, and Fe^{3+}. It is within this framework that the present $ZnN_2SS'O$ (where S = thiolate; S'= thioether) and $ZnN_2S'_2O_2$ complexes have been explored as multi-dentate chelates templated by Zn^{2+}. Their established reactivity, demonstrated in the previous chapters, has led to the examination of these complexes in the presence of a Ni^{2+} salt to probe the capability of "free" Ni^{2+} to displace Zn^{2+} within an N-, S-, and O- donor environment. An ultimate question is whether a zinc-templated ligand or zinc complex might serve as a toxic metal remediation agent.

The synthetic zinc complexes to be discussed within this chapter are preceded by similar $ZnN_2SS'O$ (Zn-1-Ac) and $NiN_2S'2O_2$ ($Ni\text{-}1\text{-}Ac_2$) analogues that have been well-

studied in their structural, electrochemical, and spectroscopic (in the case of the Ni) properties.[29, 115, 119] The synthesis of these compounds from their $[M(N_2S_2)]_n$ precursors (where N_2S_2 = N, N'-bis(2-mercaptoethyl)-1,5-diazacyclooctane; M = Ni, n=1 ; M = Zn, n = 2) was made possible by M-thiolate alkylation by one (in the case of Zn) or two (in the Ni) equivalents of an acetate moiety. The full characterization and structural and spectroscopic comparisons of these previously established Zn and Ni derivatives have provided insight into the predicted Zn/Ni metal-exchanged product from the Zn-1'-Ac ($ZnN_2SS'O$) and **Zn-1'-Ac$_2$** ($ZnN_2S'_2O_2$) reactions with Ni^{2+}.

Scheme V-1. The Zn/Ni Transmetallation Reaction Yielding **Ni-1'-Ac$_2$** as a Product from **1** Zn-1'-Ac: **1** $Ni(BF_4)_2$ and **2** Zn-1'-Ac: **1** $Ni(BF_4)_2$ Stoichiometric Reactions

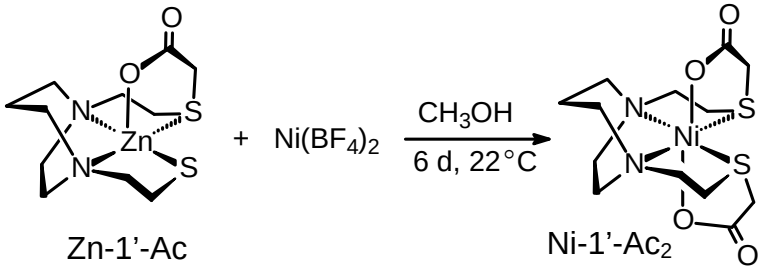

The present chapter describes the 1 Zn: 1 Ni and 2 Zn: 1 Ni stoichiometric reactions between the penta-coordinate Zn-1'-Ac complex and $Ni(BF_4)_2$ to yield the metal-exchanged product, **Ni-1'-Ac$_2$**, depicted in Scheme V-1. The zinc displacement reactions are compared to the direct synthesis of the **Ni-1'-Ac$_2$** complex through an alternate synthetic pathway, along with Zn/Ni exchange examined utilizing a hexa-coordinate Zn complex as the zinc-exchange site.

Experimental Details

Methods and Materials. All solvents used were reagent grade and were dried and distilled under N_2 using standard techniques. The N, N'–bis(2-mercaptoethyl)-1,4–diazacycloheptanezinc(II) dimer, $[Zn\text{-}1']_2$,[92] and the (N-(3-Thiabutyl)-N'-(3-thiapentaneoate)-1,4-diazacycloheptane) zinc(II), Zn-1'-Ac, were prepared according to the experimental details outlined in Chapters II and IV respectively. The N, N'-bis(2-mercaptoethyl)-1,5-diazacyclooctane nickel (II), Ni-1', was synthesized following published procedures.[55] All reactions were carried out under inert atmosphere unless otherwise noted.

Physical Measurements. Elemental analyses were performed by Atlantic Microlab, Inc. Norcross, GA, USA. Electrospray ionization mass spectra (ESI-MS) were obtained in the Laboratory for Biological Mass Spectrometry at Texas A&M University. Infrared spectra were recorded on a Bruker Tensor 37 Fourier Transform – IR spectrometer, using a CaF_2 cell with 0.1 mm path length for solution analysis. UV-Visible spectra were obtained using a Shimadzu UV-2450 spectrophotometer with 1.00 cm path length quartz cells for sample holding.

Synthesis of 1,4-diazacycloheptane-1,4-diylbis(3-thiapentanoato) zinc(II), Zn-1'-Ac$_2$. The **Zn-1'-Ac$_2$** complex was synthesized through various synthetic routes, listed below as (a'), (b), and (b'). The synthesis and characterization were performed in collaboration with Jason A. Denny.

(a'). A portion of $[Zn\text{-}1']_2$ (0.171 g, 0.301 mmol) was placed in a degassed 500 mL Schlenk flask equipped with a reflux condenser, followed by addition of 200 mL of

CH_3OH. As the suspension was stirred at 22 °C, a solution of $Na^+[ICH_2CO_2]^-$ (0.250 g, 1.202 mmol) dissolved in 25 mL of CH_3OH was added. The reaction mixture was then refluxed overnight in a 75 °C oil bath under Ar flow. After cooling to 22 °C, the clear, colorless solution was dried in vacuo. The resulting white powder was purified via silica column chromatography (5 cm x 20 cm) with CH_3OH / CH_3CN (50/50 mix) as the eluent. The products were identified with the aid of thin layer silica chromatography plates (tlc), ran in CH_3OH / CH_3CN solvent mixture, and developed with I_2 stain. The retention factors (R_f values) for each product are as follows: Zn-1'-Ac, R_f = 0.40; **Zn-1'-Ac$_2$**, R_f = 0.15; $[Zn\text{-}1']_2$, R_f = 0.00 (immobile spot). The **Zn-1'-Ac$_2$** fractions were consolidated, dried *in vacuo*, and washed three times with diethyl ether to yield 0.107 g white product (0.268 mmol, 44.3 % yield). The white powder was dissolved in CH_3OH and layered with diethyl ether to yield X-ray quality crystals. ESI-mass spectrum: $[M + Na]^+$ *m/z* = 421. IR (in CH_3CN, cm^{-1}): 1632 (s, sharp), 1377 (w, sharp), 1352 (w, br), 1331 (w, br). Elem. Anal. Calcd. (found) for $C_{13}H_{24}N_2O_5S_2Zn_1$ (**Zn-1'-Ac$_2$** + $1H_2O$): C, 37.37 (37.08); H, 5.79 (5.87); N, 6.70 (6.01).

(b). A sample of Zn-1'-Ac (0.080 g, 0.234 mmol) was dissolved in 25 mL of CH_3OH and a solution of $Na^+[ICH_2CO_2]^-$ (0.049 g, 0.236 mmol) in 5 mL of CH_3OH was added to the Zn solution via cannula. The reaction was stirred at 22 °C under an Ar blanket for 24 h. Tlc plating and staining of the product confirmed **Zn-1'-Ac$_2$** formation (R_f = 0.15). The solvent was removed *in vacuo* and the product purified by silica column chromatography (5 cm x 20 cm), using CH_3OH / CH_3CN (50/50 mix) as the eluent. The **Zn-1'-Ac$_2$** fractions were consolidated, dried, and washed with diethyl ether

to yield 0.0204 g of white solid (0.051 mmol, 21.8 % yield). ESI-mass spectrum: [M + Na]$^+$ *m/z* = 421. IR (in CH_3CN, cm^{-1}): 1632 (s, sharp), 1377 (w, sharp), 1352 (w, br), 1331 (w, br).

(b'). The Zn-1'-Ac (0.212 g, 0.621 mmol) compound in 55 mL of CH_3OH was stirred for 24 h at 22 °C under an Ar blanket. The solution was monitored with tlc plating as described in synthetic route (a'). The cloudy white solution was anaerobically filtered to remove solid [Zn-1']$_2$, and purified by silica column chromatography, also as described above, to yield 0.052 g (0.130 mmol, 20.9 % yield). ESI-mass spectrum: [M + Na]$^+$ *m/z* = 421. IR (in CH_3CN, cm^{-1}): 1632 (s, sharp), 1377 (w, sharp), 1352 (w, br), 1331 (w, br).

Direct Synthesis of 1,4-diazacycloheptane-1,4-diylbis(3-thiapentanoato) nickel (II), Ni-1'-Ac$_2$, (d). The synthesic procedure described below is similar to that found in the literature for Ni-1-Ac.[55] A portion of Ni-1' (0.100 g, 0.361 mmol) was placed in a degassed 200 mL Schlenk flask equipped with a reflux condenser, followed by addition of 40 mL of CH_3OH. As the brown nickel suspension was stirred at 22 °C, two equivalents of $Na^+[ICH_2CO_2]^-$ (0.151 g, 0.726 mmol) were dissolved in 12 mL of CH_3OH and were added. The reaction mixture was then refluxed overnight in a 80 °C oil bath under Ar flow. The resulting dark green solution was removed from the hot oil bath. After cooling to room temperature, an additional portion of $Na^+[ICH_2CO_2]^-$ (0.038 g, 0.183 mmol) in a solvent mixture of 3 mL of CH_3OH and 30 mL of CH_3CN was added. The reaction solution was stirred for an additional 24 h at 22 °C. The resulting deep blue solution was dried *in vacuo* and the product purified by silica column

chromatography (CH_3OH / CH_3CN eluent). Collection of the mobile blue band (R_f = 0.15) and consolidation and drying of the corresponding fractions yielded 0.941 g (0.239 mmol, 66.3 %) of Ni-1'-Ac solid. ESI-mass spectrum in CH_3OH: $[M + Na]^+$ *m/z* = 415. UV-vis spectrum in CH_3OH: 580, 362, 258 nm. IR (in CH_3CN, cm^{-1}): 1628 (s), 1444 (vs), 1420 (shoulder), 1375 (vs, sharp).

Synthesis of 1,4-diazacycloheptane-1,4-diylbis(3-thiapentanoato) nickel (II), Ni-1'-Ac$_2$, Zinc Displacement Reactions. The **Ni-1'-Ac$_2$** was produced through several zinc displacement reactions, listed below as (c) 1 Zn: 1 Ni, (c) 2 Zn: 1 Ni, and (c'). The synthesis and characterization were executed in collaboration with Jason A. Denny.

(c) 1 Zn: 1 Ni. The Zn-1'-Ac compound (0.345 g, 1.011 mmol) was dissolved in 150 mL of CH_3OH to yield a clear, colorless solution. A light green solution of anhydrous $Ni(BF_4)_2$ (0.235 g, 1.012 mmol) in 15 mL of CH_3OH was added via cannula to the stirring Zn solution. The reaction mixture, which displayed an immediate color change to a deep green, was stirred overnight at 22 °C under an Ar blanket. The resulting blue solution was anaerobically filtered and diethyl ether added to precipitate a blue solid. The solid was placed through a silica column (as described above in (d)) to obtain 0.0815 g of pure **Ni-1'-Ac$_2$** (0.207 mmol, 20.5 % yield). Slow evaporation of a methanol solution yielded X-ray quality crystals. ESI-mass spectrum in CH_3OH: $[M + Na]^+$ *m/z* = 415. UV-vis spectrum in CH_3OH: 580, 351, 258 nm. IR (in CH_3CN, cm^{-1}): 1628 (s), 1444 (vs), 1420 (shoulder), 1375 (vs, sharp). Elem. Anal. Calcd. (found) for $C_{13}H_{28}N_2S_2O_7Ni_1$ (**Ni-1'-Ac$_2$** + 3 H_2O): C, 34.91 (35.41); H, 6.31 (6.23); N, 6.27 (6.54).

(c) 2 Zn: 1 Ni. The Zn-1'-Ac compound (0.212 g, 0.621 mmol) was dissolved in 50 mL of CH_3OH to yield a clear, colorless solution. A light green solution of anhydrous $Ni(BF_4)_2$ (0.068 g, 0.293 mmol) in 6 mL of CH_3OH was added via cannula to the stirring Zn solution. The reaction mixture, which displayed an immediate color change to blue, was stirred for 6 d at 22 °C under an Ar blanket. The resulting solution was dried *in vacuo*, and the blue solid was placed through a silica column (as described above) to obtain 0.0904 g of pure **Ni-1'-Ac$_2$** (0.230 mmol, 78.5 % yield). ESI-mass spectrum in CH_3OH: $[M + Na]^+$ *m/z* = 415. UV-vis spectrum in CH_3OH: 580, 351, 258 nm. IR (in CH_3CN, cm^{-1}): 1628 (s), 1444 (vs), 1420 (shoulder), 1375 (vs, sharp).

(c'). A portion of the **Zn-1'-Ac$_2$** compound (0.040 g, 0.100 mmol) was dissolved in 15 mL of CH_3OH to yield a clear, colorless solution. A light green solution of anhydrous $Ni(BF_4)_2$ (0.023 g, 0.099 mmol) in 7 mL of CH_3OH was added via cannula to the stirring Zn solution. The reaction mixture, which displayed a gradual color change from light green to light blue, was stirred for 24 h at 22 °C under an Ar blanket. The resulting solution was dried *in vacuo.* Aliquots of crude product spotted on tlc plates, ran in CH_3OH / CH_3CN, and illuminated with a UV-lamp indicated formation of the **Ni-1'-Ac$_2$** complex. As the **Zn-1'-Ac$_2$** starting material and the metal-exchanged **Ni-1'-Ac$_2$** product possess the same solubility and R_f values, it was not possible to obtain a yield for pure **Ni-1'-Ac$_2$** from this experimental procedure. ESI-mass spectrum in CH_3OH: $[M + Na]^+$ *m/z* = 415.

X-ray Structure Analysis. The final structural solutions for the two structures presented in this chapter will be finalized and prepared for publication by Dr. N.

Bhuvanesh, X-ray Diffraction Laboratory at Texas A&M University. Data for **Zn-1'-Ac_2** were collected on a Bruker D8 GADDS general-purpose three-circle x-ray diffractometer (Cu Kα radiation, λ = 1.54178 Å) operating at 110 K. At the time of collection, the GADDS Hi-Star detector was past due on routine maintenance (re-gassing by Bruker) and collected insufficient data for the **Zn-1'-Ac_2** crystal (last crystal analyzed before the detector was sent to Bruker). The data solution and refinement yielded an acceptable R_{int} (approx. 6%) value but unacceptable (for publication), high R factors (approx. 17%). Graphics presented in this chapter were generated from this preliminary data; however, the **Zn-1'-Ac_2** crystals have been kept at - 20 °C and will be analyzed on the APEX-II CCD three-circle X-ray diffractometer. The **Ni-1'-Ac_2** (product from metal-exchange) single crystal data were collected on a Bruker SMART 1000 CCD based diffractometer[56] (Mo Kα radiation, λ = 0.71073 Å), also at 110 K. The data solution and refinement for the **Ni-1'-Ac_2** structure is in progress.

Results and Discussion

Scheme V-2. Reaction Scheme Summary

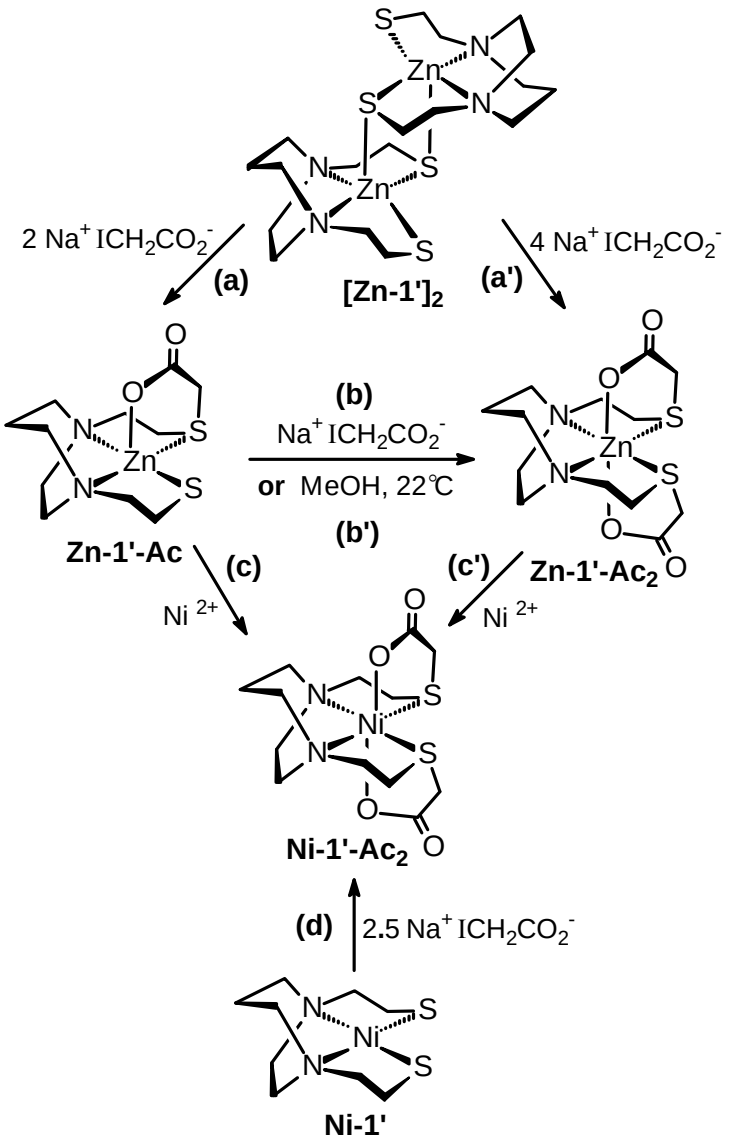

Scheme V-2 displays the overall results of the reaction sequences and products obtained in this study. Specifically, reactions (a) and (a') demonstrate the S-based reactivity of the zinc-thiolate with $Na^+[ICH_2CO_2]^-$ yielding penta- and hexa-coordinate

$ZnN_2SS'O$ and $ZnN_2S'_2O_2$ complexes respectively. Note that the former, isolated and purified, may be converted to the latter either by reaction with an additional equivalent of $Na^+[ICH_2CO_2]^-$ (path (b)), or according to a ligand reformulation (path (b')) under the conditions described below. Reactions (c) and (c') in Scheme V-2 represent the exchange of zinc by nickel in both cases resulting in the hexa-coordinate $NiN_2S'_2O_2$ complex. This **Ni-1'-Ac$_2$** complex is also the sole product of the direct synthesis of NiN_2S_2 (Ni-1') with 2.5 equivalents of $Na^+[ICH_2CO_2]^-$, Scheme V-2 reaction (d).

Complexes $[Zn\text{-}1']_2$, Ni-1', and Zn-1'-Ac have previously been characterized by X-ray crystallography.[55, 92] The synthesis, characterization, and structural properties of the $[Zn\text{-}1']_2$ and Zn-1'-Ac are discussed in great detail in Chapters II and IV respectively, while the Ni-1' molecular structure is evaluated in Chapter III. The **Zn-1'-Ac$_2$** and **Ni-1'-Ac$_2$** complexes are reported within this work, as are the conditions and details of the Zn/Ni exchange reactions. Isolated **Zn-1'-Ac$_2$** and **Ni-1'-Ac$_2$** complexes are hygroscopic and elemental analysis fit various water content, also noted in the solid state X-ray structure. As expected, the Zn complex is white and shows no d-d electronic transitions in the UV-vis spectrum. The **Ni-1'-Ac$_2$** is bright blue with prominent electronic transitions at 580, 362, and 258 nm.

Multiple Synthetic Routes Yielding Zn-1'-Ac$_2$. As described within the Experimental Details section and in Scheme V-2, the **Zn-1'-Ac$_2$** complex was synthesized through experimental procedures (a'), (b) and (b'). Tlc plating of the zinc solutions played an essential role in the monitoring and isolation of pure products. The R_f values (in 50/50 CH_3OH / CH_3CN) for each observable product are as follows: NaI,

R_f = 0.99; Zn-1'-Ac, R_f = 0.40; Zn-1'Ac_2, R_f = 0.15; and $[Zn\text{-}1']_2$ = 0.00 (immobile spot).

In synthetic route (a'), the dimeric $[Zn\text{-}1']_2$ complex was cleaved by refluxing in the presence of four equivalents of $Na^+[ICH_2CO_2]^-$ to yield the octahedral **Zn-1'-Ac_2** product. As the $[Zn\text{-}1']_2$ starting material is only partially soluble in CH_3OH, the initial reaction mixture prior to heating existed as a cloudy, white suspension. As the reaction proceeded, with heating, the entire solution became clear and colorless. After overnight refluxing and cooling, the crude solution was spotted, run, and stained on a tlc plate to reveal **Zn-1'-Ac_2**, Zn-1'-Ac, and NaI products. The silica column fractions containing **Zn-1'-Ac_2** were consolidated and dried to yield 44 % of the hexa-coordinate product. IR spectroscopy was employed to compare the acetate stretching regions of the penta-coordinate Zn-1'-Ac versus the **Zn-1'-Ac_2**. According to Cotton and Wilkinson, classical metal-acetate compounds commonly exhibit multiple bands in the 1400 to 1500 cm^{-1} range, and a high frequency band in the 1590 – 1650 cm^{-1} range indicative of uni-dentate carboxylate coordination.[118] The IR spectrum of Zn-1'-Ac in CH_3CN displayed a strong high frequency band at 1636 cm^{-1} and additional bands at 1445, 1420 (shoulder), and 1375 cm^{-1}. The six-coordinate **Zn-1'-Ac_2** yielded IR bands at 1632, 1377, 1352, and 1331 cm^{-1}. Furthermore, the $[(Zn\text{-}1'\text{-}Ac)W(CO)_5]_x$ coordination polymer, discussed in Chapter IV to contain Zn-carboxylate bridges, produced a set of IR bands at 1653 (s, br), 1460 (vs, sharp), and 1365 (m) cm^{-1} in THF. The similar arrays of stretching frequency patterns displayed by the mono-, di-, and bridging carboxylate Zn complexes support the

viewpoint stated by Cotton and Wilkinson that the IR acetate frequencies may not be very prognostic of bidentate vs bridging metal-bound acetate groups.[118]

Rather than the cleavage reaction used in route (a'), synthetic pathway (b) utilized Zn-1'-Ac as the starting material in the presence of one equivalent of $Na^+[ICH_2CO_2]^-$ at room temperature. Route (b) yielded the alkylation of the remaining available thiolate on the Zn-1'-Ac complex, forming the octahedral **Zn-1'-Ac$_2$**. The first hours of reaction were monitored by tlc plating at 30 min intervals. Starting at t = 3.25 h, NaI and Zn-1'Ac$_2$ were detected, as well as the unreacted Zn-1'-Ac, in the clear, colorless reaction solution. After 24 hours of reaction time, aside from NaI salt, **Zn-1'-Ac$_2$** was the sole Zn product detected via tlc plating.

Synthetic pathway (b') acted as a "control" experiment to examine possible acetate scavenging or ligand reformulation amongst Zn-1'-Ac molecules in a CH_3OH solution (Scheme V-3). As in route (b), this experiment was executed at 22 °C, and the first hours of reaction time were monitored by tlc plating. The tlc plates indicated the

Scheme V-3. The Self-Consuming Reaction of Zn-1'-Ac to Form the **Zn-1'-Ac$_2$** and [Zn-1']$_2$ Products Via Ligand Reconstruction

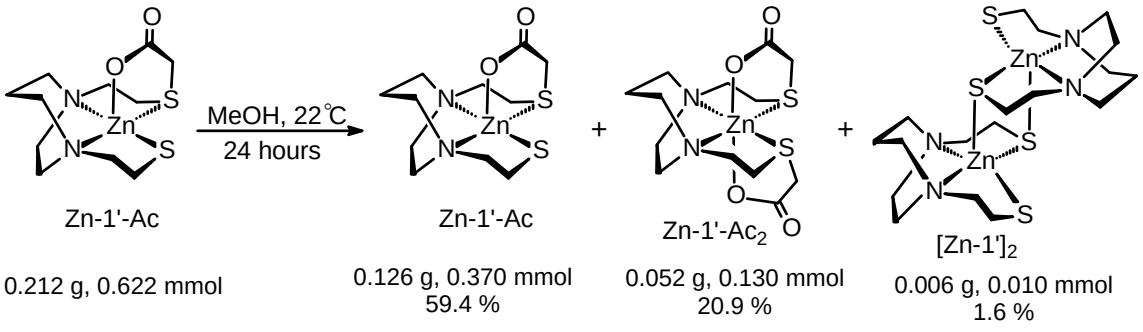

emergence of new species, $[Zn\text{-}1']_2$ and **Zn-1'-Ac$_2$**, after only 3.25 h of stirring. This correlated well with the visual appearance of cloudiness in the stirring solution, as the $[Zn\text{-}1']_2$ is only partially soluble in CH_3OH . The three species, including the starting Zn-1'-Ac compound, persisted for 24 hours of stirring. Figure V-1 displays the cloudy reaction solution (flask on the right) in comparison to the clear, colorless solution produced from route (b) described above (flask on the left). ESI-MS analysis of the stirring solution at 24 hours exhibited $[Zn\text{-}1'\text{-}Ac + Na]^+$ *m/z* = 363 and [**Zn-1'-Ac$_2$** + $Na]^+$ *m/z* = 421. The $[Zn\text{-}1']_2$ species was not observed in the ESI- mass spectrum, as the complex may not have been ionized from the sample solution due to its low solubility in CH_3OH. White solid isolated from the reaction flask weighed approx. 0.006 g. A duplicate solution was allowed to stir at 22 °C under an Ar blanket for up to 14 days and yielded the same products in solution.

Figure V-1. Schlenk flasks containing the reaction mixtures from synthetic route (b) on the left and route (b') on the right were photographed against a colored background to highlight the clear and cloudy makeup of each colorless solution.

Direct Synthesis of Ni-1'-Ac$_2$ via Iodoacetate Reaction With Ni-1'. According to reaction (d) of Scheme V-2, and identical to the preparation of Ni-1-Ac$_2$ (Ni-1 = Ni(bme-daco)),[29, 115, 119] a slight excess of $Na^+[ICH_2CO_2]^-$ was mixed with Ni-1' in a CH_3OH / CH_3CN solution under reflux conditions to yield the **Ni-1'-Ac$_2$** complex in 66.3 % yield. The synthetic conditions for the Ni-1-Ac$_2$ analogue revealed that even when a deficiency of $Na^+[ICH_2CO_2]^-$ is reacted with the Ni-1 precursor, the reaction nevertheless yielded the hexa-coordinate Ni($N_2S'_2O_2$) complex.[29, 115, 119] This suggested that the **Ni-1'-Ac$_2$** product is more stable than its proposed five-coordinate Ni-1-Ac green precursor, and readily scavenges an additional acetate group to form the octahedral complex. The reflux reaction executed with the Ni-1' complex (Experimental Details (d)) in the prescence of exactly two equivalents of $Na^+[ICH_2CO_2]^-$ resulted in a dark green solution, presumably a mixture containing the penta-coordinate intermediate. The addition of another 0.5 equivalent of the $Na^+[ICH_2CO_2]^-$ reagent in CH_3CN drove the reaction to the deep blue **Ni-1'-Ac$_2$** product solution. The direct synthesis of this complex via alkylation of the Ni-1' thiolate donor atoms was performed for comparison to the products generated from the Zn/Ni transmetallation reactions. The ESI-MS analysis, IR spectra of the acetate regions, and UV-Vis spectra of the metal-exchanged Ni complexes were matched to the directly synthesized compound.

Zinc Displacement Reactions: The Reaction of Ni(II) with Zn-1'-Ac. Depicted in Scheme V-2 (c), the Zn/Ni metal-exchange reaction was carried out in both 1 Zn: 1 Ni and at 2 Zn: 1 Ni stoichiometric ratios. The addition of the light green Ni(BF_4)$_2$ solution to an equimolar solution of Zn-1'-Ac (colorless) resulted in an

immediate color change to deep green with a gradual change to blue, and produced **Ni-1'-Ac$_2$** in 20.5 % yield. When reproduced, this reaction was commonly stirred overnight. Some duplicate reactions were stirred for up to 6 days and resulted in the same products with similar yields. As in the zinc reactions (a'), (b) and (b'), the zinc displacement reactions were monitored using tlc plating. The **Ni-1'-Ac$_2$** product, with the identical R_f as the **Zn-1'-Ac$_2$** (0.15 in CH_3OH / CH_3CN) was detected by illuminating the plates with a UV-lamp to observe the product as a colored spot. The separation of products was performed as described above for the **Zn-1'-Ac$_2$** reactions, with the added prescence of the **Ni-1'-Ac$_2$** blue mobile band and a Ni^{2+} species observed at R_f = 0.00 (immobile spot). The green immobile product was isolated from the silica column by addition of Et_3N / CH_3OH as the eluent. The pale green solution was collected, dried, and washed with benzene and ether to render a few milligrams of greenish oil. The green product was re-dissolved in CH_3OH and subjected to ESI-MS analysis. The green solution gave multiple unidentifiable species in the ESI-mass spectrum. Conversely, the purified **Ni-1'-Ac$_2$** product, isolated from the 1 Zn: 1 Ni reaction, was dissolved in CH_3OH with slow evaporation to afford deep blue X-ray quality crystals. A single crystal was analyzed by X-ray diffraction; and the structural solution and refinement are in progress.

The mixing of the light green $Ni(BF_4)_2$ solution to a two-fold molar solution of colorless Zn-1'-Ac resulted in an immediate change to a bright blue color, as pictured in Figure V-2. From this stoichiometric ratio, the green intermediate was not observed, but rather the **Ni-1'-Ac$_2$** was obtained in 78.5 % yield (with the same work-up of products as

described above). Our initial hypothesis of the mechanism is that nucleophilic attack on Ni^{2+} by the lone pair of the one available thiolate in Zn-1'-Ac drives these transmetallation reactions between Zn-1'-Ac and $Ni(BF_4)_2$. However, as shown in the next section, the presence of a thiolate is not required for rapid Zn/Ni exchange.

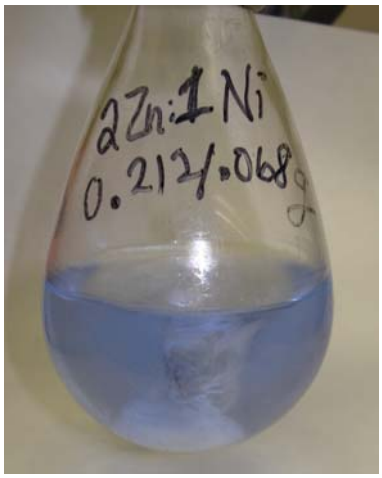

Figure V-2. Reaction flask containing the 2 Zn: 1 Ni zinc displacement reaction solution in CH_3OH. The blue color was observed upon immediate addition of the light green Ni to the colorless Zn solution.

Zinc Displacement Reactions: The Reaction of Ni(II) with Zn-1'-Ac_2. The **Zn-1'-Ac_2**, containing both of its sulfur donors "de-activated" as thioethers by the attached acetate groups, was reacted with one equivalent of $Ni(BF_4)_2$, Scheme V-2 (c'). The reaction was employed to probe the reactivity of the $ZnN_2S'_2O_2$ (where S' = "deactivated" thioether donor), thus testing the hypothesized mechanism proposed for the previous Zn / Ni reactions. The reaction was monitored with tlc plating, and after only 30 min of reaction time, indicated the emergence of the **Ni-1'-Ac_2** was indicated

under a UV lamp exposure. Figure V-3 displays a photograph of the blue reaction solution after 30 min of stirring. Thus, the reaction of the **Zn-1'-Ac$_2$** with Ni^{2+} yielded the Zn/Ni exchanged product, demonstrating that an available thiolate on the zinc complex was not a necessary for such metal-exchange to occur. Although a definite mechanism may not be confirmed by these experiments, it may be deduced that the carboxylate oxygen atoms play a role in attracting the Ni^{2+} ion, and in partnership with the Zn-thiolates, form a bridge that ultimately ends in Ni uptake and Zn ejection from the ligand chelate.

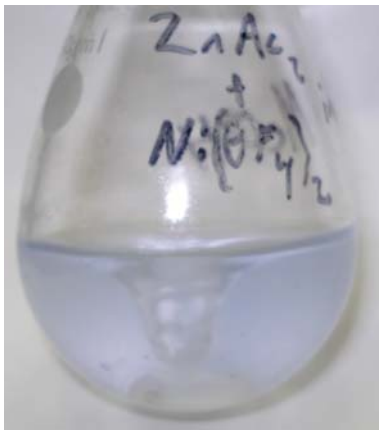

Figure V-3. A Schlenk flask containing the zinc displacement reaction of $Ni(BF_4)_2$ (light green) with **Zn-1'-Ac$_2$** (colorless) in CH_3OH. The blue color was observed after approx. 30 min of reaction time.

Molecular Structure Analysis. The **Zn-1'-Ac$_2$** crystals were obtained from layering of a methanol solution with diethyl ether, and a single crystal was subjected to X-ray diffraction analysis. Figure V-4 contains the ball-and-stick representation of the **Zn-1'-Ac$_2$** molecular structure. The pertinent bond angles and distances are listed within the caption of the figure. The octahedral zinc molecule contains an almost perfect

square planar N(1)N(2)S(1)S(2) plane, with an mean atom deviation of 0.0031 Å (without Zn). The central Zn^{2+} is displaced from the N_2S_2 plane by 0.0185 Å. Table V-1 shows the comparison of selected bond distances between the $[Zn\text{-}1']_2$ dimeric precursor, the penta-coordinate Zn-1'-Ac, and the hexa-coordinate **Zn-1'-Ac$_2$**.

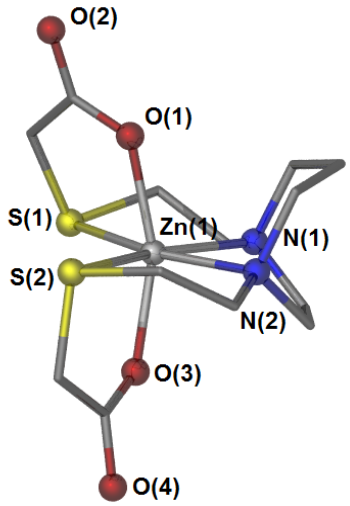

Figure V-4. A ball-and-stick representation of the **Zn-1'-Ac$_2$** molecular structure. The solvent molecules have been omitted for clarity. Selected metric parameters: Bond lengths (Å): Zn(1)–S(1), 2.551; Zn(1)–S(2), 2.582; Zn(1)–N(1), 2.171; Zn(1)–N(2), 2.171; Zn(1)–O(1), 2.036; Zn(1)–O(3), 2.040. Bond angles (°): N(1)–Zn(1)–N(2), 75.88; S(1) –Zn(1) –S(2), 114.68; O(1) –Zn(1) –O(3), 159.55.

Table V-1. Selected Bond Lengths (Å) for $[Zn\text{-}1']_2$, Zn-1'-Ac, and **Zn-1'-Ac$_2$**.

	$[Zn\text{-}1']_2$	**Zn-1'-Ac**	**Zn-1'-Ac$_2$**
Zn(1) – S(thiolate)	2.307* 2.496**	2.263	--
Zn(1) – S(thioether)	--	2.587	2.551 2.582
Zn(1) – O(1)	--	1.983	2.036 2.040

* terminal thiolate, ** bridging thiolate

Comments and Conclusions

The multiple synthetic routes successfully yielding **Zn-1'-Ac$_2$** demonstrated the facile formation of the octahedral Zn^{2+} complex. Moreover, this finding has led to the discovery of a novel feature of the penta-coordinate Zn-1'-Ac. When allowed to stir in MeOH at 22 °C, it readily reformulates into the hexa-coordinate **Zn-1'-Ac$_2$** and the dimeric [Zn-1']$_2$ precursor from which it was originally synthesized (before alkylation by $Na^+[ICH_2CO_2]^-$). This self-reactivity or cannibalism was not observed in the well-studied Zn-1-Ac (daco) analogue.[29, 115, 119] For the direct synthesis of the **Ni-1'-Ac$_2$** (Scheme V-2 (d)), excess $Na^+[ICH_2CO_2]^-$ under reflux was required in order to produce the desired **Ni-1'-Ac$_2$** as the major product. In contrast, each of the Zn/Ni transmetallation reactions took place at 22 °C with rapid formation of the Ni product. The small amount of green "unidentifiable" oil from the 1 Zn: 1 Ni transmetallation reaction was not produced in the 2 Zn: 1 Ni reaction. The green compound may be the proposed five-coordinate Ni-1'-Ac intermediate, and would thus be unlikely to exist in a solution where excess acetate ligand is available for scavenging, as in the 2 Zn-1'-Ac: 1 $Ni(BF_4)_2$ reaction.

The synthesis and isolation of the **Zn-1'-Ac$_2$** and its metal-exchange reaction with Ni^{2+} presented difficulties in isolation of pure **Ni-1'-Ac$_2$** from the reaction mixture. In retrospect, it may then be possible to consider that the **Ni-1'-Ac$_2$** products that result from each of the transmetallation reactions may contain a certain amount of **Zn-1'-Ac$_2$**. Furthermore, the fact that the Zn-1'-Ac was found to readily form **Zn-1'-Ac$_2$** in solution supports this notion that the metal-exchanged **Ni-1'-Ac$_2$** products may not be as "pure"

as initially projected. A closer look at ESI-MS analysis on the larger batches of zinc displacement reactions revealed isotopic bundles that may be assigned to **Zn-1'-Ac$_2$**. The UV-visible spectra of the metal exchanged products also differ slightly in that they possess a 351 nm band, while the directly synthesized **Ni-1'-Ac$_2$** exhibits a band at 362 nm. UV-visible spectroscopy studies are underway to determine the exact molar absorptivities of the directly synthesized **Ni-1'-Ac$_2$** and utilize a standard curve to compare the absorbance of common bands of metal-exchanged compound solutions. The spectroscopic experiment may determine whether the metal-exchanged **Ni-1'-Ac$_2$** products are contaminated with a significant amount of Zn. Consequently, the examination of these synthetic complexes to produce Zn/Ni metal-exchanged products has provided preliminary evidence, in which further investigations are underway to fully quantify and characterize the products resulting from the Ni^{2+} reactions. Additionally, the transmetallation reactions of these Zn complexes will be expanded to Pb^{2+}, Cd^{2+}, Hg^{2+} Co^{2+}, Cu^{2+}, Fe^{2+}, and Fe^{3+} to further explore the potential of such Zn-templated sites for metal exchange.

CHAPTER VI

CONCLUSIONS

As the evidence for biological interactions between Zn-containing proteins and xenobiotic metal ions continues to develop,[19, 35, 37] testing the reactivity of their synthetic models may provide further insight into the first coordination sphere effects on Zn-S sites.[3] The small molecule model experiments and isolated products, specifically from Chapters II and III, have thoroughly demonstrated the capability of such species to form stable thiolate-bridged heteronuclear aggregates as well as metal-exchanged products. The corresponding large scale direct synthesis and structural determination of the products have verified the occurrence of metal exchange between such biomimetic compounds. The isolation of the Zn/Pt bi-metallics, Chapter II complexes **II** and **III**, was not only an an exhilarating achievement resulting from an arduous quest, but formed a major advance in this area. To our knowledge, there are have been no analogous structures that model such interactions between Zn-S sites and Pt(II). As mentioned earlier, the Cambridge Crystallographic Data Centre (CCDC) contains only six crystallographic structures of Zn/Pt hetero-metallic compounds, and those are of multi-metallics with S^{2-} bridges rather than RS^{-}.[73-77]

Although these findings have confirmed that the metal ions may be bridged and exchanged within a N- and S- rich chelate ligand, it does not predict the overall repercussions these interactions may have on the entire protein structure. However, there is evidence, as observed within model peptide sequences and within the proteins

themselves, to suggest that modifications by alkylation and metallation may lead to disruption of structure, thus inhibiting function.[19, 35, 37] This then directs us to the two initial hypotheses proposed within the introduction:

> Does the ternary zinc protein-Pt-DNA adduct formation and subsequent zinc ejection enhance the cytotoxic or antiviral properties of the platinum agent?
>
> or
>
> Does the ternary adduct formation and removal of platinum by function of the zinc-finger enhance DNA repair?

As alluded to in the introduction, the two proposed implications resulting from ternary adducts and Zn/Pt metal exchange may be much more complicated than a clear cut "one or the other" scenario. As the second possibility implies that DNA repair via platinum removal within cancerous cells would be a method of resistance, one must question whether the sacrifice of the Zn-protein performing the removal (as suggested in the first hypothesis) has an overriding effect on the cell. As our biomimetic studies have not answer these questions, they have however contributed in revealing the possible basic chemical interactions that may occur between the Zn-S and Pt(II) key players in these systems.

Derivatization of the $[Zn\text{-}1']_2$ complex has led to an entirely different branch of chemical reactions, which was amply illustrated in Chapters IV and V. As the reactions with the tungsten carbonyl complexes and the Ni salt served two different purposes, both

studies continued to highlight the versatility of the small, unique metal ion to participate in a host of interactions. As mentioned in Chapter IV, zinc(II) was shown to template the bme-dach ligand into both a *cis*-dithiolato and monothiolato S-donor ligand to heavy metal tungsten carbonyl complexes. Various metal carbonyls have been well-studied as bio-markers exploiting the sensitivity of their IR active, isolated CO stretching vibrations.[120, 121] The stability of the $Zn(\mu\text{-}SR)W(CO)_x$ bonds not only extended the scope of Zn-S reactivity, but implied the potential for application of such bio-markers toward the notoriously silent Zn(II) in S-cysteinyl environments. As our findings demonstrate this stability between the two moieties, possible biological applications would require the employment of a different metal, such as iron, to probe the biological sites (to avoid introducing a harmful heavy metal). Furthermore, the structural changes observed within our Zn complexes, transforming from seriously distorted (in their unbound state) to more ordered penta- and hexacoordinate geometries in their W-modified derivatives, further supports the notion of drastic structural effects produced by Zn-S modification. Thus, our notion of bio-applications would be useful only in quantifying silent Zn-S species because it could cause conformational changes and deleterious effects from Zn-S binding of the bio-markers.

As demonstrated within Chapter IV, zinc (II) acted to *template* the bme-dach ligand in a variety of geometries and bridging interactions. This feature was also observed within its reactions with Ni(II). The purpose of exploring Zn/Ni reactions, Chapter V, was to continue to probe the conditions under which exogenous metal ions may replace Zn within its coordination environment. As mentioned earlier,

"bioinorganic chelate therapy" has long been used for the treatment of Ni(II), Hg(II), Cu(II), Pb(II), and Fe(III) poisoning.[3] Our findings in Chapter V have suggested that the **Zn-1'-Ac** and **Zn-1'-Ac$_2$** complexes readily consumed Ni(II) into their ligand chelate. The administering of free chelates or ligands into the body that do not selectively or preferentially bind one metal ion over another has posed some problems with this form of therapy.[3] The idea of using Zn-templated chelates may have the added advantages of ligand design, to target a specific metal ion for capture, along with the flexible, relatively non-toxic Zn(II) to deliver it into the system. The zinc complexes synthesized, characterized, and examined for their respective Zn-S reactivities have provided a starting point in the unearthing of relevant biological interactions, as well as seeding the notion of this small silent ion's potential for use in toxic metal remediation.

REFERENCES

(1) Pennella, M. A.; Giedroc, D. P.; Auld, D. S.; Burgess, J.; Prince, R. H. Zinc. In *Encyclopedia of Inorganic Chemistry* Vol. IX; King, R. B., Ed.; Wiley: Hoboken, NJ, 2nd Edn. 2005; pp.5867-5949.

(2) Emsley, J. Zinc. In *Nature's Building Blocks: An A-Z Guide to the Elements*; Oxford University Press: Oxford, 2003; pp. 499-505.

(3) Kaim, W.; Schwederski, B. Historical Background, Current Relevance and Perspectives, Some General Principles. In *Bioinorganic Chemistry: Inorganic Elements in the Chemistry of Life*; Meyer, G.; Nakamura, A., Eds.; Wiley: New York, 1994**;** pp.1-38.

(4) Vallee, B. L. Zinc in Biology and Biochemistry. In *Zinc Enzymes*; Spiro, T. G., Ed.; John Wiley & Sons: New York, 1983, pp. 1-24.

(5) Parkin, G. *Chem. Rev.* **2004**, *104*, 699-767.

(6) Glusker, J. P. *Adv. Protein Chem.* **1991**, *42*, 1-76.

(7) Bock, C. W.; Katz, A. K.; Glusker, J. P. *J. Am. Chem. Soc.* **1995**, *117*, 3754-3763.

(8) Vahrenkamp, H. *J. Chem. Soc. Dalton Trans.* **2007**, *42*, 4751-4759.

(9) Vallee, B. L.; Maret, W.; Bertini, I.; Luchinat, C.; Viezzoli, M. S. A Synopsis of Zinc Biology and Pathology, Methodology of Metal Exchange in Metalloproteins, and Metal Substitution as a Tool for the Investigation of Zinc Proteins. In *Zinc Enzymes*; Bertini, I.; Luchinat, C.; Maret, W.; Zeppezauer, M. Eds.; Birkhauser: Boston, 1986, pp. 1-47.

(10) da Silva, J. J. R. F.; Williams, R. J. P. Zinc: Lewis Acid Catalysis and Regulation. In *The Biological Chemistry of the Elements: The Inorganic Chemistry of Life*; Clarendon Press: Oxford, 1991; pp. 299-318.

(11) Lippard, S. J.; Berg, J. M. Overview of Bioinorganic Chemistry, Metal Ion Folding and Cross-linking of Biomolecules, Substrate Binding and Activation by Nonredox Mechanisms, and Protein Tuning of Metal Properties to Achieve Specific Functions. In *Principles of Bioinorganic Chemistry*; University Science Books: Mill Valley, CA, 1994; pp.1-20, 175-185, 257-281, 354-355.

(12) Berg, J. M.; Godwin, H. A. *Annu. Rev. Biophys. Biomol. Struct.* **1997**, *26*, 357-371.

(13) Jantz, D.; Amann, B. T.; Gatto, Jr., G. J.; Berg, J. M. *Chem. Rev*. **2004**, *104*, 789-799.

(14) Witkiewicz-Kucharczyk, A.; Bal, W. *Toxicology Letters*, **2006**, *162*, 29-42.

(15) Pavletich, N. P.; Pabo, C. O. *Science*, **1991**, *252*, 809-817.

(16) Elrod-Erickson, M.; Rould, M. A.; Nekludova, L.; Pabo, C. O. *Structure*, **1996**, *4*, 1171-1180.

(17) Tan, S. <http://www.bmb.psu.edu/faculty/tan/lab/gallery_protdna.html>

(18) Berg, J. M.; Merkle, D. L. *J. Am. Chem. Soc.* **1989**, *111*, 3759-3761.

(19) Hanas, J. S.; Larabee, J. L.; Hocker, J. R. Zinc Finger Interactions with Metals and Other Small Molecules. In *Zinc Finger Proteins: From Atomic Contact to Cellular Function*; Iuchi, S., Kuldell, N., Eds.; Landes Bioscience: Austin, TX, 2005; pp. 39-46.

(20) Lachenmann, M. J.; Ladbury, J. E.; Dong, J.; Huang, K.; Carey, P.; Weiss, M. A. *Biochem.* **2004**, *43*, 13910-13925.

(21) Corwin Jr., D. T.; Fikar, R.; Koch, S. A. *Inorg. Chem.* **1987**, *26*, 3079-3080.

(22) Corwin Jr., D. T.; Gruff, E. S.; Koch, S. A. *J. Chem. Soc., Chem.Commun.* **1987**, 966-967.

(23) Kremer-Aach, A.; Klaui, W.; Bell, R.; Strerath, A.; Wunderlich, H.; Mootz, D. *Inorg. Chem.* **1997**, *36*, 1552-1563.

(24) Shoner, S. C.; Nienstedt, A. M.; Ellison, J. J.; Kung, I. Y.; Barnhart, D.; Kovacs, J. A. *Inorg. Chem.* **1998**, *37*, 5721-5726.

(25) Otto, J.; Jolk, I.; Viland, T.; Wonnemann, R.; Krebs, B. *Inorg. Chim. Acta* **1999**, *285*, 262-268.

(26) Chang, S.; Karambelkar, V. V.; Sommer, R. D.; Rheingold, A. L.; Goldberg, D. P. *Inorg. Chem*. **2002**, *41*, 239-248.

(27) Wilker, J. J.; Lippard, S. J. *Inorg. Chem.*, **1997**, *36*, 969-978.

(28) Chiou, S. J.; Innocent, J.; Riordan, C. G.; Lam, K. C.; Liable-Sands, L.; Rheingold, A. L. *Inorg. Chem.*, **2000**, *39*, 4347-4353.

(29) Grapperhaus, C. A.; Tuntulani, T.; Reibenspies, J. H.; Darensbourg, M. Y. *Inorg. Chem.* **1998**, *37*, 4052-4058.

(30) Grapperhaus, C. A.; Mullins, C. S.; Kozlowski, P. M.; Mashuta, M. S. *Inorg. Chem*. **2004**, *43*, 2859-2866.

(31) Grapperhaus, C. A.; Mullins, C. S.; Mashuta, M. S. *Inorg. Chim*. *Acta* **2005**, *358*, 623-632.

(32) Kartalou, M.; Essigmann, J. M. *Mut. Res.* **2001**, *478*, 23-43.

(33) Sorenson, C. M.; Eastman, A. *Cancer Res.* **1988**, *48*, 4484-4488.

(34) Volckova, E.; Dudones, L. P.; Bose, R. N. *Pharm. Res.* **2002**, *19*, 124-131.

(35) Bose, R. N.; Wei, W.; Yang, W.; Evanics, F. *Inorg. Chim. Acta* **2005**, *358*, 2844–2854.

(36) Eastman, A. *Pharm. Ther.* **1987**, *34*, 155-166.

(37) Anzellotti, A. I.; Liu, Q.; Bloemink, M. J.; Scarsdale, J. N.; Farrell, N. *Chem. Biol.* **2006**, *13*, 1-10.

(38) Venter, J. C.; Adams, M. D.; Myers, E. W.; Li, P. W.; Mural, R. J.; Sutton, G. G. *Science* **2001**, *291*, 1304-1351.

(39) Schwabe, J. W. R.; Klug, A. *Nat. Struct. Biol.* **1994**, *1*, 345-349.

(40) Berg, J. M.; Shi, Y. *Science* **1996**, *271*, 1081-1085.

(41) Musah, R. A. *Curr. Topics in Med. Chem.* **2004**, *4*, 1605-1622.

(42) Huang, M.; Maynard, A.; Turpin, J. A.; Graham, L.; Janini, G. M.; Covell, D. G.; Rice, W. G. *J. Med. Chem.* **1998**, *41*, 1371-1381.

(43) Stephen A. G.; Worthy, K. M.; Towler, E.; Mikovits, J. A.; Sei, S.; Roberts, P.; Yang, Q.; Akee, R. K.; Klausmeyer, P.; McCloud, T. G.; Henderson, L.; Rein, A.; Covell, D. G.; Currens, M.; Shoemaker, R. H.; Fisher, R. J. *Biochem. Biophys. Res. Comm.* **2002**, *296*, 1228-1237.

(44) Sartori, D. A.; Miller, B.; Bierbach, U.; Farrell, N. *J. Biol. Inorg. Chem.* **2000**, *5*, 575-583.

(45) Wang, D.; Lippard, S. J. *Nature Rev., Drug Disc.* **2005**, *4*, 307-320.

(46) Sancar, A. *Annu. Rev. Biochem*. **1999**, *65*, 43-81.

(47) Farrell, N.; Qu, Y.; Roberts, J. D. Multifunctional DNA-Binding Metal Complexes. In *Topics in Biological Inorganic Chemistry*; Clarke, M. J. and Sadler, P. J., Eds.; Springer: New York, 1999; pp. 99-115.

(48) Van Houten, B.; Illenye, S.; Qu, Y.; Farrell, N. *Biochem.* **1993,** *44* (32), 11794-11801.

(49) Kloster, M.; Kostrhunova, H.; Zaludova, R.; Malina, J.; Kasparkova, J.; Brabec, V.; Farrell, N. *Biochem.* **2004**, *43*, 7776-7786.

(50) Qu, Y.; Farrell, N. *Inorg. Chem.* **1995**, *13* (34), 3573-3576.

(51) Lambert, B.; Jestin, J. L.; Brehin, P.; Oleyowski, C.; Yeung, A.; Mailliet, P.; Pretot, C.; le Pecq, J. B.; Jacquemin-Sablon, A.; Chottard, J. C. *J. Biol. Chem.* **1995**, *36* (270), 21251-21257.

(52) Darlix, J. L.; Gabus, C.; Nugeyre, M. T.; Clavel, F.; Barre-Sinoussi, F. *J. Mol. Biol.* **1990**, *216*, 689-699.

(53) Liu, Q.; Golden, M.; Darensbourg, M. Y.; Farrell, N. *Chem. Comm.* **2005**, 34, 4360-4362.

(54) Annibale, G.; Brandolisio, M.; Pitteri, B. *Polyhedron* **1995**, *3* (14), 451-462.

(55) Smee, J. J.; Miller, M. L.; Grapperhaus, C. A.; Reibenspies, J. H.; Darensbourg, M. Y. *Inorg. Chem.* **2001**, *40*, 3601-3605.

(56) SMART 1000 CCD; Bruker Analytical X-ray Systems: Madison, WI, 1999.

(57) Sheldrick, G.; *SHELXTL-PLUS, re*V*ision 4.11V, SHELXTL-PLUS users manual*; Siemens Analytical x-ray Instruments Inc.: Madison, WI, 1990.

(58) Sheldrick, G.; *SHELXS-97, Program for Crystal Structure Solution*; Universita¨t Gottingen: Gottingen, Germany, 1997.

(59) Sheldrick, G. *SHELXL-97, Program for Crystal Structure Refinement*; Universita¨t Gottingen: Gottingen, Germany, 1997.

(60) Barbour, L. J. *J. Supramol. Chem.* **2001**, *1*, 189-191.

(61) Oehlsen, M. E.; Qu, Y.; Farrell, N. *Inorg. Chem.* **2003**, *18* (42), 5498-5506.

(62) Pregosin, P. S., *Coord. Chem. Rev.* **1982**, *44*, 247-291.

(63) Addison, A. W.; Rao, T. N.; Reedijk, J.; van Rijn, J.; Verschoor, G. C. *J. Chem. Soc. Dalton Trans.* **1984**, *7*, 1349-1356.

(64) Connick, W. B.; Marsh, R. E.; Schaefer, W. P.; Gray, H. B. *Inorg. Chem.* **1997**, *36*, 913-922.

(65) *Extended Linear Chain Compounds*; Miller, J. S., Ed.; Plenum Press: New York, 1982; Vol. 1-3.

(66) Tzeng, B. C.; Lee, G. H.; Peng, S. M. *Inorg. Chem. Comm.* **2003**, *6*, 1341-1343.

(67) Rampersad, M. V.; Jeffery, S. P.; Reibenspies, J. H.; Ortiz, C. G.; Darensbourg, D. J.; Darensbourg, M. Y. *Angew. Chem. Int. Ed.* **2005**, *8* (44), 1217-1220.

(68) Golden, M. L.; Whaley, C. M.; Rampersad, M. V.; Reibenspies, J. H.; Hancock, R. D.; Darensbourg, M. Y. *Inorg. Chem.* **2005**, *4* (44), 875-883.

(69) Jeffery, S. P.; Green, K. N.; Rampersad, M. V.; Reibenspies, J. H.; Darensbourg, M. Y. *J. Chem. Soc. Dalton Trans.* **2006**, *35*, 4244-4252.

(70) Green, K. N.; Jeffery, S. P.; Reibenspies, J. H.; Darensbourg, M. Y. *J. Am. Chem. Soc.* **2006**, *19* (128), 6493-6498.

(71) Chiang, C.; Lee, J.; Dalrymple, C.; Sarahan, M. C.; Reibenspies, J. H.; Darensbourg, M. Y. *Inorg. Chem.* **2005**, *24* (44) 9007-9016.

(72) Jeffery, S. P.; Lee, J.; Darensbourg, M. Y. *Chem. Comm.* **2005**, *9*, 1122-1124.

(73) Li, Z.; Loh, Z. H.; Fong, S. W. A.; Yan, Y. K.; Henderson, W.; Mok, K. F.; Hor, T. S. A. *J. Chem. Soc., Dalton Trans.* **2000**, *7*, 1027-1031.

(74) Li, Z.; Zheng, W.; Liu, H.; Mok, K. F.; Hor, T. S. A. *Inorg. Chem.* **2003**, *42***,** 8481-8488.

(75) Bridson, J. H.; Henderson, W.; Nicholson, B. K.; Hor, T. S. A. *Inorg. Chim. Acta* **2006**, *359*, 680-684.

(76) Capdevila, M.; Carrasco, Y.; Clegg, W.; Coxall, R. A.; Gonzalez-Duarte, P.; Lledos, A.; Ramirez, J. A. *J. Chem. Soc., Dalton Trans.* **1999**, *17*, 3103-3113.

(77) Novio, F.; Mas-Balleste, R.; Gallardo, I.; Gonzalez-Duarte, P.; Lledos, A.; Vila, N. *Dalton Trans.* **2005**, *16*, 2742-2753.

(78) Djuran, I. M.; Lempers, E. L. M.; Reedijk, J. *Inorg. Chem.* **1991**, *30*, 2648-2652.

(79) Mitchell, K. A.; Streveler, K. C.; Jensen, C. M. *Inorg. Chem.* **1993**, *32*, 2608-2609.

(80) del Sucorro Murdoch, P.; Kratochwil, N. A.; Parkinson, J. A.; Patriarca, M.; Sadler, P. J. *Agnew. Chem. Int. Ed.* **1999**, *38*, 2949-2951.

(81) Mochida, I.; Mattern, J. A.; Bailar, Jr., J. C. *J. Amer. Chem. Soc*. **1975***, 97*, 11, 3021-3026.

(82) Cheng, C.-C.; Lu, Y.-L. *Chem. Commun.* **1998**, 253–254.

(83) Larabee, J. L.; Hocker, J. R.; Hanas, J. S. *Chem. Res. Toxicol.* **2005**, *18*, 1943-1954.

(84) Maynard, A. T.; Covell, D. G. *J. Am. Chem. Soc.* **2001**, *123*, 1047-1058.

(85) Myers, L. C.; Terranova, M. P.; Ferentz, A. E.; Wagner, G.; Verdine, G. L. *Science* **1993**, *261*, 1164-1167.

(86) Myers, L. C.; Wagner, G.; Verdine, G. L. *J. Am. Chem. Soc.* **1995**, *117*, 10749-10750.

(87) Bancroft, D. P.; Lepre, C. A.; Lippard, S. *J. Am. Chem. Soc.* **1990**, *112*, 6860-6871.

(88) Eastman, A. *Chem. Biol. Interact.* **1987**, *61*, 241-248.

(89) Tuntulani, T.; Musie, G.; Reibenspies, J. H.; Darensbourg, M. Y. *Inorg. Chem*., **1995**, *34*, 6279-6286.

(90) Darensbourg, M. Y.; Tuntulani, T.; Reibenspies J. H. *Inorg. Chem., 34*, **1995**, 6287-6294.

(91) Grapperhaus, C. A.; Maguire, M. J.; Tuntulani, T.; Darensbourg, M. Y. *Inorg. Chem.*, **1997**, *36*, 1860-1866.

(92) Almaraz, E.; de Paula, Q. A.; Liu, Q.; Reibenspies, J. H.; Darensbourg, M. Y.; Farrell, N. *J. Am. Chem. Soc.,* **2008**, *130*, 6272-6280.

(93) Kaim, W.; Schwederski, B. Chemotherapy with Compounds of Some Nonessential Elements: Gold-Containing Drugs Used in the Therapy of Rheumatoid Arthritis. In *Bioinorganic Chemistry: Inorganic Elements in the*

Chemistry of Life; Meyer, G.; Nakamura, A., Eds.; Wiley: New York, 1994**;** pp.374-375.

(94) Lippard, S. J.; Berg, J. M. Overview of Bioinorganic Chemistry: Metals in Medicine. In *Principles of Bioinorganic Chemistry*; University Science Books: Mill Valley, CA, 1994; pp.16-18.

(95) Bateman, A.; Birney, E.; Cerruti, L.; Durbin, R.; Etwiller, L.; Eddy, S. R.; Griffiths-Jones, S.; Howe, K. L.; Marshall, M.; Sonnhammer, E. L. L. *Nucl. Acids Res.*, **2002**, *30*, 276-280.

(96) Bruker-Nonius Inc., *FRAMBO*, Version 4.1.13, Madison, WI, 2003.

(97) Sheldrick, G. *CELL-NOW*, University of Göttingen, Germany, 2003.

(98) Bruker-Nonius Inc., *SAINT*, Madison, WI, 2003.

(99) Bruker-Nonius, *APEX II*. Version 2008.6-0. Bruker-Nonius Inc., Madison, WI, 2008.

(100) Sheldrick, G. *SADABS*. University of Göttingen, Germany, 2006.

(101) Sheldrick, G. *Acta Cryst.*, **2008**, *A64*, 112-122, and related references therein.

(102) Maret, W. *Antioxid. Redox Sig.* **2006**, *8*, 1419-1441.

(103) Karlin, S.; Zhu, Z.- Y. *Proc. Natl. Acad. Sci. U.S.A.* **1997**,*94*, 14231-14236.

(104) Maret, W. *Biochem.* **2004**, *43*, 3301-3309.

(105) Matthews, R. G.; Goulding, C. W. *Curr. Opin. Chem. Biol.* **1997**, *1*, 332-339.

(106) Hightower, K. E.; Fierke, C. A. *Curr. Opin. Chem. Biol.* **1999**, *3*, 176-181.

(107) Darnault, C.; Volbeda, A.; Kim, E. J.; Legrand, P.; Vernede, X.; Lindahl, P. A.; Fontecilla-Camps, J. C. *Nat. Struct. Biol.* **2003**, *10*, 271-279.

(108) Song, L.; Wang, M.; Shi, J.; Xue, Z.; Wang, M.- X.; Qian, S. *Biochem. Biophys. Res. Commun.* **2007**, *362*, 319-324.

(109) Beerheide, W.; Bernard, H. U.; Tan, Y. J.; Ganesan, A.; Rice, W. G.; Ting, A. *J. Natl. Cancer Inst.* **1999**, *91*, 1211-1220.

(110) Farrell, N. F. *Coord. Chem. Rev.* **2002**, *232*, 1-4.

(111) Garcia, C. C.; Damonte, E. B. *Infect. Disord. Drug Targets* **2007**, *7*, 204-212.

(112) Lazarczyk, M.; Favre, M. *J. Virol.* **2008**, *82*, 11486-11494.

(113) Darensbourg, D. J.; Kump, R. L. *Inorg. Chem*. **1978**, *17*, 2680-2682.

(114) Rampersad, M. V.; Jeffery, S. P.; Golden, M. L.; Lee, J.; Reibenspies, J. H.; Darensbourg, D. J.; Darensbourg, M. Y. *J. Am. Chem. Soc.* **2005**, *127*, 17323-17334.

(115) Goodman, D. C.; Tuntulani, T.; Farmer, P. J.; Reibenspies, J. H.; Darensbourg, M. Y. *Angew. Chem. Int. Ed. Engl.* **1993**, *32*, 116–119.

(116) Phelps, A. L.; Rampersad, M. V.; Fitch, S. B.; Darensbourg, M. Y.; Darensbourg, D. J. *Inorg. Chem.* **2006**, *45*, 119-126.

(117) Cotton, F. A.; Kraihanzel, C. S. *J. Am. Chem. Soc.* **1962**, *84*, 4432-4438.

(118) Cotton, F. A.; Wilkinson, G. Chemistry of the Transition Elements: Classical Complexes. In *Advanced Inorganic Chemistry: A Comprehensive Text, Third Edition*; Interscience: New York, 1972; pp. 620-681.

(119) Goodman, D. C.; Farmer, P. J.; Reibenspies, J. H.; Darensbourg, M. Y. *Inorg. Chem.* **1996**, *35*, 4989-4994.

(120) Metzler-Nolte, N. *Angew. Chem. Int. Ed.* **2001**, *40*, 1040-1043.

(121) Salmain, M.; Stephenson, G. R. Metallo-carbonyl Probes for Infrared Spectroscopy and Organometallic Components for Organometallic Bioprobes – Opening up the Advantages of IR-based Read-out Methods. In *Bioorganometallics: Biomolecules, Labeling, Medicine*; Jaouen, G., Ed.; Wiley-VCH Verlag GmbH & Co. KGaA: Weinheim, Germany, 2006; pp. 202-205, 220-226.

(122) Emsley, J. Nickel. In *Nature's Building Blocks: An A-Z Guide to the Elements*; Oxford University Press: Oxford, 2003; pp. 277-282.

APPENDIX

Table A-1. Crystal data and structure refinement for **[Zn(bme-dach)]$_2$**.

Empirical formula	C_{18} H_{36} N_4 S_4 Zn_2	
Formula weight	567.49	
Temperature	110(2) K	
Wavelength	1.54178 Å	
Crystal system	Monoclinic	
Space group	P2(1)/n	
Unit cell dimensions	a = 8.1341(9) Å	α= 90°.
	b = 10.4101(11) Å	β= 94.148(7)°.
	c = 13.6281(14) Å	γ = 90°.
Volume	1151.0(2) Å^3	
Z	2	
Density (calculated)	1.637 Mg/m^3	
Absorption coefficient	6.046 mm^{-1}	
F(000)	592	
Crystal size	0.10 x 0.05 x 0.01 mm^3	
Theta range for data collection	5.35 to 59.15°.	
Index ranges	-9<=h<=9, -11<=k<=11, -14<=l<=15	
Reflections collected	8402	
Independent reflections	1626 [R(int) = 0.0624]	
Completeness to theta = 59.15°	97.8 %	
Absorption correction	Semi-empirical from equivalents	

Table A-1. (Continued).

Max. and min. transmission	0.9704 and 0.5831
Refinement method	Full-matrix least-squares on F^2
Data / restraints / parameters	1626 / 0 / 127
Goodness-of-fit on F^2	1.046
Final R indices [I>2sigma(I)]	R1 = 0.0462, wR2 = 0.1124
R indices (all data)	R1 = 0.0713, wR2 = 0.1274
Largest diff. peak and hole	1.278 and -0.482 e.Å^{-3}

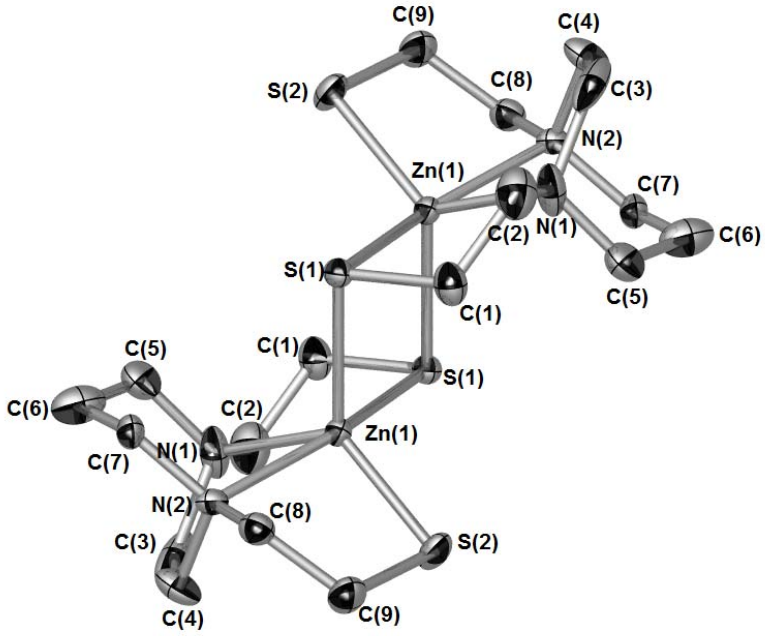

[Zn(bme-dach)]$_2$, half of the dimer is symmetry-generated from the other half.

Table A-2. Bond lengths [Å] for **[Zn(bme-dach)]$_2$**.

Zn(1)-N(1)	2.181(6)
Zn(1)-N(2)	2.274(5)
Zn(1)-S(2)	2.3077(17)
Zn(1)-S(1)#1	2.4170(16)
Zn(1)-S(1)	2.4960(17)
S(1)-C(1)	1.838(7)
S(1)-Zn(1)#1	2.4170(16)
S(2)-C(9)	1.827(7)
N(1)-C(5)	1.427(10)
N(1)-C(2)	1.507(10)
N(1)-C(3)	1.552(10)
N(2)-C(8)	1.454(8)
N(2)-C(7)	1.462(8)
N(2)-C(4)	1.481(8)
C(1)-C(2)	1.512(10)
C(1)-H(1A)	0.9900
C(1)-H(1B)	0.9900
C(2)-H(2A)	0.9900
C(2)-H(2B)	0.9900
C(3)-C(4)	1.554(11)
C(3)-H(3A)	0.9900
C(3)-H(3B)	0.9900
C(4)-H(4A)	0.9900
C(4)-H(4B)	0.9900
C(5)-C(6)	1.469(11)
C(5)-H(5A)	0.9900
C(5)-H(5B)	0.9900
C(6)-C(7)	1.497(10)
C(6)-H(6A)	0.9900
C(6)-H(6B)	0.9900
C(7)-H(7A)	0.9900
C(7)-H(7B)	0.9900
C(8)-C(9)	1.521(9)
C(8)-H(8A)	0.9900
C(8)-H(8B)	0.9900
C(9)-H(9A)	0.9900
C(9)-H(9B)	0.9900

Table A-3. Bond angles [°] for **[Zn(bme-dach)]$_2$**.

N(1)-Zn(1)-N(2)	71.94(19)
N(1)-Zn(1)-S(2)	128.51(17)
N(2)-Zn(1)-S(2)	85.11(13)
N(1)-Zn(1)-S(1)#1	113.18(18)
N(2)-Zn(1)-S(1)#1	98.13(13)
S(2)-Zn(1)-S(1)#1	115.34(7)
N(1)-Zn(1)-S(1)	84.83(15)
N(2)-Zn(1)-S(1)	156.62(13)
S(2)-Zn(1)-S(1)	108.28(6)
S(1)#1-Zn(1)-S(1)	93.30(6)
C(1)-S(1)-Zn(1)#1	100.0(2)
C(1)-S(1)-Zn(1)	93.9(2)
Zn(1)#1-S(1)-Zn(1)	86.70(6)
C(9)-S(2)-Zn(1)	98.8(2)
C(5)-N(1)-C(2)	113.5(6)
C(5)-N(1)-C(3)	110.5(5)
C(2)-N(1)-C(3)	106.5(6)
C(5)-N(1)-Zn(1)	108.0(5)
C(2)-N(1)-Zn(1)	110.7(4)
C(3)-N(1)-Zn(1)	107.5(4)
C(8)-N(2)-C(7)	110.9(5)
C(8)-N(2)-C(4)	114.4(5)
C(7)-N(2)-C(4)	110.1(5)
C(8)-N(2)-Zn(1)	103.7(4)
C(7)-N(2)-Zn(1)	111.4(4)
C(4)-N(2)-Zn(1)	106.1(4)
C(2)-C(1)-S(1)	110.3(5)
C(2)-C(1)-H(1A)	109.6
S(1)-C(1)-H(1A)	109.6
C(2)-C(1)-H(1B)	109.6
S(1)-C(1)-H(1B)	109.6
H(1A)-C(1)-H(1B)	108.1
N(1)-C(2)-C(1)	111.2(6)
N(1)-C(2)-H(2A)	109.4
C(1)-C(2)-H(2A)	109.4
N(1)-C(2)-H(2B)	109.4
C(1)-C(2)-H(2B)	109.4
H(2A)-C(2)-H(2B)	108.0
N(1)-C(3)-C(4)	110.4(5)
N(1)-C(3)-H(3A)	109.6
C(4)-C(3)-H(3A)	109.6
N(1)-C(3)-H(3B)	109.6
C(4)-C(3)-H(3B)	109.6
H(3A)-C(3)-H(3B)	108.1
N(2)-C(4)-C(3)	110.5(5)

Table A-3. (Continued).

N(2)-C(4)-H(4A)	109.5
C(3)-C(4)-H(4A)	109.5
N(2)-C(4)-H(4B)	109.5
C(3)-C(4)-H(4B)	109.5
H(4A)-C(4)-H(4B)	108.1
N(1)-C(5)-C(6)	115.9(7)
N(1)-C(5)-H(5A)	108.3
C(6)-C(5)-H(5A)	108.3
N(1)-C(5)-H(5B)	108.3
C(6)-C(5)-H(5B)	108.3
H(5A)-C(5)-H(5B)	107.4
C(5)-C(6)-C(7)	115.1(7)
C(5)-C(6)-H(6A)	108.5
C(7)-C(6)-H(6A)	108.5
C(5)-C(6)-H(6B)	108.5
C(7)-C(6)-H(6B)	108.5
H(6A)-C(6)-H(6B)	107.5
N(2)-C(7)-C(6)	113.9(6)
N(2)-C(7)-H(7A)	108.8
C(6)-C(7)-H(7A)	108.8
N(2)-C(7)-H(7B)	108.8
C(6)-C(7)-H(7B)	108.8
H(7A)-C(7)-H(7B)	107.7
N(2)-C(8)-C(9)	112.7(5)
N(2)-C(8)-H(8A)	109.1
C(9)-C(8)-H(8A)	109.1
N(2)-C(8)-H(8B)	109.1
C(9)-C(8)-H(8B)	109.1
H(8A)-C(8)-H(8B)	107.8
C(8)-C(9)-S(2)	114.6(5)
C(8)-C(9)-H(9A)	108.6
S(2)-C(9)-H(9A)	108.6
C(8)-C(9)-H(9B)	108.6
S(2)-C(9)-H(9B)	108.6
H(9A)-C(9)-H(9B)	107.6

Symmetry transformations used to generate equivalent atoms:
#1 -x,-y,-z

Table A-4. Crystal data and structure refinement for **Pt(bme-dach)**.

Empirical formula	$C_9 H_{18} N_2 Pt S_2$	
Formula weight	413.46	
Temperature	110(2) K	
Wavelength	0.71073 Å	
Crystal system	Orthorhombic	
Space group	Pnma	
Unit cell dimensions	a = 9.965(4) Å	α= 90°.
	b = 15.076(7) Å	β= 90°.
	c = 7.497(3) Å	γ = 90°.
Volume	1126.3(9) $Å^3$	
Z	4	
Density (calculated)	2.438 Mg/m^3	
Absorption coefficient	12.792 mm^{-1}	
F(000)	784	
Crystal size	0.30 x 0.10 x 0.10 mm^3	
Theta range for data collection	2.70 to 24.97°.	
Index ranges	-11<=h<=11, -17<=k<=17, -8<=l<=8	
Reflections collected	4616	
Independent reflections	854 [R(int) = 0.0627]	
Completeness to theta = 24.97°	83.3 %	
Absorption correction	Semi-empirical from equivalents	

Table A-4. (Continued).

Max. and min. transmission	0.3611 and 0.1140
Refinement method	Full-matrix least-squares on F^2
Data / restraints / parameters	854 / 30 / 67
Goodness-of-fit on F^2	1.011
Final R indices [I>2sigma(I)]	R1 = 0.0491, wR2 = 0.1257
R indices (all data)	R1 = 0.0567, wR2 = 0.1320
Largest diff. peak and hole	2.161 and -1.783 e.Å^{-3}

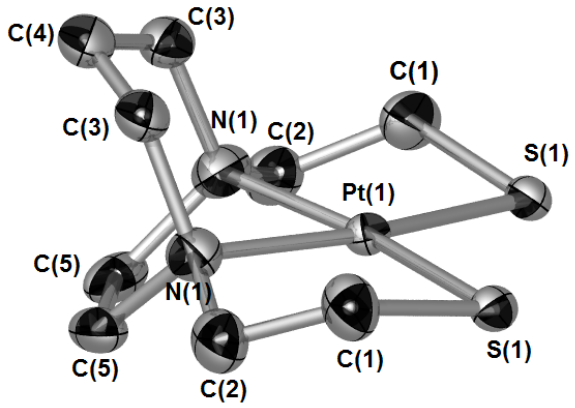

Pt(bme-dach), half of the molecule is symmetry-generated from the other half.

Table A-5. Bond lengths [Å] for **Pt(bme-dach).**

Pt(1)-N(1)#1	2.089(13)
Pt(1)-N(1)	2.089(13)
Pt(1)-S(1)#1	2.298(3)
Pt(1)-S(1)	2.298(3)
S(1)-C(1)	1.838(15)
N(1)-C(2)	1.46(2)
N(1)-C(3)	1.481(14)
N(1)-C(5)	1.489(16)
C(1)-C(2)	1.47(2)
C(1)-H(1A)	0.9900
C(1)-H(1B)	0.9900
C(2)-H(2A)	0.9900
C(2)-H(2B)	0.9900
C(3)-C(4)	1.427(15)
C(3)-H(3A)	0.9900
C(3)-H(3B)	0.9900
C(4)-C(3)#1	1.427(15)
C(4)-H(4A)	0.9600
C(4)-H(4B)	0.9600
C(5)-C(5)#1	1.70(2)
C(5)-H(5A)	0.9601
C(5)-H(5B)	0.9600

Table A-6. Bond angles [°] for **Pt(bme-dach)**.

N(1)#1-Pt(1)-N(1)	80.6(8)
N(1)#1-Pt(1)-S(1)#1	88.5(4)
N(1)-Pt(1)-S(1)#1	169.1(4)
N(1)#1-Pt(1)-S(1)	169.1(4)
N(1)-Pt(1)-S(1)	88.5(4)
S(1)#1-Pt(1)-S(1)	102.45(17)
C(1)-S(1)-Pt(1)	94.4(6)
C(2)-N(1)-C(3)	118.5(11)
C(2)-N(1)-C(5)	106.3(9)
C(3)-N(1)-C(5)	109.6(10)
C(2)-N(1)-Pt(1)	111.4(9)
C(3)-N(1)-Pt(1)	106.3(8)
C(5)-N(1)-Pt(1)	103.8(8)
C(2)-C(1)-S(1)	114.0(11)
C(2)-C(1)-H(1A)	108.7
S(1)-C(1)-H(1A)	108.7
C(2)-C(1)-H(1B)	108.7
S(1)-C(1)-H(1B)	108.7
H(1A)-C(1)-H(1B)	107.6
N(1)-C(2)-C(1)	110.6(12)
N(1)-C(2)-H(2A)	109.5
C(1)-C(2)-H(2A)	109.5
N(1)-C(2)-H(2B)	109.5
C(1)-C(2)-H(2B)	109.5
H(2A)-C(2)-H(2B)	108.1
C(4)-C(3)-N(1)	119.7(11)
C(4)-C(3)-H(3A)	107.4
N(1)-C(3)-H(3A)	107.4
C(4)-C(3)-H(3B)	107.4
N(1)-C(3)-H(3B)	107.4
H(3A)-C(3)-H(3B)	106.9
C(3)#1-C(4)-C(3)	114.6(16)
C(3)#1-C(4)-H(4A)	108.1
C(3)-C(4)-H(4A)	108.1
C(3)#1-C(4)-H(4B)	109.0
C(3)-C(4)-H(4B)	109.0
H(4A)-C(4)-H(4B)	107.8
N(1)-C(5)-C(5)#1	109.7(7)
N(1)-C(5)-H(5A)	110.3
C(5)#1-C(5)-H(5A)	109.6
N(1)-C(5)-H(5B)	109.3
C(5)#1-C(5)-H(5B)	109.6
H(5A)-C(5)-H(5B)	108.2

Symmetry transformations used to generate equivalent atoms: #1 x, -y+1/2, z

Table A-7. Crystal data and structure refinement for **[(Zn(bme-dach)Cl)(Pt(dien))]Cl**.

Empirical formula	C_{14} H_{37} Cl_2 N_5 O_2 Pt S_2 Zn	
Formula weight	702.97	
Temperature	110(2) K	
Wavelength	0.71073 Å	
Crystal system	Monoclinic	
Space group	P2(1)/c	
Unit cell dimensions	a = 14.372(3) Å	α= 90°.
	b = 12.196(2) Å	β= 112.923(2)°.
	c = 14.497(3) Å	γ = 90°.
Volume	2340.3(7) $Å^3$	
Z	4	
Density (calculated)	1.995 Mg/m^3	
Absorption coefficient	7.422 mm^{-1}	
F(000)	1384	
Crystal size	0.10 x 0.05 x 0.05 mm^3	
Theta range for data collection	2.26 to 25.00°.	
Index ranges	-17<=h<=17, -14<=k<=14, -17<=l<=17	
Reflections collected	21570	
Independent reflections	4071 [R(int) = 0.0382]	
Completeness to theta = 25.00°	98.8 %	

Table A-7. (Continued).

Absorption correction	Semi-empirical from equivalents
Max. and min. transmission	0.7079 and 0.5240
Refinement method	Full-matrix least-squares on F^2
Data / restraints / parameters	4071 / 0 / 256
Goodness-of-fit on F^2	1.030
Final R indices [I>2sigma(I)]	R1 = 0.0187, wR2 = 0.0402
R indices (all data)	R1 = 0.0229, wR2 = 0.0417
Largest diff. peak and hole	0.628 and -0.465 e.Å^{-3}

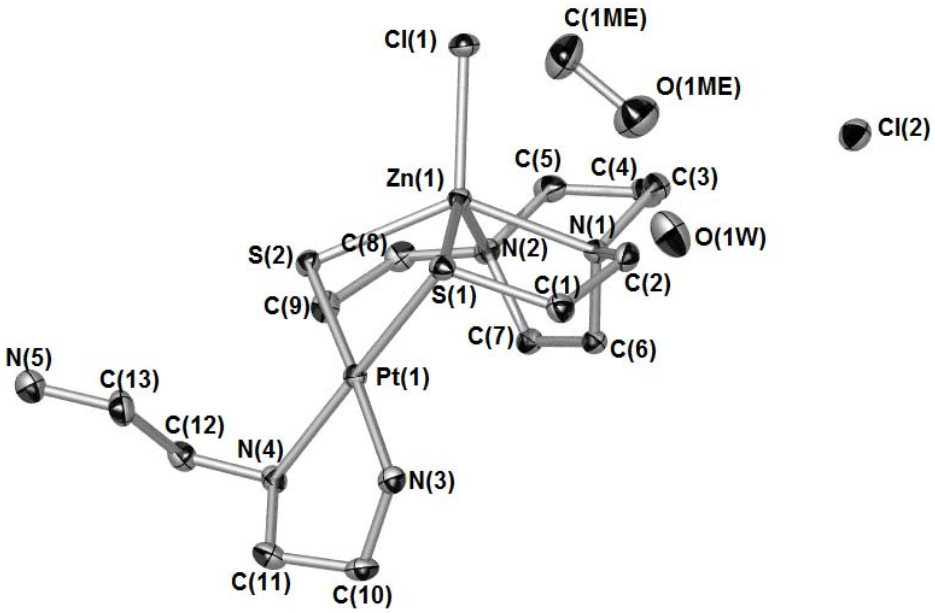

[(Zn(bme-dach)Cl)(Pt(dien))]Cl

Table A-8. Bond lengths [Å] for **[(Zn(bme-dach)Cl)(Pt(dien))]Cl**.

Pt(1)-N(3)	2.069(3)
Pt(1)-N(4)	2.103(3)
Pt(1)-S(1)	2.3078(9)
Pt(1)-S(2)	2.3107(9)
Zn(1)-N(1)	2.148(3)
Zn(1)-N(2)	2.167(3)
Zn(1)-Cl(1)	2.2575(9)
Zn(1)-S(2)	2.4210(10)
Zn(1)-S(1)	2.4567(10)
S(1)-C(1)	1.832(3)
S(2)-C(9)	1.841(3)
N(1)-C(2)	1.478(4)
N(1)-C(6)	1.486(4)
N(1)-C(3)	1.489(4)
N(2)-C(7)	1.475(4)
N(2)-C(8)	1.483(4)
N(2)-C(5)	1.486(4)
N(3)-C(10)	1.486(4)
N(3)-H(3)	0.85(4)
N(3)-H(3AA)	0.78(4)
N(4)-C(11)	1.484(4)
N(4)-C(12)	1.492(4)
N(4)-H(4)	0.84(4)
N(5)-C(13)	1.475(5)
N(5)-H(1N5)	0.8999
N(5)-H(2N5)	0.9000
C(1)-C(2)	1.519(5)
C(1)-H(1A)	0.9900
C(1)-H(1B)	0.9900
C(2)-H(2A)	0.9900
C(2)-H(2B)	0.9900
C(3)-C(4)	1.521(5)
C(3)-H(3A)	0.9900
C(3)-H(3B)	0.9900
C(4)-C(5)	1.518(5)
C(4)-H(4A)	0.9900
C(4)-H(4B)	0.9900
C(5)-H(5A)	0.9900
C(5)-H(5B)	0.9900
C(6)-C(7)	1.551(5)
C(6)-H(6A)	0.9900
C(6)-H(6B)	0.9900
C(7)-H(7A)	0.9900
C(7)-H(7B)	0.9900
C(8)-C(9)	1.511(5)

Table A-8. (Continued).

C(8)-H(8A)	0.9900
C(8)-H(8B)	0.9900
C(9)-H(9A)	0.9900
C(9)-H(9B)	0.9900
C(10)-C(11)	1.493(5)
C(10)-H(10A)	0.9900
C(10)-H(10B)	0.9900
C(11)-H(11A)	0.9900
C(11)-H(11B)	0.9900
C(12)-C(13)	1.513(5)
C(12)-H(12A)	0.9900
C(12)-H(12B)	0.9900
C(13)-H(13A)	0.9900
C(13)-H(13B)	0.9900
O(1W)-H(1W1)	0.8500
O(1W)-H(1W2)	0.8500
O(1ME)-C(1ME)	1.381(5)
O(1ME)-H(1)	0.8500
C(1ME)-H(1MA)	0.9600
C(1ME)-H(1MB)	0.9600
C(1ME)-H(1MC)	0.9600

Table A-9. Bond angles [°] for **[(Zn(bme-dach)Cl)(Pt(dien))]Cl**.

N(3)-Pt(1)-N(4)	82.56(12)
N(3)-Pt(1)-S(1)	94.03(9)
N(4)-Pt(1)-S(1)	175.91(8)
N(3)-Pt(1)-S(2)	177.65(10)
N(4)-Pt(1)-S(2)	95.36(8)
S(1)-Pt(1)-S(2)	88.01(3)
N(1)-Zn(1)-N(2)	75.07(10)
N(1)-Zn(1)-Cl(1)	109.04(8)
N(2)-Zn(1)-Cl(1)	108.62(8)
N(1)-Zn(1)-S(2)	136.17(8)
N(2)-Zn(1)-S(2)	85.44(8)
Cl(1)-Zn(1)-S(2)	114.35(3)
N(1)-Zn(1)-S(1)	84.60(8)
N(2)-Zn(1)-S(1)	135.05(8)
Cl(1)-Zn(1)-S(1)	115.87(3)
S(2)-Zn(1)-S(1)	82.26(3)
C(1)-S(1)-Pt(1)	110.14(12)
C(1)-S(1)-Zn(1)	97.25(11)
Pt(1)-S(1)-Zn(1)	85.03(3)
C(9)-S(2)-Pt(1)	107.39(12)
C(9)-S(2)-Zn(1)	97.35(11)
Pt(1)-S(2)-Zn(1)	85.79(3)
C(2)-N(1)-C(6)	112.5(3)
C(2)-N(1)-C(3)	108.7(3)
C(6)-N(1)-C(3)	111.3(3)
C(2)-N(1)-Zn(1)	110.2(2)
C(6)-N(1)-Zn(1)	106.21(19)
C(3)-N(1)-Zn(1)	107.9(2)
C(7)-N(2)-C(8)	112.4(3)
C(7)-N(2)-C(5)	110.9(3)
C(8)-N(2)-C(5)	108.9(3)
C(7)-N(2)-Zn(1)	105.8(2)
C(8)-N(2)-Zn(1)	109.0(2)
C(5)-N(2)-Zn(1)	109.7(2)
C(10)-N(3)-Pt(1)	109.3(2)
C(10)-N(3)-H(3)	108(2)
Pt(1)-N(3)-H(3)	110(2)
C(10)-N(3)-H(3AA)	107(3)
Pt(1)-N(3)-H(3AA)	104(3)
H(3)-N(3)-H(3AA)	118(4)
C(11)-N(4)-C(12)	112.0(3)
C(11)-N(4)-Pt(1)	107.5(2)
C(12)-N(4)-Pt(1)	119.7(2)
C(11)-N(4)-H(4)	103(2)
C(12)-N(4)-H(4)	108(2)

Table A-9. (Continued).

Pt(1)-N(4)-H(4)	105(2)
C(13)-N(5)-H(1N5)	104.5
C(13)-N(5)-H(2N5)	111.1
H(1N5)-N(5)-H(2N5)	107.7
C(2)-C(1)-S(1)	112.6(2)
C(2)-C(1)-H(1A)	109.1
S(1)-C(1)-H(1A)	109.1
C(2)-C(1)-H(1B)	109.1
S(1)-C(1)-H(1B)	109.1
H(1A)-C(1)-H(1B)	107.8
N(1)-C(2)-C(1)	113.6(3)
N(1)-C(2)-H(2A)	108.8
C(1)-C(2)-H(2A)	108.8
N(1)-C(2)-H(2B)	108.8
C(1)-C(2)-H(2B)	108.8
H(2A)-C(2)-H(2B)	107.7
N(1)-C(3)-C(4)	112.7(3)
N(1)-C(3)-H(3A)	109.0
C(4)-C(3)-H(3A)	109.0
N(1)-C(3)-H(3B)	109.0
C(4)-C(3)-H(3B)	109.0
H(3A)-C(3)-H(3B)	107.8
C(5)-C(4)-C(3)	117.0(3)
C(5)-C(4)-H(4A)	108.0
C(3)-C(4)-H(4A)	108.0
C(5)-C(4)-H(4B)	108.0
C(3)-C(4)-H(4B)	108.0
H(4A)-C(4)-H(4B)	107.3
N(2)-C(5)-C(4)	112.3(3)
N(2)-C(5)-H(5A)	109.1
C(4)-C(5)-H(5A)	109.1
N(2)-C(5)-H(5B)	109.1
C(4)-C(5)-H(5B)	109.1
H(5A)-C(5)-H(5B)	107.9
N(1)-C(6)-C(7)	111.3(3)
N(1)-C(6)-H(6A)	109.4
C(7)-C(6)-H(6A)	109.4
N(1)-C(6)-H(6B)	109.4
C(7)-C(6)-H(6B)	109.4
H(6A)-C(6)-H(6B)	108.0
N(2)-C(7)-C(6)	111.5(3)
N(2)-C(7)-H(7A)	109.3
C(6)-C(7)-H(7A)	109.3
N(2)-C(7)-H(7B)	109.3
C(6)-C(7)-H(7B)	109.3
H(7A)-C(7)-H(7B)	108.0

Table A-9. (Continued).

N(2)-C(8)-C(9)	113.7(3)
N(2)-C(8)-H(8A)	108.8
C(9)-C(8)-H(8A)	108.8
N(2)-C(8)-H(8B)	108.8
C(9)-C(8)-H(8B)	108.8
H(8A)-C(8)-H(8B)	107.7
C(8)-C(9)-S(2)	112.3(2)
C(8)-C(9)-H(9A)	109.1
S(2)-C(9)-H(9A)	109.1
C(8)-C(9)-H(9B)	109.1
S(2)-C(9)-H(9B)	109.1
H(9A)-C(9)-H(9B)	107.9
N(3)-C(10)-C(11)	107.9(3)
N(3)-C(10)-H(10A)	110.1
C(11)-C(10)-H(10A)	110.1
N(3)-C(10)-H(10B)	110.1
C(11)-C(10)-H(10B)	110.1
H(10A)-C(10)-H(10B)	108.4
N(4)-C(11)-C(10)	109.0(3)
N(4)-C(11)-H(11A)	109.9
C(10)-C(11)-H(11A)	109.9
N(4)-C(11)-H(11B)	109.9
C(10)-C(11)-H(11B)	109.9
H(11A)-C(11)-H(11B)	108.3
N(4)-C(12)-C(13)	113.0(3)
N(4)-C(12)-H(12A)	109.0
C(13)-C(12)-H(12A)	109.0
N(4)-C(12)-H(12B)	109.0
C(13)-C(12)-H(12B)	109.0
H(12A)-C(12)-H(12B)	107.8
N(5)-C(13)-C(12)	112.8(3)
N(5)-C(13)-H(13A)	109.0
C(12)-C(13)-H(13A)	109.0
N(5)-C(13)-H(13B)	109.0
C(12)-C(13)-H(13B)	109.0
H(13A)-C(13)-H(13B)	107.8
H(1W1)-O(1W)-H(1W2)	114.1
C(1ME)-O(1ME)-H(1)	105.7
O(1ME)-C(1ME)-H(1MA)	109.2
O(1ME)-C(1ME)-H(1MB)	108.9
H(1MA)-C(1ME)-H(1MB)	109.5
O(1ME)-C(1ME)-H(1MC)	110.3
H(1MA)-C(1ME)-H(1MC)	109.5
H(1MB)-C(1ME)-H(1MC)	109.5

Symmetry transformations used to generate equivalent atoms: -x, y+1/2, -z+1/2

Table A-10. Crystal data and structure refinement for **[Zn(bme-dach)Cl]$_2$Pt**.

Empirical formula	C_{18} H_{36} Cl_2 N_4 Pt S_4 Zn_2
Formula weight	833.48
Temperature	110(2) K
Wavelength	1.54178 A
Crystal system	Orthorhombic
space group	Pbca
Unit cell dimensions	a = 13.0193(15) Å α = 90 °. b = 14.7971(17) Å β = 90 °. c = 26.831(3) Å γ = 90 °.
Volume	5169.0(10) Å^3
Z	8
Calculated density	2.142 Mg/m^3
Absorption coefficient	17.129 mm^{-1}
F(000)	3264
Crystal size	0.12 x 0.02 x 0.02 mm
Theta range for data collection	3.29 to 60.00 °.
Limiting indices	-14<=h<=14, -16<=k<=16, -30<=l<=28
Reflections collected / unique	34974 / 3607 [R(int) = 0.1204]
Completeness to theta = 60.00	93.9 %
Absorption correction	Semi-empirical from equivalents
Max. and min. transmission	0.7257 and 0.2330
Refinement method	Full-matrix least-squares on F^2

Table A-10. (Continued).

Data / restraints / parameters	3607 / 252 / 280
Goodness-of-fit on F^2	1.009
Final R indices [I>2sigma(I)]	R1 = 0.0307, wR2 = 0.0563
R indices (all data)	R1 = 0.0492, wR2 = 0.0595
Largest diff. peak and hole	0.882 and -0.557 e.A^-3

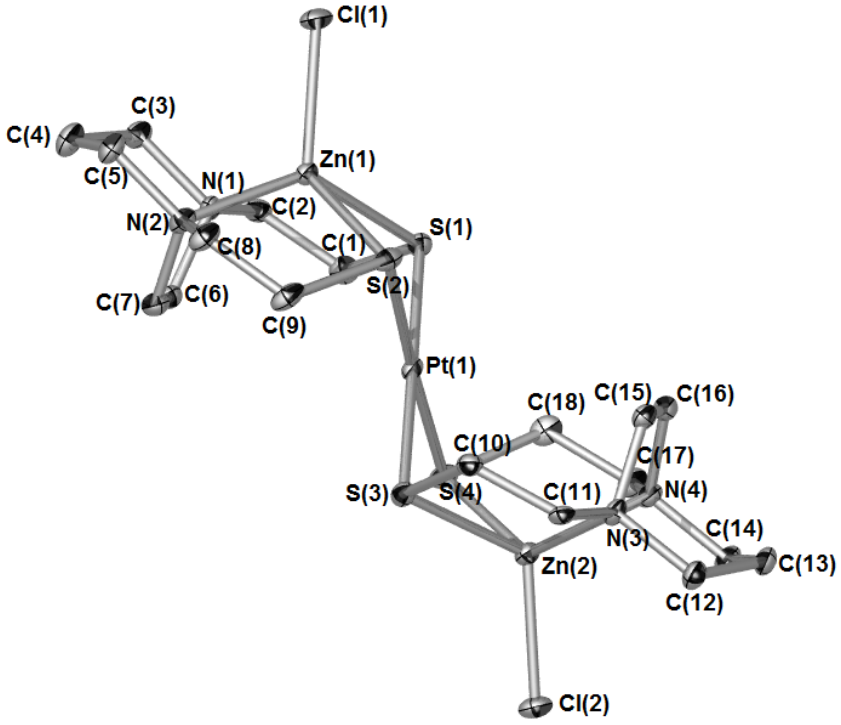

$[Zn(bme\text{-}dach)Cl]_2Pt$

Table A-11. Bond lengths [Å] for **[Zn(bme-dach)Cl]$_2$Pt**.

Pt(1)-S(1)	2.3401(14)
Pt(1)-S(2)	2.3407(15)
Pt(1)-S(3)	2.3437(15)
Pt(1)-S(4)	2.3465(15)
Zn(1)-N(1)	2.178(5)
Zn(1)-N(2)	2.196(5)
Zn(1)-Cl(1)	2.2520(17)
Zn(1)-S(2)	2.4159(17)
Zn(1)-S(1)	2.4390(16)
Zn(2)-N(4)	2.172(5)
Zn(2)-N(3)	2.195(5)
Zn(2)-Cl(2)	2.2559(16)
Zn(2)-S(3)	2.4295(17)
Zn(2)-S(4)	2.4349(16)
S(1)-C(1)	1.818(6)
S(2)-C(9)	1.857(6)
S(3)-C(10)	1.827(6)
S(4)-C(18)	1.863(6)
N(1)-C(2)	1.439(7)
N(1)-C(6)	1.470(7)
N(1)-C(3)	1.504(7)
N(2)-C(7)	1.456(8)
N(2)-C(5)	1.474(8)
N(2)-C(8)	1.475(8)
N(3)-C(11)	1.477(7)
N(3)-C(12)	1.478(7)
N(3)-C(15)	1.490(7)
N(4)-C(17)	1.465(8)
N(4)-C(16)	1.483(8)
N(4)-C(14)	1.485(7)
C(1)-C(2)	1.529(8)
C(1)-H(1A)	0.9900
C(1)-H(1B)	0.9900
C(2)-H(2A)	0.9900
C(2)-H(2B)	0.9900
C(3)-C(4)	1.531(8)
C(3)-H(3A)	0.9900
C(3)-H(3B)	0.9900
C(4)-C(5)	1.511(9)
C(4)-H(4A)	0.9900
C(4)-H(4B)	0.9900
C(5)-H(5A)	0.9900
C(5)-H(5B)	0.9900
C(6)-C(7)	1.569(8)

Table A-11. (Continued).

C(6)-H(6A)	0.9900
C(6)-H(6B)	0.9900
C(7)-H(7A)	0.9900
C(7)-H(7B)	0.9900
C(8)-C(9)	1.513(8)
C(8)-H(8A)	0.9900
C(8)-H(8B)	0.9900
C(9)-H(9A)	0.9900
C(9)-H(9B)	0.9900
C(10)-C(11)	1.527(8)
C(10)-H(10A)	0.9900
C(10)-H(10B)	0.9900
C(11)-H(11A)	0.9900
C(11)-H(11B)	0.9900
C(12)-C(13)	1.529(8)
C(12)-H(12A)	0.9900
C(12)-H(12B)	0.9900
C(13)-C(14)	1.524(9)
C(13)-H(13A)	0.9900
C(13)-H(13B)	0.9900
C(14)-H(14A)	0.9900
C(14)-H(14B)	0.9900
C(15)-C(16)	1.538(8)
C(15)-H(15A)	0.9900
C(15)-H(15B)	0.9900
C(16)-H(16A)	0.9900
C(16)-H(16B)	0.9900
C(17)-C(18)	1.519(8)
C(17)-H(17A)	0.9900
C(17)-H(17C)	0.9900
C(18)-H(18C)	0.9900
C(18)-H(18A)	0.9900

Table A-12. Bond angles [°] for **[Zn(bme-dach)Cl]$_2$Pt**.

S(1)-Pt(1)-S(2)	86.39(5)
S(1)-Pt(1)-S(3)	179.38(6)
S(2)-Pt(1)-S(3)	93.93(5)
S(1)-Pt(1)-S(4)	92.86(5)
S(2)-Pt(1)-S(4)	177.41(5)
S(3)-Pt(1)-S(4)	86.84(5)
N(1)-Zn(1)-N(2)	74.92(18)
N(1)-Zn(1)-Cl(1)	108.00(13)
N(2)-Zn(1)-Cl(1)	109.64(14)
N(1)-Zn(1)-S(2)	135.07(13)
N(2)-Zn(1)-S(2)	84.81(14)
Cl(1)-Zn(1)-S(2)	116.56(6)
N(1)-Zn(1)-S(1)	84.41(13)
N(2)-Zn(1)-S(1)	135.21(14)
Cl(1)-Zn(1)-S(1)	114.47(6)
S(2)-Zn(1)-S(1)	82.59(5)
N(4)-Zn(2)-N(3)	74.51(18)
N(4)-Zn(2)-Cl(2)	106.54(14)
N(3)-Zn(2)-Cl(2)	110.46(13)
N(4)-Zn(2)-S(3)	134.89(14)
N(3)-Zn(2)-S(3)	84.32(13)
Cl(2)-Zn(2)-S(3)	118.17(6)
N(4)-Zn(2)-S(4)	85.55(14)
N(3)-Zn(2)-S(4)	136.23(13)
Cl(2)-Zn(2)-S(4)	112.47(6)
S(3)-Zn(2)-S(4)	83.02(5)
C(1)-S(1)-Pt(1)	107.5(2)
C(1)-S(1)-Zn(1)	97.6(2)
Pt(1)-S(1)-Zn(1)	85.09(5)
C(9)-S(2)-Pt(1)	108.2(2)
C(9)-S(2)-Zn(1)	98.7(2)
Pt(1)-S(2)-Zn(1)	85.60(5)
C(10)-S(3)-Pt(1)	107.4(2)
C(10)-S(3)-Zn(2)	98.72(19)
Pt(1)-S(3)-Zn(2)	83.20(5)
C(18)-S(4)-Pt(1)	105.4(2)
C(18)-S(4)-Zn(2)	96.9(2)
Pt(1)-S(4)-Zn(2)	83.03(5)
C(2)-N(1)-C(6)	113.2(5)
C(2)-N(1)-C(3)	109.7(4)
C(6)-N(1)-C(3)	110.7(4)
C(2)-N(1)-Zn(1)	109.5(4)
C(6)-N(1)-Zn(1)	105.8(3)
C(3)-N(1)-Zn(1)	107.7(4)

Table A-12. (Continued).

C(7)-N(2)-C(5)	111.5(5)
C(7)-N(2)-C(8)	112.8(5)
C(5)-N(2)-C(8)	109.9(5)
C(7)-N(2)-Zn(1)	105.0(3)
C(5)-N(2)-Zn(1)	108.6(4)
C(8)-N(2)-Zn(1)	108.9(4)
C(11)-N(3)-C(12)	108.4(4)
C(11)-N(3)-C(15)	112.1(4)
C(12)-N(3)-C(15)	111.9(4)
C(11)-N(3)-Zn(2)	109.6(3)
C(12)-N(3)-Zn(2)	110.6(4)
C(15)-N(3)-Zn(2)	104.2(3)
C(17)-N(4)-C(16)	113.7(5)
C(17)-N(4)-C(14)	109.2(5)
C(16)-N(4)-C(14)	110.5(5)
C(17)-N(4)-Zn(2)	109.0(4)
C(16)-N(4)-Zn(2)	104.9(4)
C(14)-N(4)-Zn(2)	109.5(4)
C(2)-C(1)-S(1)	112.5(4)
C(2)-C(1)-H(1A)	109.1
S(1)-C(1)-H(1A)	109.1
C(2)-C(1)-H(1B)	109.1
S(1)-C(1)-H(1B)	109.1
H(1A)-C(1)-H(1B)	107.8
N(1)-C(2)-C(1)	114.5(5)
N(1)-C(2)-H(2A)	108.6
C(1)-C(2)-H(2A)	108.6
N(1)-C(2)-H(2B)	108.6
C(1)-C(2)-H(2B)	108.6
H(2A)-C(2)-H(2B)	107.6
N(1)-C(3)-C(4)	113.8(5)
N(1)-C(3)-H(3A)	108.8
C(4)-C(3)-H(3A)	108.8
N(1)-C(3)-H(3B)	108.8
C(4)-C(3)-H(3B)	108.8
H(3A)-C(3)-H(3B)	107.7
C(5)-C(4)-C(3)	115.7(5)
C(5)-C(4)-H(4A)	108.3
C(3)-C(4)-H(4A)	108.3
C(5)-C(4)-H(4B)	108.3
C(3)-C(4)-H(4B)	108.3
H(4A)-C(4)-H(4B)	107.4
N(2)-C(5)-C(4)	114.5(5)
N(2)-C(5)-H(5A)	108.6
C(4)-C(5)-H(5A)	108.6

Table A-12. (Continued).

N(2)-C(5)-H(5B)	108.6
C(4)-C(5)-H(5B)	108.6
H(5A)-C(5)-H(5B)	107.6
N(1)-C(6)-C(7)	111.6(5)
N(1)-C(6)-H(6A)	109.3
C(7)-C(6)-H(6A)	109.3
N(1)-C(6)-H(6B)	109.3
C(7)-C(6)-H(6B)	109.3
H(6A)-C(6)-H(6B)	108.0
N(2)-C(7)-C(6)	112.2(5)
N(2)-C(7)-H(7A)	109.2
C(6)-C(7)-H(7A)	109.2
N(2)-C(7)-H(7B)	109.2
C(6)-C(7)-H(7B)	109.2
H(7A)-C(7)-H(7B)	107.9
N(2)-C(8)-C(9)	115.3(5)
N(2)-C(8)-H(8A)	108.5
C(9)-C(8)-H(8A)	108.5
N(2)-C(8)-H(8B)	108.5
C(9)-C(8)-H(8B)	108.5
H(8A)-C(8)-H(8B)	107.5
C(8)-C(9)-S(2)	111.6(4)
C(8)-C(9)-H(9A)	109.3
S(2)-C(9)-H(9A)	109.3
C(8)-C(9)-H(9B)	109.3
S(2)-C(9)-H(9B)	109.3
H(9A)-C(9)-H(9B)	108.0
C(11)-C(10)-S(3)	112.8(4)
C(11)-C(10)-H(10A)	109.0
S(3)-C(10)-H(10A)	109.0
C(11)-C(10)-H(10B)	109.0
S(3)-C(10)-H(10B)	109.0
H(10A)-C(10)-H(10B)	107.8
N(3)-C(11)-C(10)	114.1(5)
N(3)-C(11)-H(11A)	108.7
C(10)-C(11)-H(11A)	108.7
N(3)-C(11)-H(11B)	108.7
C(10)-C(11)-H(11B)	108.7
H(11A)-C(11)-H(11B)	107.6
N(3)-C(12)-C(13)	112.5(5)
N(3)-C(12)-H(12A)	109.1
C(13)-C(12)-H(12A)	109.1
N(3)-C(12)-H(12B)	109.1
C(13)-C(12)-H(12B)	109.1
H(12A)-C(12)-H(12B)	107.8

Table A-12. (Continued).

C(14)-C(13)-C(12)	115.7(5)
C(14)-C(13)-H(13A)	108.3
C(12)-C(13)-H(13A)	108.3
C(14)-C(13)-H(13B)	108.3
C(12)-C(13)-H(13B)	108.3
H(13A)-C(13)-H(13B)	107.4
N(4)-C(14)-C(13)	113.9(5)
N(4)-C(14)-H(14A)	108.8
C(13)-C(14)-H(14A)	108.8
N(4)-C(14)-H(14B)	108.8
C(13)-C(14)-H(14B)	108.8
H(14A)-C(14)-H(14B)	107.7
N(3)-C(15)-C(16)	111.2(5)
N(3)-C(15)-H(15A)	109.4
C(16)-C(15)-H(15A)	109.4
N(3)-C(15)-H(15B)	109.4
C(16)-C(15)-H(15B)	109.4
H(15A)-C(15)-H(15B)	108.0
N(4)-C(16)-C(15)	112.5(5)
N(4)-C(16)-H(16A)	109.1
C(15)-C(16)-H(16A)	109.1
N(4)-C(16)-H(16B)	109.1
C(15)-C(16)-H(16B)	109.1
H(16A)-C(16)-H(16B)	107.8
N(4)-C(17)-C(18)	114.8(5)
N(4)-C(17)-H(17A)	108.6
C(18)-C(17)-H(17A)	108.6
N(4)-C(17)-H(17C)	108.6
C(18)-C(17)-H(17C)	108.6
H(17A)-C(17)-H(17C)	107.5
C(17)-C(18)-S(4)	112.4(4)
C(17)-C(18)-H(18C)	109.1
S(4)-C(18)-H(18C)	109.1
C(17)-C(18)-H(18A)	109.1
S(4)-C(18)-H(18A)	109.1
H(18C)-C(18)-H(18A)	107.9

Symmetry transformations used to generate equivalent atoms: -x+1/2, -y, z+1/2

Table A-13. Crystal data and structure refinement for **Pd(bme-dach)**.

Empirical formula	$C_9 H_{18} N_2 Pd S_2$	
Formula weight	324.77	
Temperature	110(2) K	
Wavelength	0.71073 Å	
Crystal system	Orthorhombic	
Space group	Pnma	
Unit cell dimensions	a = 9.961(5) Å	α= 90°.
	b = 15.105(7) Å	β= 90°.
	c = 7.514(4) Å	γ = 90°.
Volume	1130.5(9) $Å^3$	
Z	4	
Density (calculated)	1.908 Mg/m^3	
Absorption coefficient	1.974 mm^{-1}	
F(000)	656	
Crystal size	0.22 x 0.05 x 0.05 mm^3	
Theta range for data collection	2.70 to 27.49°.	
Index ranges	-12<=h<=12, -19<=k<=13, -9<=l<=9	
Reflections collected	7572	
Independent reflections	1347 [R(int) = 0.0877]	
Completeness to theta = 27.49°	99.9 %	

Table A-13. (Continued).

Absorption correction	Semi-empirical from equivalents
Max. and min. transmission	0.9060 and 0.6763
Refinement method	Full-matrix least-squares on F^2
Data / restraints / parameters	1347 / 24 / 71
Goodness-of-fit on F^2	1.098
Final R indices [I>2sigma(I)]	R1 = 0.0618, wR2 = 0.1614
R indices (all data)	R1 = 0.0905, wR2 = 0.1809
Largest diff. peak and hole	2.311 and -1.693 e.$Å^{-3}$

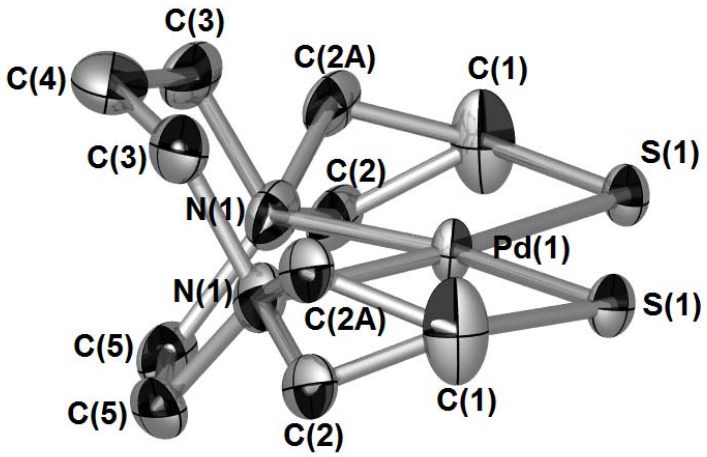

Pd(bme-dach), half of the molecule is symmetry-generated from the other half.

Table A-14. Bond lengths [Å] for **Pd(bme-dach)**.

Pd(1)-N(1)#1	2.074(7)
Pd(1)-N(1)	2.074(7)
Pd(1)-S(1)	2.2825(19)
Pd(1)-S(1)#1	2.2825(19)
S(1)-C(1)	1.808(9)
C(1)-C(2A)	1.41(3)
C(1)-C(2)	1.445(16)
C(1)-H(1A)	0.9900
C(1)-H(1B)	0.9900
C(2)-N(1)	1.515(14)
C(2)-H(2A)	0.9900
C(2)-H(2B)	0.9900
C(2A)-N(1)	1.57(3)
C(2A)-H(2A1)	0.9900
C(2A)-H(2A2)	0.9900
C(3)-C(4)	1.378(11)
C(3)-N(1)	1.465(11)
C(3)-H(3A)	0.9900
C(3)-H(3B)	0.9900
C(4)-C(3)#1	1.378(11)
C(4)-H(4A)	0.9900
C(4)-H(4B)	0.9900
C(5)-N(1)	1.518(11)
C(5)-C(5)#1	1.674(18)
C(5)-H(5A)	0.9900
C(5)-H(5B)	0.9900

Table A-15. Bond angles [°] for **Pd(bme-dach)**.

N(1)#1-Pd(1)-N(1)	79.0(4)
N(1)#1-Pd(1)-S(1)	168.6(2)
N(1)-Pd(1)-S(1)	89.7(2)
N(1)#1-Pd(1)-S(1)#1	89.7(2)
N(1)-Pd(1)-S(1)#1	168.6(2)
S(1)-Pd(1)-S(1)#1	101.70(10)
C(1)-S(1)-Pd(1)	95.5(3)
C(2A)-C(1)-C(2)	42.3(13)
C(2A)-C(1)-S(1)	119.6(13)
C(2)-C(1)-S(1)	115.6(8)
C(2A)-C(1)-H(1A)	67.5
C(2)-C(1)-H(1A)	108.4
S(1)-C(1)-H(1A)	108.4
C(2A)-C(1)-H(1B)	131.0
C(2)-C(1)-H(1B)	108.4
S(1)-C(1)-H(1B)	108.4
H(1A)-C(1)-H(1B)	107.4
C(1)-C(2)-N(1)	112.7(9)
C(1)-C(2)-H(2A)	109.1
N(1)-C(2)-H(2A)	109.1
C(1)-C(2)-H(2B)	109.1
N(1)-C(2)-H(2B)	109.1
H(2A)-C(2)-H(2B)	107.8
C(1)-C(2A)-N(1)	111.7(18)
C(1)-C(2A)-H(2A1)	109.3
N(1)-C(2A)-H(2A1)	109.3
C(1)-C(2A)-H(2A2)	109.3
N(1)-C(2A)-H(2A2)	109.3
H(2A1)-C(2A)-H(2A2)	107.9
C(4)-C(3)-N(1)	117.6(9)
C(4)-C(3)-H(3A)	107.9
N(1)-C(3)-H(3A)	107.9
C(4)-C(3)-H(3B)	107.9
N(1)-C(3)-H(3B)	107.9
H(3A)-C(3)-H(3B)	107.2
C(3)-C(4)-C(3)#1	119.1(13)
C(3)-C(4)-H(4A)	107.5
C(3)#1-C(4)-H(4A)	107.5
C(3)-C(4)-H(4B)	107.5
C(3)#1-C(4)-H(4B)	107.5
H(4A)-C(4)-H(4B)	107.0
N(1)-C(5)-C(5)#1	108.5(4)
N(1)-C(5)-H(5A)	110.0
C(5)#1-C(5)-H(5A)	110.0
N(1)-C(5)-H(5B)	110.0

Table A-15. (Continued).

C(5)#1-C(5)-H(5B)	110.0
H(5A)-C(5)-H(5B)	108.4
C(3)-N(1)-C(2)	117.8(8)
C(3)-N(1)-C(5)	110.0(7)
C(2)-N(1)-C(5)	106.2(7)
C(3)-N(1)-C(2A)	82.4(12)
C(2)-N(1)-C(2A)	39.1(12)
C(5)-N(1)-C(2A)	138.3(13)
C(3)-N(1)-Pd(1)	106.5(5)
C(2)-N(1)-Pd(1)	109.8(6)
C(5)-N(1)-Pd(1)	105.9(5)
C(2A)-N(1)-Pd(1)	108.3(10)

Symmetry transformations used to generate equivalent atoms:
#1 x, -y+1/2, z

Table A-16. Crystal data and structure refinement for **[Au(bme-dach)]BPh_4**.

Empirical formula	C_{33} H_{38} Au B N_2 S_2	
Formula weight	734.55	
Temperature	110(2) K	
Wavelength	1.54178 Å	
Crystal system	Monoclinic	
Space group	P21/c	
Unit cell dimensions	a = 10.643(4) Å	α= 90°.
	b = 14.184(5) Å	β= 117.051(18)°.
	c = 21.407(7) Å	γ = 90°.
Volume	2878.1(18) $Å^3$	
Z	4	
Density (calculated)	1.695 Mg/m^3	
Absorption coefficient	11.149 mm^{-1}	
F(000)	1464	
Crystal size	0.02 x 0.02 x 0.02 mm^3	
Theta range for data collection	3.88 to 60.82°.	
Index ranges	-12<=h<=11, -16<=k<=15, -23<=l<=23	
Reflections collected	20083	
Independent reflections	4222 [R(int) = 0.3155]	
Completeness to theta = 60.82°	96.7 %	

Table A-16. (Continued).

Absorption correction	Semi-empirical from equivalents
Max. and min. transmission	0.8078 and 0.8078
Refinement method	Full-matrix least-squares on F^2
Data / restraints / parameters	4222 / 346 / 353
Goodness-of-fit on F^2	1.062
Final R indices [I>2sigma(I)]	R1 = 0.0948, wR2 = 0.2289
R indices (all data)	R1 = 0.1704, wR2 = 0.2721
Extinction coefficient	0.00020(7)
Largest diff. peak and hole	3.253 and -2.930 e.$Å^{-3}$

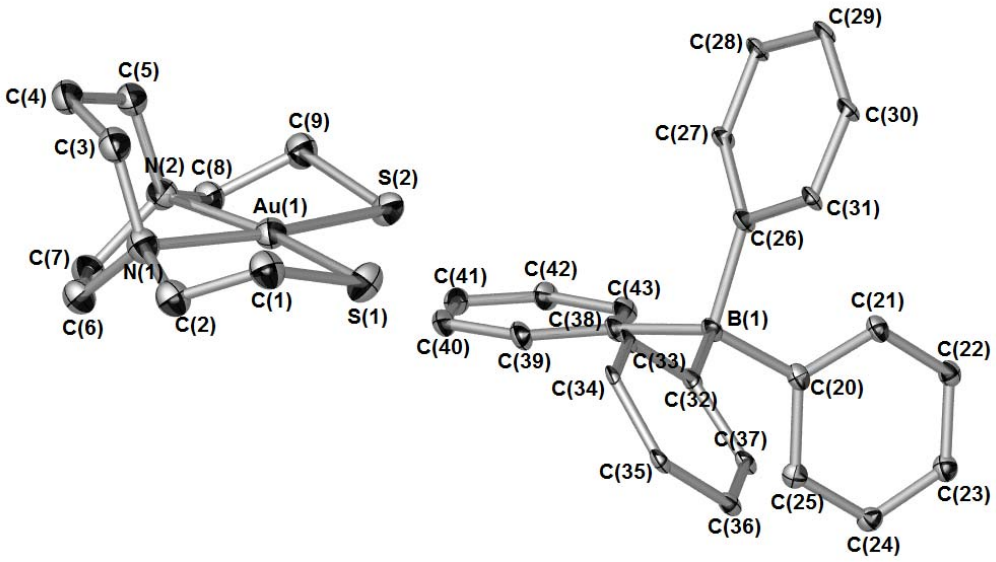

[Au(bme-dach)]BPh_4

Table A-17. Bond lengths [Å] for **[Au(bme-dach)]BPh_4**.

B(1)-C(20)	1.59(3)
B(1)-C(26)	1.63(3)
B(1)-C(38)	1.65(3)
B(1)-C(32)	1.68(3)
Au(1)-N(2)	2.12(2)
Au(1)-N(1)	2.18(2)
Au(1)-S(1)	2.290(6)
Au(1)-S(2)	2.293(6)
S(1)-C(1)	1.86(2)
S(2)-C(9)	1.90(3)
N(1)-C(2)	1.41(3)
N(1)-C(3)	1.47(3)
N(1)-C(6)	1.49(3)
N(2)-C(5)	1.44(3)
N(2)-C(8)	1.50(3)
N(2)-C(7)	1.51(3)
C(1)-C(2)	1.50(3)
C(1)-H(1A)	0.9900
C(1)-H(1B)	0.9900
C(2)-H(2A)	0.9900
C(2)-H(2B)	0.9900
C(3)-C(4)	1.52(3)
C(3)-H(3A)	0.9900
C(3)-H(3B)	0.9900
C(4)-C(5)	1.52(3)
C(4)-H(4A)	0.9900
C(4)-H(4B)	0.9900
C(5)-H(5A)	0.9900
C(5)-H(5B)	0.9900
C(6)-C(7)	1.50(3)
C(6)-H(6A)	0.9900
C(6)-H(6B)	0.9900
C(7)-H(7A)	0.9900
C(7)-H(7B)	0.9900
C(8)-C(9)	1.46(3)
C(8)-H(8A)	0.9900
C(8)-H(8B)	0.9900
C(9)-H(9A)	0.9900
C(9)-H(9B)	0.9900
C(20)-C(21)	1.39(3)
C(20)-C(25)	1.43(3)
C(21)-C(22)	1.40(3)
C(21)-H(21)	0.9500
C(22)-C(23)	1.35(3)

Table A-17. (Continued).

C(22)-H(22)	0.9500
C(23)-C(24)	1.35(3)
C(23)-H(23)	0.9500
C(24)-C(25)	1.40(3)
C(24)-H(24)	0.9500
C(25)-H(25)	0.9500
C(26)-C(27)	1.41(3)
C(26)-C(31)	1.44(3)
C(27)-C(28)	1.35(3)
C(27)-H(27)	0.9500
C(28)-C(29)	1.41(3)
C(28)-H(28)	0.9500
C(29)-C(30)	1.38(3)
C(29)-H(29)	0.9500
C(30)-C(31)	1.36(3)
C(30)-H(30)	0.9500
C(31)-H(31)	0.9500
C(32)-C(33)	1.39(3)
C(32)-C(37)	1.43(3)
C(33)-C(34)	1.35(3)
C(33)-H(33)	0.9500
C(34)-C(35)	1.40(3)
C(34)-H(34)	0.9500
C(35)-C(36)	1.44(3)
C(35)-H(35)	0.9500
C(36)-C(37)	1.44(3)
C(36)-H(36)	0.9500
C(37)-H(37)	0.9500
C(38)-C(43)	1.40(3)
C(38)-C(39)	1.42(3)
C(39)-C(40)	1.35(3)
C(39)-H(39)	0.9500
C(40)-C(41)	1.45(3)
C(40)-H(40)	0.9500
C(41)-C(42)	1.35(3)
C(41)-H(41)	0.9500
C(42)-C(43)	1.39(3)
C(42)-H(42)	0.9500
C(43)-H(43)	0.9500

Table A-18. Bond angles [°] for **[Au(bme-dach)]BPh$_4$**.

C(20)-B(1)-C(26)	106.7(17)
C(20)-B(1)-C(38)	109.4(18)
C(26)-B(1)-C(38)	109.9(17)
C(20)-B(1)-C(32)	113.6(18)
C(26)-B(1)-C(32)	104.4(17)
C(38)-B(1)-C(32)	112.6(17)
N(2)-Au(1)-N(1)	79.2(8)
N(2)-Au(1)-S(1)	169.4(6)
N(1)-Au(1)-S(1)	90.3(6)
N(2)-Au(1)-S(2)	91.1(5)
N(1)-Au(1)-S(2)	170.2(6)
S(1)-Au(1)-S(2)	99.5(2)
C(1)-S(1)-Au(1)	93.9(8)
C(9)-S(2)-Au(1)	93.5(8)
C(2)-N(1)-C(3)	118(2)
C(2)-N(1)-C(6)	116.3(19)
C(3)-N(1)-C(6)	112.5(19)
C(2)-N(1)-Au(1)	104.9(15)
C(3)-N(1)-Au(1)	102.5(14)
C(6)-N(1)-Au(1)	99.3(13)
C(5)-N(2)-C(8)	114.2(19)
C(5)-N(2)-C(7)	114.5(19)
C(8)-N(2)-C(7)	113.5(18)
C(5)-N(2)-Au(1)	105.4(15)
C(8)-N(2)-Au(1)	105.8(15)
C(7)-N(2)-Au(1)	101.8(14)
C(2)-C(1)-S(1)	109.2(17)
C(2)-C(1)-H(1A)	109.8
S(1)-C(1)-H(1A)	109.8
C(2)-C(1)-H(1B)	109.8
S(1)-C(1)-H(1B)	109.8
H(1A)-C(1)-H(1B)	108.3
N(1)-C(2)-C(1)	117(2)
N(1)-C(2)-H(2A)	108.0
C(1)-C(2)-H(2A)	108.0
N(1)-C(2)-H(2B)	108.0
C(1)-C(2)-H(2B)	108.0
H(2A)-C(2)-H(2B)	107.2
N(1)-C(3)-C(4)	116(2)
N(1)-C(3)-H(3A)	108.4
C(4)-C(3)-H(3A)	108.4
N(1)-C(3)-H(3B)	108.4
C(4)-C(3)-H(3B)	108.4
H(3A)-C(3)-H(3B)	107.5
C(3)-C(4)-C(5)	112(2)

Table A-18. (Continued).

C(3)-C(4)-H(4A)	109.2
C(5)-C(4)-H(4A)	109.2
C(3)-C(4)-H(4B)	109.2
C(5)-C(4)-H(4B)	109.2
H(4A)-C(4)-H(4B)	107.9
N(2)-C(5)-C(4)	114(2)
N(2)-C(5)-H(5A)	108.7
C(4)-C(5)-H(5A)	108.7
N(2)-C(5)-H(5B)	108.7
C(4)-C(5)-H(5B)	108.7
H(5A)-C(5)-H(5B)	107.6
N(1)-C(6)-C(7)	117(2)
N(1)-C(6)-H(6A)	108.0
C(7)-C(6)-H(6A)	108.0
N(1)-C(6)-H(6B)	108.0
C(7)-C(6)-H(6B)	108.0
H(6A)-C(6)-H(6B)	107.2
C(6)-C(7)-N(2)	112(2)
C(6)-C(7)-H(7A)	109.3
N(2)-C(7)-H(7A)	109.3
C(6)-C(7)-H(7B)	109.3
N(2)-C(7)-H(7B)	109.3
H(7A)-C(7)-H(7B)	107.9
C(9)-C(8)-N(2)	114(2)
C(9)-C(8)-H(8A)	108.7
N(2)-C(8)-H(8A)	108.7
C(9)-C(8)-H(8B)	108.7
N(2)-C(8)-H(8B)	108.7
H(8A)-C(8)-H(8B)	107.6
C(8)-C(9)-S(2)	109.4(17)
C(8)-C(9)-H(9A)	109.8
S(2)-C(9)-H(9A)	109.8
C(8)-C(9)-H(9B)	109.8
S(2)-C(9)-H(9B)	109.8
H(9A)-C(9)-H(9B)	108.2
C(21)-C(20)-C(25)	114(2)
C(21)-C(20)-B(1)	125.8(19)
C(25)-C(20)-B(1)	120.2(19)
C(20)-C(21)-C(22)	123(2)
C(20)-C(21)-H(21)	118.4
C(22)-C(21)-H(21)	118.4
C(23)-C(22)-C(21)	121(2)
C(23)-C(22)-H(22)	119.7
C(21)-C(22)-H(22)	119.7
C(22)-C(23)-C(24)	119(2)
C(22)-C(23)-H(23)	120.3

Table A-18. (Continued).

C(24)-C(23)-H(23)	120.3
C(23)-C(24)-C(25)	121(2)
C(23)-C(24)-H(24)	119.5
C(25)-C(24)-H(24)	119.5
C(24)-C(25)-C(20)	122(2)
C(24)-C(25)-H(25)	119.2
C(20)-C(25)-H(25)	119.2
C(27)-C(26)-C(31)	110.1(18)
C(27)-C(26)-B(1)	127.0(19)
C(31)-C(26)-B(1)	122.4(18)
C(28)-C(27)-C(26)	127(2)
C(28)-C(27)-H(27)	116.6
C(26)-C(27)-H(27)	116.6
C(27)-C(28)-C(29)	120(2)
C(27)-C(28)-H(28)	119.8
C(29)-C(28)-H(28)	119.8
C(30)-C(29)-C(28)	116.4(18)
C(30)-C(29)-H(29)	121.8
C(28)-C(29)-H(29)	121.8
C(31)-C(30)-C(29)	122(2)
C(31)-C(30)-H(30)	119.2
C(29)-C(30)-H(30)	119.2
C(30)-C(31)-C(26)	125(2)
C(30)-C(31)-H(31)	117.6
C(26)-C(31)-H(31)	117.6
C(33)-C(32)-C(37)	118.0(19)
C(33)-C(32)-B(1)	121.9(18)
C(37)-C(32)-B(1)	120.0(18)
C(34)-C(33)-C(32)	123(2)
C(34)-C(33)-H(33)	118.4
C(32)-C(33)-H(33)	118.4
C(33)-C(34)-C(35)	122(2)
C(33)-C(34)-H(34)	119.1
C(35)-C(34)-H(34)	119.1
C(34)-C(35)-C(36)	118.0(19)
C(34)-C(35)-H(35)	121.0
C(36)-C(35)-H(35)	121.0
C(37)-C(36)-C(35)	119.2(19)
C(37)-C(36)-H(36)	120.4
C(35)-C(36)-H(36)	120.4
C(32)-C(37)-C(36)	120(2)
C(32)-C(37)-H(37)	120.2
C(36)-C(37)-H(37)	120.2
C(43)-C(38)-C(39)	117(2)
C(43)-C(38)-B(1)	119.6(19)
C(39)-C(38)-B(1)	123.4(19)

Table A-18. (Continued).

C(40)-C(39)-C(38)	122(2)
C(40)-C(39)-H(39)	119.0
C(38)-C(39)-H(39)	119.0
C(39)-C(40)-C(41)	119(2)
C(39)-C(40)-H(40)	120.3
C(41)-C(40)-H(40)	120.3
C(42)-C(41)-C(40)	119(2)
C(42)-C(41)-H(41)	120.5
C(40)-C(41)-H(41)	120.5
C(41)-C(42)-C(43)	121(2)
C(41)-C(42)-H(42)	119.4
C(43)-C(42)-H(42)	119.4
C(42)-C(43)-C(38)	122(2)
C(42)-C(43)-H(43)	119.1
C(38)-C(43)-H(43)	119.1

Symmetry transformations used to generate equivalent atoms: x, -y-1/2, z-1/2

Table A-19. Crystal data and structure refinement for **[Zn(bme-dach)Cl]$_2$Pd**.

Empirical formula	$C_{9.50}\ H_{18.50}\ Cl_{2.50}\ N_2\ Pd_{0.50}\ S_2\ Zn$	
Formula weight	432.08	
Temperature	110(2) K	
Wavelength	1.54178 Å	
Crystal system	Monoclinic	
Space group	P2(1)/c	
Unit cell dimensions	a = 7.4293(2) Å	α= 90°.
	b = 12.4008(4) Å	β= 97.128(2)°.
	c = 16.6452(6) Å	γ = 90°.
Volume	1521.66(8) Å^3	
Z	4	
Density (calculated)	1.886 Mg/m^3	
Absorption coefficient	13.312 mm^{-1}	
F(000)	868	
Crystal size	0.13 x 0.12 x 0.04 mm^3	
Theta range for data collection	4.46 to 59.28°.	
Index ranges	-8<=h<=8, -13<=k<=13, -18<=l<=18	
Reflections collected	9433	
Independent reflections	2190 [R(int) = 0.0585]	
Completeness to theta = 59.28°	99.0 %	

Table A-19. (Continued).

Absorption correction	Semi-empirical from equivalents
Max. and min. transmission	0.6180 and 0.2765
Refinement method	Full-matrix least-squares on F^2
Data / restraints / parameters	2190 / 0 / 178
Goodness-of-fit on F^2	1.040
Final R indices [I>2sigma(I)]	R1 = 0.0295, wR2 = 0.0769
R indices (all data)	R1 = 0.0349, wR2 = 0.0799
Largest diff. peak and hole	0.518 and -0.969 e.Å^{-3}

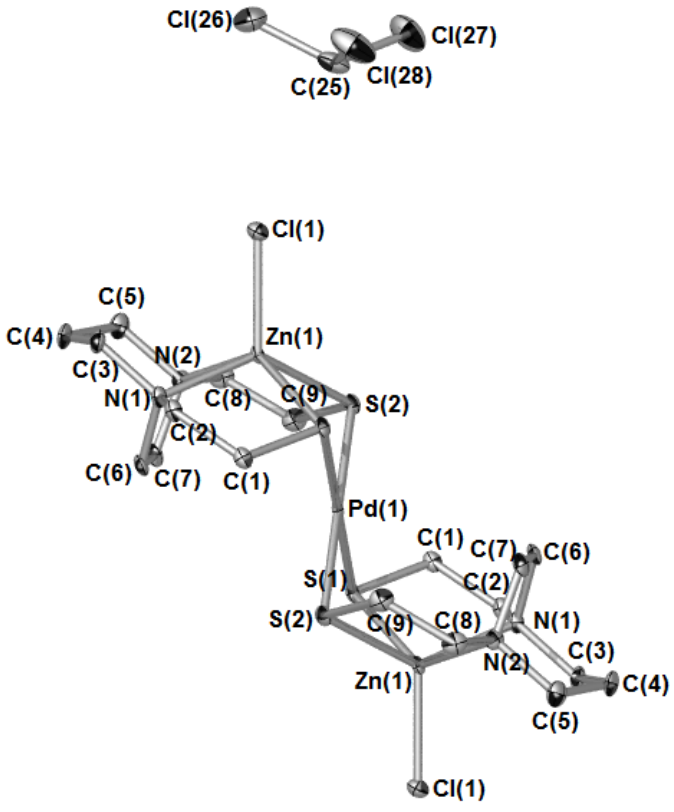

[Zn(bme-dach)Cl]$_2$Pd, half of the molecule is symmetry-generated from the other half.

Table A-20. Bond lengths [Å] for **[Zn(bme-dach)Cl]$_2$Pd**.

Pd(1)-S(1)	2.3510(8)
Pd(1)-S(1)#1	2.3510(8)
Pd(1)-S(2)#1	2.3543(8)
Pd(1)-S(2)	2.3543(8)
Pd(1)-Zn(1)#1	3.1610(4)
Zn(1)-N(1)	2.157(2)
Zn(1)-N(2)	2.185(2)
Zn(1)-Cl(1)	2.2415(9)
Zn(1)-S(2)	2.4219(9)
Zn(1)-S(1)	2.4373(9)
S(1)-C(1)	1.826(3)
S(2)-C(9)	1.835(3)
N(1)-C(2)	1.476(4)
N(1)-C(6)	1.476(4)
N(1)-C(3)	1.497(4)
N(2)-C(7)	1.472(4)
N(2)-C(8)	1.483(4)
N(2)-C(5)	1.489(4)
C(1)-C(2)	1.533(4)
C(3)-C(4)	1.522(5)
C(4)-C(5)	1.516(5)
C(6)-C(7)	1.560(4)
C(8)-C(9)	1.528(5)
C(25)-Cl(28)#2	1.514(9)
C(25)-C(25)#2	1.597(16)
C(25)-Cl(27)#2	1.662(9)
C(25)-Cl(27)	1.751(9)
C(25)-Cl(26)	1.758(10)
C(25)-Cl(28)	1.761(9)
Cl(26)-Cl(28)#2	2.359(5)
Cl(26)-Cl(27)#2	2.429(6)
Cl(27)-C(25)#2	1.662(9)
Cl(27)-Cl(26)#2	2.429(6)
Cl(28)-C(25)#2	1.515(9)
Cl(28)-Cl(26)#2	2.359(5)

Table A-21. Bond angles [°]for **[Zn(bme-dach)Cl]$_2$Pd**.

S(1)-Pd(1)-S(1)#1	180.0
S(1)-Pd(1)-S(2)#1	93.68(3)
S(1)#1-Pd(1)-S(2)#1	86.32(3)
S(1)-Pd(1)-S(2)	86.32(3)
S(1)#1-Pd(1)-S(2)	93.68(3)
S(2)#1-Pd(1)-S(2)	180.00(3)
S(1)-Pd(1)-Zn(1)#1	130.13(2)
S(1)#1-Pd(1)-Zn(1)#1	49.87(2)
S(2)#1-Pd(1)-Zn(1)#1	49.49(2)
S(2)-Pd(1)-Zn(1)#1	130.51(2)
N(1)-Zn(1)-N(2)	74.75(9)
N(1)-Zn(1)-Cl(1)	107.09(7)
N(2)-Zn(1)-Cl(1)	108.32(7)
N(1)-Zn(1)-S(2)	135.66(7)
N(2)-Zn(1)-S(2)	84.93(7)
Cl(1)-Zn(1)-S(2)	116.68(3)
N(1)-Zn(1)-S(1)	84.25(7)
N(2)-Zn(1)-S(1)	134.77(7)
Cl(1)-Zn(1)-S(1)	116.07(3)
S(2)-Zn(1)-S(1)	82.96(3)
C(1)-S(1)-Pd(1)	107.68(10)
C(1)-S(1)-Zn(1)	98.58(10)
Pd(1)-S(1)-Zn(1)	82.60(3)
C(9)-S(2)-Pd(1)	106.03(11)
C(9)-S(2)-Zn(1)	98.46(11)
Pd(1)-S(2)-Zn(1)	82.86(3)
C(2)-N(1)-C(6)	112.5(2)
C(2)-N(1)-C(3)	107.8(2)
C(6)-N(1)-C(3)	111.4(2)
C(2)-N(1)-Zn(1)	110.13(18)
C(6)-N(1)-Zn(1)	104.87(18)
C(3)-N(1)-Zn(1)	110.14(19)
C(7)-N(2)-C(8)	112.7(2)
C(7)-N(2)-C(5)	111.3(2)
C(8)-N(2)-C(5)	108.7(2)
C(7)-N(2)-Zn(1)	104.06(18)
C(8)-N(2)-Zn(1)	109.62(19)
C(5)-N(2)-Zn(1)	110.47(19)
C(2)-C(1)-S(1)	112.5(2)
N(1)-C(2)-C(1)	114.0(2)
N(1)-C(3)-C(4)	113.1(3)
C(5)-C(4)-C(3)	115.9(3)
N(2)-C(5)-C(4)	113.1(3)
N(1)-C(6)-C(7)	111.2(2)
N(2)-C(7)-C(6)	111.6(2)

Table A-21. (Continued).

N(2)-C(8)-C(9)	114.4(3)
C(8)-C(9)-S(2)	113.4(2)
Cl(28)#2-C(25)-C(25)#2	68.9(5)
Cl(28)#2-C(25)-Cl(27)#2	130.1(6)
C(25)#2-C(25)-Cl(27)#2	65.0(5)
Cl(28)#2-C(25)-Cl(27)	20.0(3)
C(25)#2-C(25)-Cl(27)	59.3(5)
Cl(27)#2-C(25)-Cl(27)	124.3(5)
Cl(28)#2-C(25)-Cl(26)	92.0(5)
C(25)#2-C(25)-Cl(26)	114.5(8)
Cl(27)#2-C(25)-Cl(26)	90.4(4)
Cl(27)-C(25)-Cl(26)	111.8(4)
Cl(28)#2-C(25)-Cl(28)	122.2(5)
C(25)#2-C(25)-Cl(28)	53.4(4)
Cl(27)#2-C(25)-Cl(28)	20.4(2)
Cl(27)-C(25)-Cl(28)	110.2(5)
Cl(26)-C(25)-Cl(28)	110.3(5)
C(25)-Cl(26)-Cl(28)#2	39.9(3)
C(25)-Cl(26)-Cl(27)#2	43.2(3)
Cl(28)#2-Cl(26)-Cl(27)#2	73.96(13)
C(25)#2-Cl(27)-C(25)	55.7(5)
C(25)#2-Cl(27)-Cl(26)#2	46.4(4)
C(25)-Cl(27)-Cl(26)#2	83.3(4)
C(25)#2-Cl(28)-C(25)	57.8(5)
C(25)#2-Cl(28)-Cl(26)#2	48.1(4)
C(25)-Cl(28)-Cl(26)#2	85.2(3)

Symmetry transformations used to generate equivalent atoms:
#1 -x+1,-y+1,-z+1 #2 -x,-y+1,-z

Table A-22. Crystal data and structure refinement for **Zn-1'-Ac**.

Empirical formula	C_{11} H_{20} N_2 O_2 S_2 Zn	
Formula weight	341.78	
Temperature	110(2) K	
Wavelength	0.71073 Å	
Crystal system	Orthorhombic	
Space group	P2(1)2(1)2(1)	
Unit cell dimensions	a = 9.266(9) Å	α= 90°.
	b = 12.332(12) Å	β= 90°.
	c = 12.472(12) Å	γ = 90°.
Volume	1425(2) $Å^3$	
Z	4	
Density (calculated)	1.593 Mg/m^3	
Absorption coefficient	2.012 mm^{-1}	
F(000)	712	
Crystal size	0.20 x 0.10 x 0.10 mm^3	
Theta range for data collection	2.74 to 25.00°.	
Index ranges	-10<=h<=10, -14<=k<=14, -14<=l<=14	
Reflections collected	11041	
Independent reflections	2462 [R(int) = 0.0678]	
Completeness to theta = 25.00°	98.6 %	

Table A-22. (Continued).

Absorption correction	Semi-empirical from equivalents
Max. and min. transmission	0.8242 and 0.6891
Refinement method	Full-matrix least-squares on F^2
Data / restraints / parameters	2462 / 0 / 163
Goodness-of-fit on F^2	1.049
Final R indices [I>2sigma(I)]	R1 = 0.0261, wR2 = 0.0432
R indices (all data)	R1 = 0.0352, wR2 = 0.0451
Absolute structure parameter	0.008(12)
Largest diff. peak and hole	0.225 and -0.201 e.Å^{-3}

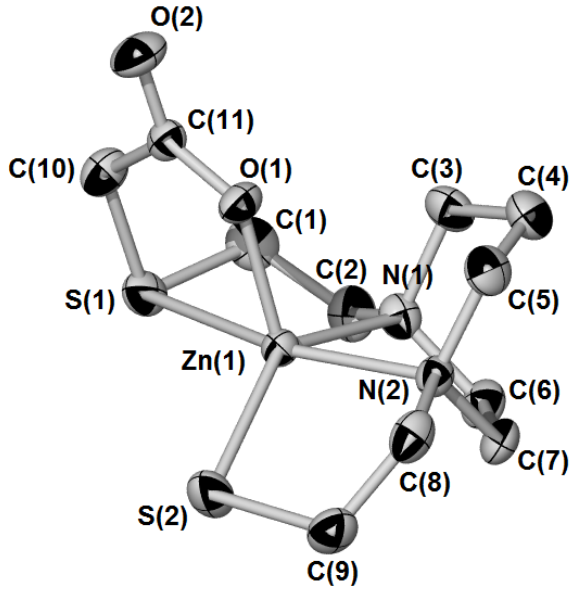

Zn-1'-Ac

Table A-23. Bond lengths [Å] for **Zn-1'-Ac**.

Zn(1)-O(1)	1.983(2)
Zn(1)-N(1)	2.159(3)
Zn(1)-N(2)	2.171(3)
Zn(1)-S(2)	2.2631(18)
Zn(1)-S(1)	2.587(3)
S(1)-C(10)	1.810(3)
S(1)-C(1)	1.826(4)
O(1)-C(11)	1.270(4)
N(1)-C(2)	1.457(4)
N(1)-C(6)	1.491(4)
N(1)-C(3)	1.509(4)
C(1)-C(2)	1.505(5)
C(1)-H(1A)	0.9900
C(1)-H(1B)	0.9900
S(2)-C(9)	1.820(4)
O(2)-C(11)	1.229(3)
N(2)-C(8)	1.459(4)
N(2)-C(5)	1.482(4)
N(2)-C(7)	1.489(4)
C(2)-H(2A)	0.9900
C(2)-H(2B)	0.9900
C(3)-C(4)	1.523(5)
C(3)-H(3A)	0.9900
C(3)-H(3B)	0.9900
C(4)-C(5)	1.516(5)
C(4)-H(4A)	0.9900
C(4)-H(4B)	0.9900
C(5)-H(5A)	0.9900
C(5)-H(5B)	0.9900
C(6)-C(7)	1.531(5)
C(6)-H(6A)	0.9900
C(6)-H(6B)	0.9900
C(7)-H(7A)	0.9900
C(7)-H(7B)	0.9900
C(8)-C(9)	1.528(4)
C(8)-H(8A)	0.9900
C(8)-H(8B)	0.9900
C(9)-H(9A)	0.9900
C(9)-H(9B)	0.9900
C(10)-C(11)	1.510(4)
C(10)-H(10A)	0.9900
C(10)-H(10B)	0.9900

Table A-24. Bond angles [°] for **Zn-1'-Ac**.

O(1)-Zn(1)-N(1)	105.24(10)
O(1)-Zn(1)-N(2)	101.39(9)
N(1)-Zn(1)-N(2)	75.21(10)
O(1)-Zn(1)-S(2)	116.78(9)
N(1)-Zn(1)-S(2)	137.38(7)
N(2)-Zn(1)-S(2)	89.31(7)
O(1)-Zn(1)-S(1)	82.46(7)
N(1)-Zn(1)-S(1)	83.65(8)
N(2)-Zn(1)-S(1)	158.81(7)
S(2)-Zn(1)-S(1)	107.72(4)
C(10)-S(1)-C(1)	102.57(17)
C(10)-S(1)-Zn(1)	92.05(11)
C(1)-S(1)-Zn(1)	92.74(12)
C(11)-O(1)-Zn(1)	126.4(2)
C(2)-N(1)-C(6)	110.7(2)
C(2)-N(1)-C(3)	111.7(3)
C(6)-N(1)-C(3)	110.1(3)
C(2)-N(1)-Zn(1)	111.7(2)
C(6)-N(1)-Zn(1)	107.35(19)
C(3)-N(1)-Zn(1)	105.12(18)
C(2)-C(1)-S(1)	111.2(2)
C(2)-C(1)-H(1A)	109.4
S(1)-C(1)-H(1A)	109.4
C(2)-C(1)-H(1B)	109.4
S(1)-C(1)-H(1B)	109.4
H(1A)-C(1)-H(1B)	108.0
C(9)-S(2)-Zn(1)	97.47(10)
C(8)-N(2)-C(5)	111.5(2)
C(8)-N(2)-C(7)	112.0(2)
C(5)-N(2)-C(7)	111.3(2)
C(8)-N(2)-Zn(1)	106.83(19)
C(5)-N(2)-Zn(1)	109.34(19)
C(7)-N(2)-Zn(1)	105.56(19)
N(1)-C(2)-C(1)	113.9(3)
N(1)-C(2)-H(2A)	108.8
C(1)-C(2)-H(2A)	108.8
N(1)-C(2)-H(2B)	108.8
C(1)-C(2)-H(2B)	108.8
H(2A)-C(2)-H(2B)	107.7
N(1)-C(3)-C(4)	113.8(3)
N(1)-C(3)-H(3A)	108.8
C(4)-C(3)-H(3A)	108.8

Table A-24. (Continued).

N(1)-C(3)-H(3B)	108.8
C(4)-C(3)-H(3B)	108.8
H(3A)-C(3)-H(3B)	107.7
C(5)-C(4)-C(3)	116.0(3)
C(5)-C(4)-H(4A)	108.3
C(3)-C(4)-H(4A)	108.3
C(5)-C(4)-H(4B)	108.3
C(3)-C(4)-H(4B)	108.3
H(4A)-C(4)-H(4B)	107.4
N(2)-C(5)-C(4)	112.6(3)
N(2)-C(5)-H(5A)	109.1
C(4)-C(5)-H(5A)	109.1
N(2)-C(5)-H(5B)	109.1
C(4)-C(5)-H(5B)	109.1
H(5A)-C(5)-H(5B)	107.8
N(1)-C(6)-C(7)	111.5(3)
N(1)-C(6)-H(6A)	109.3
C(7)-C(6)-H(6A)	109.3
N(1)-C(6)-H(6B)	109.3
C(7)-C(6)-H(6B)	109.3
H(6A)-C(6)-H(6B)	108.0
N(2)-C(7)-C(6)	112.2(3)
N(2)-C(7)-H(7A)	109.2
C(6)-C(7)-H(7A)	109.2
N(2)-C(7)-H(7B)	109.2
C(6)-C(7)-H(7B)	109.2
H(7A)-C(7)-H(7B)	107.9
N(2)-C(8)-C(9)	113.6(3)
N(2)-C(8)-H(8A)	108.8
C(9)-C(8)-H(8A)	108.8
N(2)-C(8)-H(8B)	108.8
C(9)-C(8)-H(8B)	108.8
H(8A)-C(8)-H(8B)	107.7
C(8)-C(9)-S(2)	113.8(2)
C(8)-C(9)-H(9A)	108.8
S(2)-C(9)-H(9A)	108.8
C(8)-C(9)-H(9B)	108.8
S(2)-C(9)-H(9B)	108.8
H(9A)-C(9)-H(9B)	107.7
C(11)-C(10)-S(1)	118.6(2)
C(11)-C(10)-H(10A)	107.7
S(1)-C(10)-H(10A)	107.7

Table A-24. (Continued).

C(11)-C(10)-H(10B)	107.7
S(1)-C(10)-H(10B)	107.7
H(10A)-C(10)-H(10B)	107.1
O(2)-C(11)-O(1)	124.7(3)
O(2)-C(11)-C(10)	115.6(3)
O(1)-C(11)-C(10)	119.7(3)

Symmetry transformations used to generate equivalent atoms: -x+1/2, -y, z+1/2

Table A-25. Crystal data and structure refinement for **$[(Zn\text{-}1'\text{-}Ac)W(CO)_5]_x$**.

Empirical formula	$C_{16}\ H_{18}\ N_2\ O_7\ S_2\ W\ Zn$	
Formula weight	663.66	
Temperature	110(2) K	
Wavelength	1.54178 Å	
Crystal system	Monoclinic	
Space group	P21	
Unit cell dimensions	a = 9.481(2) Å	α= 90°.
	b = 10.843(3) Å	β= 104.965(11)°.
	c = 10.599(3) Å	γ = 90°.
Volume	1052.6(4) $Å^3$	
Z	2	
Density (calculated)	2.094 Mg/m^3	
Absorption coefficient	13.576 mm^{-1}	
F(000)	640	
Crystal size	0.10 x 0.01 x 0.01 mm^3	
Theta range for data collection	4.32 to 59.98°.	
Index ranges	-10<=h<=10, -12<=k<=12, -10<=l<=11	
Reflections collected	7542	
Independent reflections	2765 [R(int) = 0.3011]	
Completeness to theta = 59.98°	95.8 %	
Absorption correction	Semi-empirical from equivalents	

Table A-25. (Continued).

Max. and min. transmission	0.8762 and 0.3438
Refinement method	Full-matrix least-squares on F^2
Data / restraints / parameters	2765 / 210 / 263
Goodness-of-fit on F^2	1.013
Final R indices [I>2sigma(I)]	R1 = 0.0719, wR2 = 0.1507
R indices (all data)	R1 = 0.1257, wR2 = 0.1853
Absolute structure parameter	0.0(3)
Largest diff. peak and hole	0.950 and -0.874 e.Å^{-3}

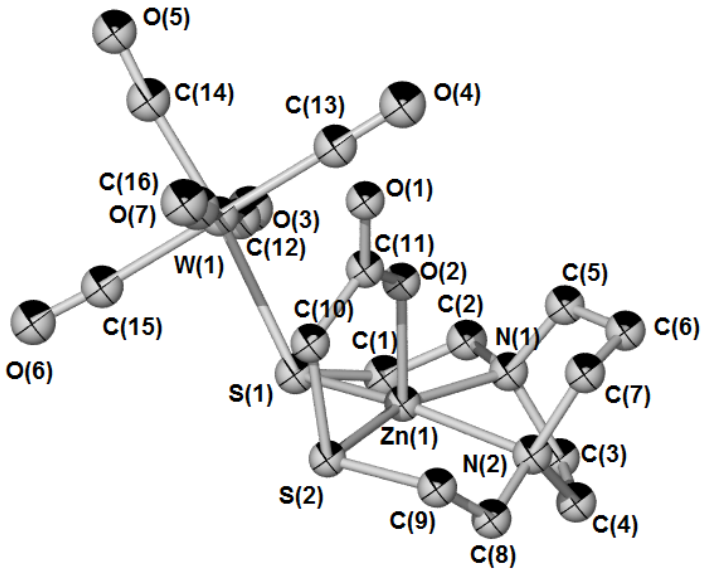

(Zn-1'-Ac)W(CO)$_5$ unit within the coordination polymer

Table A-26. Bond lengths [Å] for **$[(Zn\text{-}1'\text{-}Ac)W(CO)_5]_x$**.

W(1)-C(13)	2.02(3)
W(1)-C(14)	2.02(3)
W(1)-C(16)	2.04(3)
W(1)-C(15)	2.04(3)
W(1)-C(12)	2.08(3)
W(1)-S(1)	2.591(7)
Zn(1)-O(2)	2.074(18)
Zn(1)-N(1)	2.121(19)
Zn(1)-O(1)#1	2.265(17)
Zn(1)-N(2)	2.277(18)
Zn(1)-S(1)	2.403(7)
Zn(1)-S(2)	2.548(7)
S(1)-C(1)	1.79(3)
O(1)-C(11)	1.25(3)
O(1)-Zn(1)#2	2.265(17)
N(1)-C(5)	1.41(4)
N(1)-C(3)	1.51(3)
N(1)-C(2)	1.53(3)
C(1)-C(2)	1.37(4)
C(1)-H(6A)	0.9900
C(1)-H(6B)	0.9900
S(2)-C(10)	1.85(3)
S(2)-C(9)	1.85(2)
O(2)-C(11)	1.20(3)
N(2)-C(7)	1.47(4)
N(2)-C(8)	1.53(3)
N(2)-C(4)	1.55(3)
C(2)-H(7A)	0.9900
C(2)-H(7B)	0.9900
O(3)-C(12)	1.15(3)
C(3)-C(4)	1.53(3)
C(3)-H(8A)	0.9900
C(3)-H(8B)	0.9900
O(4)-C(13)	1.17(3)
C(4)-H(9A)	0.9900
C(4)-H(9B)	0.9900
O(5)-C(14)	1.12(3)
C(5)-C(6)	1.39(3)
C(5)-H(10A)	0.9900
C(5)-H(10B)	0.9900
O(6)-C(15)	1.15(3)
C(6)-C(7)	1.38(3)
C(6)-H(11A)	0.9900
C(6)-H(11B)	0.9900
O(7)-C(16)	1.15(3)
C(7)-H(12A)	0.9900

Table A-26. (Continued).

C(7)-H(12B)	0.9900
C(8)-C(9)	1.31(3)
C(8)-H(13A)	0.9900
C(8)-H(13B)	0.9900
C(9)-H(14A)	0.9900
C(9)-H(14B)	0.9900
C(10)-C(11)	1.53(4)

Table A-27. Bond angles [°] for **[(Zn-1'-Ac)W(CO)$_5$]$_x$**.

C(13)-W(1)-C(14)	90.6(12)
C(13)-W(1)-C(16)	90.2(13)
C(14)-W(1)-C(16)	86.7(12)
C(13)-W(1)-C(15)	177.2(13)
C(14)-W(1)-C(15)	89.1(11)
C(16)-W(1)-C(15)	92.5(12)
C(13)-W(1)-C(12)	89.0(12)
C(14)-W(1)-C(12)	90.7(11)
C(16)-W(1)-C(12)	177.3(12)
C(15)-W(1)-C(12)	88.3(12)
C(13)-W(1)-S(1)	94.8(8)
C(14)-W(1)-S(1)	174.6(9)
C(16)-W(1)-S(1)	93.3(9)
C(15)-W(1)-S(1)	85.5(8)
C(12)-W(1)-S(1)	89.4(7)
O(2)-Zn(1)-N(1)	97.8(9)
O(2)-Zn(1)-O(1)#1	167.7(7)
N(1)-Zn(1)-O(1)#1	93.6(8)
O(2)-Zn(1)-N(2)	94.4(8)
N(1)-Zn(1)-N(2)	74.1(7)
O(1)#1-Zn(1)-N(2)	84.1(8)
O(2)-Zn(1)-S(1)	101.7(5)
N(1)-Zn(1)-S(1)	89.1(6)
O(1)#1-Zn(1)-S(1)	83.2(5)
N(2)-Zn(1)-S(1)	158.2(6)
O(2)-Zn(1)-S(2)	81.3(5)
N(1)-Zn(1)-S(2)	158.1(5)
O(1)#1-Zn(1)-S(2)	86.4(5)
N(2)-Zn(1)-S(2)	84.2(5)
S(1)-Zn(1)-S(2)	112.6(3)
C(1)-S(1)-Zn(1)	90.4(9)
C(1)-S(1)-W(1)	107.0(9)
Zn(1)-S(1)-W(1)	120.0(3)
C(11)-O(1)-Zn(1)#2	135.4(17)
C(5)-N(1)-C(3)	112(2)
C(5)-N(1)-C(2)	112(2)
C(3)-N(1)-C(2)	108(2)
C(5)-N(1)-Zn(1)	109.0(17)
C(3)-N(1)-Zn(1)	106.8(15)
C(2)-N(1)-Zn(1)	108.7(15)
C(2)-C(1)-S(1)	120(2)
C(2)-C(1)-H(6A)	107.3
S(1)-C(1)-H(6A)	107.3
C(2)-C(1)-H(6B)	107.3
S(1)-C(1)-H(6B)	107.3

Table A-27. (Continued).

H(6A)-C(1)-H(6B)	106.9
C(10)-S(2)-C(9)	100.4(14)
C(10)-S(2)-Zn(1)	93.7(8)
C(9)-S(2)-Zn(1)	93.3(7)
C(11)-O(2)-Zn(1)	125.8(17)
C(7)-N(2)-C(8)	124(2)
C(7)-N(2)-C(4)	109(2)
C(8)-N(2)-C(4)	114(2)
C(7)-N(2)-Zn(1)	105.5(15)
C(8)-N(2)-Zn(1)	99.7(14)
C(4)-N(2)-Zn(1)	99.3(14)
C(1)-C(2)-N(1)	115(2)
C(1)-C(2)-H(7A)	108.4
N(1)-C(2)-H(7A)	108.4
C(1)-C(2)-H(7B)	108.4
N(1)-C(2)-H(7B)	108.4
H(7A)-C(2)-H(7B)	107.5
N(1)-C(3)-C(4)	106.7(19)
N(1)-C(3)-H(8A)	110.4
C(4)-C(3)-H(8A)	110.4
N(1)-C(3)-H(8B)	110.4
C(4)-C(3)-H(8B)	110.4
H(8A)-C(3)-H(8B)	108.6
C(3)-C(4)-N(2)	116(2)
C(3)-C(4)-H(9A)	108.2
N(2)-C(4)-H(9A)	108.2
C(3)-C(4)-H(9B)	108.2
N(2)-C(4)-H(9B)	108.2
H(9A)-C(4)-H(9B)	107.4
C(6)-C(5)-N(1)	119(2)
C(6)-C(5)-H(10A)	107.6
N(1)-C(5)-H(10A)	107.6
C(6)-C(5)-H(10B)	107.6
N(1)-C(5)-H(10B)	107.6
H(10A)-C(5)-H(10B)	107.1
C(7)-C(6)-C(5)	114(2)
C(7)-C(6)-H(11A)	108.8
C(5)-C(6)-H(11A)	108.8
C(7)-C(6)-H(11B)	108.8
C(5)-C(6)-H(11B)	108.8
H(11A)-C(6)-H(11B)	107.7
C(6)-C(7)-N(2)	115(2)
C(6)-C(7)-H(12A)	108.5
N(2)-C(7)-H(12A)	108.5
C(6)-C(7)-H(12B)	108.5
N(2)-C(7)-H(12B)	108.5

Table A-27. (Continued).

H(12A)-C(7)-H(12B)	107.5
C(9)-C(8)-N(2)	121(2)
C(9)-C(8)-H(13A)	107.2
N(2)-C(8)-H(13A)	107.2
C(9)-C(8)-H(13B)	107.2
N(2)-C(8)-H(13B)	107.2
H(13A)-C(8)-H(13B)	106.8
C(8)-C(9)-S(2)	109(2)
C(8)-C(9)-H(14A)	110.0
S(2)-C(9)-H(14A)	110.0
C(8)-C(9)-H(14B)	110.0
S(2)-C(9)-H(14B)	110.0
H(14A)-C(9)-H(14B)	108.4
C(11)-C(10)-S(2)	115.0(17)
O(2)-C(11)-O(1)	131(3)
O(2)-C(11)-C(10)	122(2)
O(1)-C(11)-C(10)	108(2)
O(3)-C(12)-W(1)	172(2)
O(4)-C(13)-W(1)	176(3)
O(5)-C(14)-W(1)	175(3)
O(6)-C(15)-W(1)	168(3)
O(7)-C(16)-W(1)	180(3)

Symmetry transformations used to generate equivalent atoms:
#1 -x+1,y+1/2,-z+1 #2 -x+1,y-1/2,-z+1

Table A-28. Crystal data and structure refinement for **[Et_4N][(Zn-1'-Cl)$W(CO)_4$]**.

Empirical formula	$C_{21.50}$ H_{41} Cl_2 N_3 O_5 S_2 W Zn	
Formula weight	805.81	
Temperature	110(2) K	
Wavelength	0.71073 Å	
Crystal system	Monoclinic	
Space group	C2/c	
Unit cell dimensions	a = 23.781(3) Å	α= 90°.
	b = 8.5401(12) Å	β= 107.227(2)°.
	c = 30.599(4) Å	γ = 90°.
Volume	5935.5(15) $Å^3$	
Z	8	
Density (calculated)	1.803 Mg/m^3	
Absorption coefficient	5.037 mm^{-1}	
F(000)	3208	
Crystal size	0.20 x 0.10 x 0.10 mm^3	
Theta range for data collection	2.55 to 25.00°.	
Index ranges	-28<=h<=28, -10<=k<=10, -36<=l<=36	
Reflections collected	26462	
Independent reflections	5106 [R(int) = 0.1190]	
Completeness to theta = 25.00°	97.8 %	

Table A-28. (Continued).

Absorption correction	Semi-empirical from equivalents
Max. and min. transmission	0.6328 and 0.4324
Refinement method	Full-matrix least-squares on F^2
Data / restraints / parameters	5106 / 0 / 324
Goodness-of-fit on F^2	1.019
Final R indices [I>2sigma(I)]	R1 = 0.0301, wR2 = 0.0612
R indices (all data)	R1 = 0.0374, wR2 = 0.0633
Largest diff. peak and hole	1.980 and -1.486 e.Å^{-3}

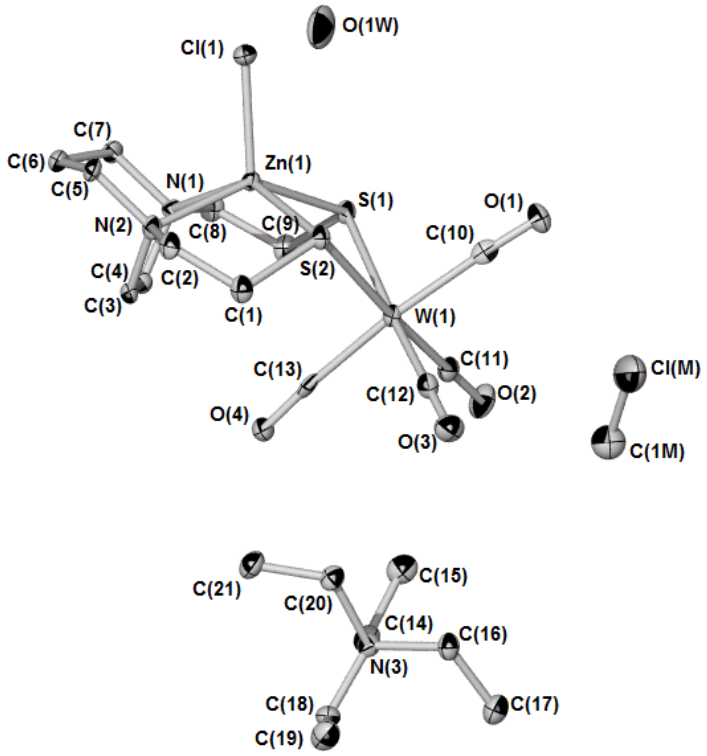

$[Et_4N][(Zn\text{-}1'\text{-}Cl)W(CO)_4$

Table A-29. Bond lengths [Å] for **[Et_4N][(Zn-1'-Cl)$W(CO)_4$]**.

W(1)-C(12)	1.950(5)
W(1)-C(11)	1.962(5)
W(1)-C(13)	2.012(5)
W(1)-C(10)	2.041(5)
W(1)-S(2)	2.5912(11)
W(1)-S(1)	2.5915(11)
Zn(1)-N(2)	2.182(3)
Zn(1)-N(1)	2.232(4)
Zn(1)-Cl(1)	2.2902(12)
Zn(1)-S(1)	2.3845(11)
Zn(1)-S(2)	2.4055(12)
ClM-C(1M)	1.582(13)
ClM-C(1M)#1	1.695(11)
C(1M)-C(1M)#1	1.42(2)
C(1M)-ClM#1	1.695(11)
C(1M)-H(1MA)	0.9600
C(1M)-H(1MB)	0.9599
O(1W)-H(1W1)	0.8500
O(1W)-H(2W1)	0.8500
S(2)-C(1)	1.834(4)
S(1)-C(9)	1.830(5)
O(3)-C(12)	1.166(5)
O(2)-C(11)	1.160(5)
O(4)-C(13)	1.152(6)
O(1)-C(10)	1.154(5)
N(1)-C(4)	1.473(5)
N(1)-C(8)	1.480(5)
N(1)-C(7)	1.492(5)
N(2)-C(3)	1.465(6)
N(2)-C(2)	1.473(6)
N(2)-C(5)	1.491(5)
N(3)-C(18)	1.515(6)
N(3)-C(14)	1.517(6)
N(3)-C(16)	1.521(6)
N(3)-C(20)	1.523(5)
C(1)-C(2)	1.517(6)
C(1)-H(1A)	0.9900
C(1)-H(1B)	0.9900
C(2)-H(2A)	0.9900
C(2)-H(2B)	0.9900
C(3)-C(4)	1.551(6)
C(3)-H(3A)	0.9900
C(3)-H(3B)	0.9900
C(4)-H(4A)	0.9900
C(4)-H(4B)	0.9900

Table A-29. (Continued).

C(5)-C(6)	1.545(7)
C(5)-H(5A)	0.9900
C(5)-H(5B)	0.9900
C(6)-C(7)	1.514(6)
C(6)-H(6A)	0.9900
C(6)-H(6B)	0.9900
C(7)-H(7A)	0.9900
C(7)-H(7B)	0.9900
C(8)-C(9)	1.521(6)
C(8)-H(8A)	0.9900
C(8)-H(8B)	0.9900
C(9)-H(9A)	0.9900
C(9)-H(9B)	0.9900
C(14)-C(15)	1.506(7)
C(14)-H(14A)	0.9900
C(14)-H(14B)	0.9900
C(15)-H(15A)	0.9800
C(15)-H(15B)	0.9800
C(15)-H(15C)	0.9800
C(16)-C(17)	1.520(6)
C(16)-H(16A)	0.9900
C(16)-H(16B)	0.9900
C(17)-H(17A)	0.9800
C(17)-H(17B)	0.9800
C(17)-H(17C)	0.9800
C(18)-C(19)	1.496(6)
C(18)-H(18A)	0.9900
C(18)-H(18B)	0.9900
C(19)-H(19A)	0.9800
C(19)-H(19B)	0.9800
C(19)-H(19C)	0.9800
C(20)-C(21)	1.519(6)
C(20)-H(20A)	0.9900
C(20)-H(20B)	0.9900
C(21)-H(21A)	0.9800
C(21)-H(21B)	0.9800
C(21)-H(21C)	0.9800

Table A-30. Bond angles [°] for **[Et_4N][(Zn-1'-Cl)$W(CO)_4$]**.

C(12)-W(1)-C(11)	89.56(18)
C(12)-W(1)-C(13)	88.65(18)
C(11)-W(1)-C(13)	86.74(18)
C(12)-W(1)-C(10)	90.35(18)
C(11)-W(1)-C(10)	86.80(18)
C(13)-W(1)-C(10)	173.48(16)
C(12)-W(1)-S(2)	92.72(13)
C(11)-W(1)-S(2)	176.61(13)
C(13)-W(1)-S(2)	95.82(12)
C(10)-W(1)-S(2)	90.67(12)
C(12)-W(1)-S(1)	174.00(14)
C(11)-W(1)-S(1)	95.23(13)
C(13)-W(1)-S(1)	95.21(12)
C(10)-W(1)-S(1)	86.32(12)
S(2)-W(1)-S(1)	82.34(3)
N(2)-Zn(1)-N(1)	73.21(13)
N(2)-Zn(1)-Cl(1)	106.44(10)
N(1)-Zn(1)-Cl(1)	107.24(9)
N(2)-Zn(1)-S(1)	140.84(11)
N(1)-Zn(1)-S(1)	85.07(9)
Cl(1)-Zn(1)-S(1)	111.02(4)
N(2)-Zn(1)-S(2)	86.83(10)
N(1)-Zn(1)-S(2)	141.44(9)
Cl(1)-Zn(1)-S(2)	109.97(5)
S(1)-Zn(1)-S(2)	90.84(4)
C(1M)-ClM-C(1M)#1	51.0(7)
C(1M)#1-C(1M)-ClM	68.6(10)
C(1M)#1-C(1M)-ClM#1	60.4(8)
ClM-C(1M)-ClM#1	129.0(7)
C(1M)#1-C(1M)-H(1MA)	122.3
ClM-C(1M)-H(1MA)	101.9
ClM#1-C(1M)-H(1MA)	104.7
C(1M)#1-C(1M)-H(1MB)	131.4
ClM-C(1M)-H(1MB)	105.5
ClM#1-C(1M)-H(1MB)	107.6
H(1MA)-C(1M)-H(1MB)	106.3
H(1W1)-O(1W)-H(2W1)	114.9
C(1)-S(2)-Zn(1)	95.49(14)
C(1)-S(2)-W(1)	111.45(16)
Zn(1)-S(2)-W(1)	89.24(4)
C(9)-S(1)-Zn(1)	97.76(14)
C(9)-S(1)-W(1)	111.93(16)
Zn(1)-S(1)-W(1)	89.69(4)
C(4)-N(1)-C(8)	112.0(3)
C(4)-N(1)-C(7)	110.6(3)

Table A-30. (Continued).

C(8)-N(1)-C(7)	109.3(3)
C(4)-N(1)-Zn(1)	106.9(2)
C(8)-N(1)-Zn(1)	110.0(3)
C(7)-N(1)-Zn(1)	107.9(3)
C(3)-N(2)-C(2)	112.0(3)
C(3)-N(2)-C(5)	110.5(4)
C(2)-N(2)-C(5)	110.0(3)
C(3)-N(2)-Zn(1)	108.5(2)
C(2)-N(2)-Zn(1)	108.1(3)
C(5)-N(2)-Zn(1)	107.7(3)
C(18)-N(3)-C(14)	107.2(4)
C(18)-N(3)-C(16)	111.2(3)
C(14)-N(3)-C(16)	110.9(3)
C(18)-N(3)-C(20)	111.0(3)
C(14)-N(3)-C(20)	110.5(3)
C(16)-N(3)-C(20)	106.0(3)
C(2)-C(1)-S(2)	111.0(3)
C(2)-C(1)-H(1A)	109.4
S(2)-C(1)-H(1A)	109.4
C(2)-C(1)-H(1B)	109.4
S(2)-C(1)-H(1B)	109.4
H(1A)-C(1)-H(1B)	108.0
N(2)-C(2)-C(1)	113.4(3)
N(2)-C(2)-H(2A)	108.9
C(1)-C(2)-H(2A)	108.9
N(2)-C(2)-H(2B)	108.9
C(1)-C(2)-H(2B)	108.9
H(2A)-C(2)-H(2B)	107.7
N(2)-C(3)-C(4)	111.7(3)
N(2)-C(3)-H(3A)	109.3
C(4)-C(3)-H(3A)	109.3
N(2)-C(3)-H(3B)	109.3
C(4)-C(3)-H(3B)	109.3
H(3A)-C(3)-H(3B)	107.9
N(1)-C(4)-C(3)	111.5(4)
N(1)-C(4)-H(4A)	109.3
C(3)-C(4)-H(4A)	109.3
N(1)-C(4)-H(4B)	109.3
C(3)-C(4)-H(4B)	109.3
H(4A)-C(4)-H(4B)	108.0
N(2)-C(5)-C(6)	112.7(4)
N(2)-C(5)-H(5A)	109.1
C(6)-C(5)-H(5A)	109.1
N(2)-C(5)-H(5B)	109.1
C(6)-C(5)-H(5B)	109.0
H(5A)-C(5)-H(5B)	107.8

Table A-30. (Continued).

C(7)-C(6)-C(5)	116.1(4)
C(7)-C(6)-H(6A)	108.3
C(5)-C(6)-H(6A)	108.3
C(7)-C(6)-H(6B)	108.3
C(5)-C(6)-H(6B)	108.3
H(6A)-C(6)-H(6B)	107.4
N(1)-C(7)-C(6)	112.8(3)
N(1)-C(7)-H(7A)	109.0
C(6)-C(7)-H(7A)	109.0
N(1)-C(7)-H(7B)	109.0
C(6)-C(7)-H(7B)	109.0
H(7A)-C(7)-H(7B)	107.8
N(1)-C(8)-C(9)	112.0(3)
N(1)-C(8)-H(8A)	109.2
C(9)-C(8)-H(8A)	109.2
N(1)-C(8)-H(8B)	109.2
C(9)-C(8)-H(8B)	109.2
H(8A)-C(8)-H(8B)	107.9
C(8)-C(9)-S(1)	111.8(3)
C(8)-C(9)-H(9A)	109.3
S(1)-C(9)-H(9A)	109.3
C(8)-C(9)-H(9B)	109.3
S(1)-C(9)-H(9B)	109.3
H(9A)-C(9)-H(9B)	107.9
O(1)-C(10)-W(1)	175.5(4)
O(2)-C(11)-W(1)	179.5(5)
O(3)-C(12)-W(1)	179.4(5)
O(4)-C(13)-W(1)	175.7(4)
C(15)-C(14)-N(3)	115.2(4)
C(15)-C(14)-H(14A)	108.5
N(3)-C(14)-H(14A)	108.5
C(15)-C(14)-H(14B)	108.5
N(3)-C(14)-H(14B)	108.5
H(14A)-C(14)-H(14B)	107.5
C(14)-C(15)-H(15A)	109.5
C(14)-C(15)-H(15B)	109.5
H(15A)-C(15)-H(15B)	109.5
C(14)-C(15)-H(15C)	109.5
H(15A)-C(15)-H(15C)	109.5
H(15B)-C(15)-H(15C)	109.5
C(17)-C(16)-N(3)	114.2(4)
C(17)-C(16)-H(16A)	108.7
N(3)-C(16)-H(16A)	108.7
C(17)-C(16)-H(16B)	108.7
N(3)-C(16)-H(16B)	108.7
H(16A)-C(16)-H(16B)	107.6

Table A-30. (Continued).

C(16)-C(17)-H(17A)	109.5
C(16)-C(17)-H(17B)	109.5
H(17A)-C(17)-H(17B)	109.5
C(16)-C(17)-H(17C)	109.5
H(17A)-C(17)-H(17C)	109.5
H(17B)-C(17)-H(17C)	109.5
C(19)-C(18)-N(3)	116.3(4)
C(19)-C(18)-H(18A)	108.2
N(3)-C(18)-H(18A)	108.2
C(19)-C(18)-H(18B)	108.2
N(3)-C(18)-H(18B)	108.2
H(18A)-C(18)-H(18B)	107.4
C(18)-C(19)-H(19A)	109.5
C(18)-C(19)-H(19B)	109.5
H(19A)-C(19)-H(19B)	109.5
C(18)-C(19)-H(19C)	109.5
H(19A)-C(19)-H(19C)	109.5
H(19B)-C(19)-H(19C)	109.5
C(21)-C(20)-N(3)	114.7(4)
C(21)-C(20)-H(20A)	108.6
N(3)-C(20)-H(20A)	108.6
C(21)-C(20)-H(20B)	108.6
N(3)-C(20)-H(20B)	108.6
H(20A)-C(20)-H(20B)	107.6
C(20)-C(21)-H(21A)	109.5
C(20)-C(21)-H(21B)	109.5
H(21A)-C(21)-H(21B)	109.5
C(20)-C(21)-H(21C)	109.5
H(21A)-C(21)-H(21C)	109.5
H(21B)-C(21)-H(21C)	109.5

Symmetry transformations used to generate equivalent atoms:
#1 -x+1/2,-y-1/2,-z

VITA

Elky Almaraz received her Bachelor of Science degree in chemistry from The University of Texas – Pan American in 2003. She began her graduate studies under the advisement of Prof. M. Y. Darensbourg at Texas A&M University in the Fall of 2003, and received her Ph.D. in chemistry in May 2009. Elky may be contacted through her parents, Alejandro and Eugenia Almaraz, or through the Texas A&M University Department of Chemistry, P.O. Box 30012, College Station, TX 77842. Her email address is elky713@gmail.com.